



UNIVERSITY OF THE
WITWATERSRAND,
JOHANNESBURG

**WSe₂ nanostructures decorated with platinum
nanocrystals as electrocatalysts for hydrogen
evolution reaction**

A dissertation submitted to the Faculty of Science, University of the Witwatersrand in
partial fulfilment of the requirements for the degree of Master of Science in
Chemistry

By

Thokozani Ngcobo

Student number:

1367697

Supervisors: Prof. Nosipho Moloto and Dr. Siziwe Gqoba

Declaration

I declare that the work reported herein is my own independent work, submitted at the School of Chemistry, University of the Witwatersrand, Johannesburg. This work has not been submitted for any degree or examination in any other institution of higher learning.

Candidate name: Thokozani Ngcobo



Date:

07/06/2023

Supervisor: Nosipho Moloto



Date:

07/06/2023

Abstract

Research into tungsten diselenide (WSe_2), a two-dimensional layered transition metal dichalcogenide (TMD) material, has increased due to its physical and chemical properties. These properties are considered unique and tunable for targeted applications such as electronic, optical, and catalytic use. WSe_2 has comparable bandgap in relation to other selenides which makes it candidate to use as an electrocatalyst for hydrogen evolution reactions (HER). Colloidal synthesis is a cheap, flexible method that allows reaction parameters to be manipulated to influence the desired outcome. Therefore, the effects of concentration, temperature, time, capping agents and tungsten precursors was investigated to find the optimal conditions for the synthesis of WSe_2 nanoflowers. WSe_2 nanoflowers were favoured at 320 °C for 120 min in oleyl alcohol when the concentration was 1:4 for W:Se. When the concentration, time and temperature decreased, WSe_2 favoured nanorod structures. However, when oleylamine was used as a capping agent, agglomeration of the nanoflowers was observed. The metal precursors all favoured oleyl alcohol as the capping agent resulting in defined nanoflowers being formed. The thickness of the nanoflowers varied depending on the precursor used. Tungsten chloride (WCl_6) formed densely packed nanoflowers whereas tungsten hexacarbonyl ($W(CO)_6$) and tungstic acid (H_2WO_4) had less layers forming nanoflower-like structure. H_2WO_4 also produced mixture of WSe_2 and WO_3 due to the oxidation of the precursor. The semiconducting 2H phase was obtained from all three tungsten precursors which is required for electrocatalytic activity. To improve the electrocatalytic activity, platinum was decorated on the surface of WSe_2 . The electrochemical characteristics of Pt/ WSe_2 nanohybrids formed from various metal precursors were studied using techniques such as linear sweep voltammetry (LSV), cyclic voltammetry (CV), and electrical impedance spectroscopy (EIS). Analysis revealed that $W(CO)_6$ -Pt/ WSe_2 nanohybrids exhibited enhanced electrochemical performance in hydrogen evolution reaction, as evidenced by lower Tafel slope and overpotential at 10mA/cm², in comparison to the other two precursors.

Acknowledgements

Firstly, I would like to thank God for granting me this opportunity. I am thankful to my mother for her unwavering love, prayers, and support, I am nothing without her. I would like to thank my supervisors, Prof. Nosipho Moloto and Dr Siziwe Gqoba, I really appreciate the guidance and support throughout this journey. I would like to thank Wits MMU for providing instrumentation and running analysis, Dr Abhishek Panday for allowing me to run XRD and NMISA for XPS. I would like to credit Dr Victor Mashindi and Dr Zakhele Ndala for helping with electrochemical studies. Then I would like to extend my gratitude to all my lab co-workers, thank you for helping throughout this project. I would like to express appreciation to my family and friends for being supportive and patient with me throughout this journey. To my partner, I appreciate your continuous support. Then I would like to thank me for believing in myself and not giving up. Finally, I would like to thank the National Research Foundation for the funding.

Dedication

I dedicate this to my parents; I hope I continue to make you proud.

List of presentation

1. Poster presentation and flash talk at University of the Witwatersrand School of Chemistry 1st annual MSc poster presentations held at University of the Witwatersrand (September 2022) (1st place)
2. Poster presentation at Catalysis Society of South Africa (CATSA) held at Drakensberg, KZN (November 2022)
3. Oral presentation at Catalysis and Materials (CATMAT) seminar held at University of the Witwatersrand, School of Chemistry (2022)

Table of Contents

Declaration.....	ii
Abstract.....	iii
Acknowledgements.....	iv
Dedication.....	v
List of presentation.....	vi
List of figures.....	x
List of tables.....	xiii
List of Abbreviations.....	xiv
Synopsis.....	xvi
Chapter 1.....	1
Introduction.....	1
1.1 Background.....	1
1.2 Rationale.....	2
1.3 Aim of the project.....	2
1.4 References.....	4
Chapter 2.....	5
Literature Review.....	5
2.1. Transition metal dichalcogenides.....	5
2.2. Electronic and structural properties of TMDs.....	6
2.3. Tungsten diselenide.....	7
2.4 Synthesis of TMDs.....	8
2.4.1. Top-down approach.....	9
2.4.2. Bottom-up approach.....	10
2.5. Colloidal growth mechanism.....	13
2.6. Photoelectrochemical water splitting.....	15
2.7. Hydrogen evolution reaction (HER).....	18
2.8. Transition metal doping.....	21
2. 9 References.....	22
Chapter 3.....	29
Synthesis of WSe ₂ nanostructures with varying reaction parameters.....	29
3.1. Introduction.....	29
3.2. Method and materials.....	31
3.2.1. Chemicals.....	31

3.2.2. Experimental procedure	31
3.2.3. Characterization	31
3.3. Results	32
3.3.1. Effect of concentration	32
3.3.2. Effect of temperature and time	36
3.5. Conclusion	41
3.5 References	42
Chapter 4	45
Synthesis of WSe₂ nanostructures by varying the tungsten precursor and capping ligand.....	45
4.1. Introduction	45
4.2. Method and materials	46
4.2.1. Chemicals	46
4.2.2. Experimental Procedure	46
4.2.3. Characterization	46
4.2. Results	47
4.2.1. Capping ligand: OA	47
4.2.2. Capping ligand: OLA	52
4.3. Conclusion	57
4.4. References	58
Chapter 5	61
Pt nanocrystals decorated on WSe₂ to form Pt/WSe₂ nanohybrids.....	61
5.1. Introduction	61
5.2. Methods and Materials	62
5.2.2. Characterization	62
5.3. Results and Discussion	62
5.4. Conclusion	74
5.5. References	75
Chapter 6	77
Pt/WSe₂ nanohybrids as the electrode in electrocatalytic HER	77
6.1. Introduction	77
6.2. Experimental	78
6.2.1. Chemicals	78
6.2.2. Electrochemical measurements and preparation of the working electrode.....	78
6.3. Results and Discussion	79
6.4. Conclusion	84

6.5. References	85
Chapter 7	88
General conclusions and recommendations	88
7.1. Conclusions	88

List of figures

Figure 2.1: Periodic table showing the transition metals and chalcogen atoms found in transition metal dichalcogenides [9].....	6
Figure 2.2: Simplified electronic structure of group 6 TMDs showing the co-existence of the split direct band gap and the indirect band gap [16].	7
Figure 2.3: Crystal structure and stacking sequence of 1T, 2H and 3R WSe ₂ phases [23].	8
Figure 2.4: Diagram of the classical nucleation theory showing the relationship of the free energy (ΔG) and the radius (r) of the nuclei [41]......	13
Figure 2.5: Diagram summarising LaMer's theory based on the separation of nucleation and growth [44].	14
Figure 2.6: Diagram showing basic electrochemical cell [53].	16
Figure 2.7: Diagram showing the mechanism of the electron-hole pair [58].	17
Figure 2.3: HER mechanism that takes place on the surface of the electrocatalyst [64].	19
Table 3.1: Summary of experimental conditions.	31
Figure 3.1: PXRD patterns of WSe ₂ nanoparticles synthesized at various mole ratios (*) indicates WO ₃	33
Figure 3.2: Raman spectroscopy of WSe ₂ nanoparticles synthesized at various mole ratios.	34
Table 3.2: Raman frequencies and their vibrational assignment.....	34
Figure 3.3: UV-vis absorption spectra of WSe ₂ nanoparticles synthesized at various mole ratios.	35
Figure 3.4: TEM images of WSe ₂ nanoparticles synthesized at various mole ratios.	36
3.5: PXRD patterns of WSe ₂ nanoparticles synthesized at various temperatures for (a) 120 min and (b) 60 min (*) indicates WO ₃	37
Figure 3.6: Raman spectra of WSe ₂ nanoparticles synthesized at various temperatures for (a) 120 min and (b) 60 min.....	38
Figure 3.7: UV-vis spectra of WSe ₂ nanoparticles synthesized at various temperatures for (a) 120 min and (b) 60 min.....	39
Figure 3.8: UV-vis spectra of WSe ₂ nanoparticles synthesized at various temperatures for (a) 120 min and (b) 60 min.....	40
.....	40

Figure 4.1: PXRD patterns of WSe ₂ nanoparticles synthesized using different tungsten precursors, (*) indicates WO ₃	48
.....	48
Figure 4.2: Raman spectroscopy of WSe ₂ nanoparticles synthesized with different tungsten precursors.....	49
.....	49
Figure 4.3: UV-vis absorption spectra of WSe ₂ nanoparticles synthesized using different tungsten precursors.	50
.....	50
Figure 4.4: TEM images of WSe ₂ nanoparticles synthesized with different tungsten precursors (a) WCl ₆ -WSe ₂ , (b) W(CO) ₆ -WSe ₂ , (c) H ₂ WO ₄ -WSe ₂	51
Figure 4.5: FTIR spectra of pure OA capping agent and capped-WSe ₂ nanoparticles synthesized using different tungsten precursors.....	52
Figure 4.6: PXRD patterns of WSe ₂ nanoparticles synthesized using different tungsten precursors, (*) indicates WO ₃	53
Figure 4.7: Raman spectroscopy of WSe ₂ nanoparticles synthesized with different tungsten precursors.....	54
Figure 4.8: UV-vis absorption spectra of WSe ₂ nanoparticles synthesized using different tungsten precursors.	55
Figure 4.9: TEM images of WSe ₂ nanoparticles synthesized with different tungsten precursors (a) WCl ₆ -WSe ₂ , (b) W(CO) ₆ -WSe ₂ , (c) H ₂ WO ₄ -WSe ₂	56
Figure 4.10: FTIR spectra of pure OLA capping agent and capped- WSe ₂ nanoparticles synthesized using different tungsten precursors.	57
Figure 5.1: PXRD patterns showing the Pt/WSe ₂ nanohybrids synthesized using different tungsten precursors.	63
Figure 5.2: UV-vis absorption spectra showing the Pt/WSe ₂ nanohybrids synthesized using different tungsten precursors.....	64
Figure 5.3: TEM images of Pt/WSe ₂ synthesized with different tungsten precursors (a) WCl ₆ , (b) WCl ₆ , (c) W(CO) ₆ , (d) W(CO) ₆ , (e) H ₂ WO ₄ , (f) H ₂ WO ₄	66
Figure 5.4: XPS survey spectra of Pt/WSe ₂ synthesized using WCl ₆ precursor.	67
Figure 5.5: High resolution core level spectra of WCl ₆ Pt/WSe ₂ nanohybrid with the focus on C1s, O1s, W4f7, Se3ds and Pt4f7.	68
Table 5.1: A summary of the stoichiometric assignments of the atomic composition, which were obtained from fitting the XPS spectra presented in Fig. 5.4 and 5.5.	68

Figure 5.6: XPS survey spectra of Pt/WSe ₂ synthesized using W(CO) ₆ precursor. .	69
Figure 5.7: High resolution core level spectra of W(CO) ₆ Pt/WSe ₂ nanohybrid with the focus on C1s.....	70
Table 5.2: A summary of the stoichiometric assignments of the atomic composition, which were obtained from fitting the XPS spectra presented in Fig. 5.6 and 5.7.....	70
Figure 5.8: XPS survey spectra of Pt/WSe ₂ synthesized using H ₂ WO ₄ precursor. ..	72
Figure 5.9: High resolution core level spectra of H ₂ WO ₄ Pt/WSe ₂ nanohybrid with the focus on C1s, O1s, W4f7, Se3ds and Pt4f7.....	73
Table 5.3: A summary of the stoichiometric assignments of the atomic composition, which were obtained from fitting the XPS spectra presented in Fig. 5.8 and 5.9.....	73
Figure 6.1: (a) LSV polarization curves of Pt/C, WCl ₆ , W(CO) ₆ and H ₂ WO ₄ Pt/WSe ₂ nanohybrids at a scan rate of 10 mV/s; (b) corresponding Tafel plots for Pt/C, WCl ₆ , W(CO) ₆ and H ₂ WO ₄ Pt/WSe ₂ nanohybrids.....	81
Table 6.1: Comparison of catalytic activity of WSe ₂ electrocatalysts in 0.5 M H ₂ SO ₄	81
Figure 6.2: Cyclic voltammograms of WCl ₆ , W(CO) ₆ and H ₂ WO ₄ - derived Pt/WSe ₂ nanohybrids at a scan rate of 10 mV/s.	82
Figure 6.3: Nyquist plots of WCl ₆ , W(CO) ₆ and H ₂ WO ₄ Pt/WSe ₂ nanohybrids.	83
Figure 6.4: Equivalent circuit of the measured impedance spectra.....	83
Table 6.2: Electrocatalytic parameters of the Pt/WSe ₂ nanohybrids using different tungsten precursors.....	84

List of tables

Table 3.1: Summary of experimental conditions.	31
Table 3.2: Raman frequencies and their vibrational assignment.	34
Table 5.1: A summary of the stoichiometric assignments of the atomic composition, which were obtained from fitting the XPS spectra presented in Fig. 5.4 and 5.5.	68
Table 5.2: A summary of the stoichiometric assignments of the atomic composition, which were obtained from fitting the XPS spectra presented in Fig. 5.6 and 5.7.	70
Table 5.3: A summary of the stoichiometric assignments of the atomic composition, which were obtained from fitting the XPS spectra presented in Fig. 5.8 and 5.9.	73
Table 6.1: Comparison of catalytic activity of WSe ₂ electrocatalysts in 0.5 M H ₂ SO ₄	81
Table 6.2: Electrocatalytic parameters of the Pt/WSe ₂ nanohybrids using different tungsten precursors.	84

List of Abbreviations

b – Tafel slope
CE – Counter electrode
CNT – Classical Nucleation Theory
CV – Cyclic Voltammetry
CVD – Chemical vapour deposition
 e^- - Electron
eV – Electron Volts
EIS – Electrical Impedance Spectroscopy
eq – Equation
FTIR – Fourier Transform Infrared
 H^+ - Hydrogen ion
 H_{ads} – Adsorbed hydrogen
HER – Hydrogen Evolution Reaction
J – Current density
 J_0 – Exchange current density
LSV – Linear sweep voltammetry
NP – Nanoparticles
OA – Oleyl alcohol
OER – Oxygen Evolution Reaction
OLA – Oleylamine
PEC – Photoelectrochemical
Pt – Platinum
Pt/C – Platinum on carbon
Pt/WSe₂ – Platinum decorated on tungsten diselenide
PXRD – Powder x-ray diffraction
 R_{ct} – Charge transfer resistance
RHE – Reversible hydrogen electrode
TEM – Transmission electron microscopy
TMD – Transition metal dichalcogenide
UV-vis – Ultraviolet visible spectroscopy
W – Tungsten

WE – Working electrode

WSe₂ – Tungsten diselenide

XPS – X-ray photoelectron spectroscopy

XRD – X-ray diffraction

Synopsis

The aim of the study was to synthesize 2D layered tungsten diselenide (WSe_2) nanostructures using the colloidal synthesis method. Then decorating the WSe_2 nanostructures with platinum nanocrystals to form nanohybrids and evaluate their electrocatalytic properties for potential application in water-splitting electrocatalytic HER. The layout of the dissertation is shown below:

- Chapter 1: is the background, motivation and rationale for the study including the aims and objectives.
- Chapter 2: is the literature review of transition metal dichalcogenides, particularly the properties of WSe_2 and various methods used to synthesize the materials. In addition, a short review on electrocatalytic HER and the application of WSe_2 as an electrocatalyst for water-splitting reactions.
- Chapter 3: reports on how varying the reaction parameters affects the properties of WSe_2 .
- Chapter 4: reports on the effect of the tungsten precursor and capping agent used on the properties of WSe_2 .
- Chapter 5: reports on the synthesis of Pt decorated on the surface of WSe_2 nanostructures.
- Chapter 6: reports on the investigation of Pt/ WSe_2 nanohybrids as electrocatalysts for HER.
- Chapter 7: evaluates the conclusions and suggests possible future work.

Chapter 1

Introduction

1.1 Background

Rolling blackouts otherwise known as load shedding has become a miserable experience for every person that depends on the South African national grid to supply electricity. For something that started off as a short-term resolution to mitigate electricity supply to meet the demand, it has now become part of everyday life and does not appear to be ending soon. This issue is not exclusive to South Africa as many countries are struggling to meet the increasing demand for electricity. As they heavily rely on non-renewable energy sources. Fossil fuels have been the main source of energy for decades as there was a large supply that has been decreasing over time. Fossil fuel-based energy is derived from burning fossil fuels which has a negative impact on human health and the environment. This is because fossil fuel combustion emits toxic particles, gases and carbon dioxide otherwise known as greenhouse gases into the atmosphere [1]. Greenhouse gases have a negative effect as they are pollutants in the atmosphere but prevent heat from escaping [2]. This is known as the “greenhouse effect” which causes global warming. Therefore alternative, sustainable clean energy sources are needed.

Clean and sustainable fuels are therefore required [3]. These have the ability to provide energy with zero or almost zero emissions that causes air pollution and greenhouse gases [4]. Therefore, they can be used to lessen the reliance on fossil fuel-based energy. To use sustainable sources for energy, they require the use of technologies that are economically feasible to generate electricity. Hydrogen is considered a fuel that can serve as a storable source [5]. Water splitting is a process whereby water is electrochemically broken down into its molecular constituents [6]. The process occurs within a cell where both the anodic oxygen evolution reaction (OER) and the cathodic hydrogen evolution reaction (HER) take place. [7]. This results in the formation of hydrogen and oxygen gas whereby the hydrogen produced can be used as fuel for energy.

Layered structures like WSe₂ are classified as transition metal dichalcogenides (TMDs) have semiconducting and catalytic properties making them suitable candidates to use in electrocatalytic generation of H₂. WSe₂ has attractive properties such as high morphology anisotropy, substantial surface area and ample active sites for redox reactions to take place [8]. The semiconducting properties of WSe₂ promotes the fast electron transfer required for HER [9]. However, it is not as effective as Pt which has high electrocatalytic performance due to its optimal hydrogen absorption energy, as a result of low overpotential and fast kinetics [10]. Although Pt is favourable for electrochemical reactions, it is not suitable for industrial application as it is pricey and scarce. Therefore, the electrocatalytic activity of WSe₂ can be improved by decorating it with Pt. The use of less Pt in combination with WSe₂ would not only decrease its overall cost but also enhance its electrocatalytic activity, resulting in a considerable improvement in the overall electrocatalytic performance of the hybrid material.

1.2 Rationale

The increase in demand for clean alternative energy requires the use of inexpensive techniques to generate electricity at a large scale. Photoelectrochemical generation of H₂ is considered an ideal solution as hydrogen is generated by splitting water into H₂ and O₂ gas. This process requires the use of an electrocatalyst. Generally, Pt is widely acknowledged as the most effective electrocatalyst but not suitable for commercial use as it is expensive. Therefore, to reduce the cost, we propose the use of WSe₂ which has semiconducting properties required for HER. WSe₂ can be obtained using cheap synthetic methods which could result in the formation of 2D layered WSe₂ materials. Colloidal synthesis is an easy, scalable technique that can be implemented for WSe₂. The reaction parameters can be modified to optimize the formation of WSe₂ in high yields. To improve the electrocatalytic activity of WSe₂, we propose decorating the surface with Pt nanocrystals. This will enhance the catalytic activity of the material by also reducing the amount of Pt used, therefore lowering the cost for industrial use.

1.3 Aim of the project

The main aim of this project was to evaluate the use of colloidal synthesis for WSe₂ nanostructures and to determine how certain parameters as well as tungsten

precursor affect the resultant WSe_2 . The WSe_2 obtained were then decorated with Pt, used to investigate the electrochemical properties of these nanomaterials for electrocatalytic HER. Therefore, to achieve the aim, the following objectives were identified:

- Colloidal synthesis and characterization of WSe_2 nanostructures by varying the reaction conditions such as the ratio of W:Se precursor, time, and temperature.
- Colloidal synthesis and characterization of WSe_2 nanostructures using different tungsten precursors and different organic capping agents.
- Ex-situ synthesis and characterization of Pt/ WSe_2 nanohybrids.
- Investigate the electrochemical properties of Pt/ WSe_2 nanohybrids for electrocatalytic HER.

1.4 References

- [1] F. Perera, "Multiple Threats to Child Health from Fossil Fuels Combustion: Impacts of Air Pollution and Climate Change," *Environmental Health Perspectives*, vol. 125, no. 2, pp. 141-148, 2017.
- [2] P. T. Latake, P. Pawar and A. Ranveer, "The Greenhouse Effect and Its Impacts on Environment," *International Journal of Innovative Research and Creative Technology*, vol. 1, no. 3, pp. 333-337, 2015.
- [3] S. R. Bull, "Renewable Energy Today and Tomorrow," *Proceedings of the IEEE*, vol. 89, no. 8, pp. 1216-1226, 2001.
- [4] N. Panwar, S. Kaushik and S. Kothari, "Role of renewable energy sources in environmental protection: A review," *Renewable and Sustainable Energy Reviews*, vol. 15, pp. 1513-1524, 2011.
- [5] Q. Zhu, Y. Qu, D. Liu, K. Ng and H. Pan, "Two-Dimensional Layered Materials: High-Efficient Electrocatalysts for Hydrogen Evolution Reaction," *ACS Applied Nano Materials*, vol. 3, pp. 6270-6296, 2020.
- [6] S. Cao, L. Piao and X. Chen, "Emerging photocatalysts for hydrogen evolution," *Trends in Chemistry*, vol. 2, pp. 57-70, 2020.
- [7] K. Khan, A. Tareen, M. Aslam, Y. Zhang, R. Wang, Z. Ouyang, Z. Gou and H. Zhang, "Recent advances in two-dimensional materials and their nanocomposites in sustainable energy conversion applications," *Nanoscale*, vol. 11, pp. 21622-21678, 2019.
- [8] P. Zhou, G. Collins, Z. Hens, K. Ryan, H. Geaney and S. Singh, "Colloidal WSe₂ nanocrystals as anodes for lithium-ion batteries," *Nanoscale*, vol. 12, p. 22307, 2020.
- [9] A. Azam, J. Yang, W. Li, J.-K. Huang and S. Li, "Tungsten diselenide (WSe₂) quantum dots: Fundamental, properties, synthesis and applications," *Progress in Materials Science*, vol. 132, p. 101042, 2023.
- [10] M. Dehcheshmeh and A. Kiani, "Synthesis of Pt nano catalyst in the presence of carbon monoxide: Superior activity towards hydrogen evolution reaction," *International Journal of Hydrogen Energy*, vol. 44, pp. 23969-23974, 2019.

Chapter 2

Literature Review

2.1. Transition metal dichalcogenides

Due to their optoelectronic properties, two-dimensional (2D) layered materials, specifically transition metal dichalcogenides (TMDs), have garnered a lot of attention and been thoroughly studied as promising emerging materials [1] [2]. The diverse range of chemical and physical properties exhibited by TMDs presents them as promising candidates for numerous applications. Their attractive properties arise from their layered structure containing weak van der Waals bonds [3]. TMDs are typically denoted by the chemical formula MX_2 , where M represents a transition metal belonging to groups 4-10 (e.g. Mo, W, Nb), while X denotes a chalcogen, usually S, Se, or Te [4] [5]. The covalent bonds between the X-M-X layers hold them together. [6]. The transition metal is the central atom that is encircled in a layer of two chalcogen atoms and can result in two phases: the octahedral phase (1T) and the prismatic phase (2H) depending on their stacking arrangement [7]. When the stacking sequence follows an AbA BaB pattern, it leads to the formation of the 2H phase, while an AbA CaC BcB stacking sequence results in the rhombohedral phase, commonly referred to as the 3R phase (see figure 2.3) [8].

The compositions and crystal structures influence the chemical and physical properties required for their application. The physicochemical properties of the material are influenced by various factors, including the ability to regulate its composition, thickness, crystalline phase, surface chemistry, as well as the presence of vacancies and other defects [1]. They have chemical and optical properties that vary from insulating to metallic behaviour and sizable band gaps [3]. The unique properties of these materials make them well-suited for a wide range of applications, including use as semiconductors, in electrochemistry, and as electrocatalysts [5].

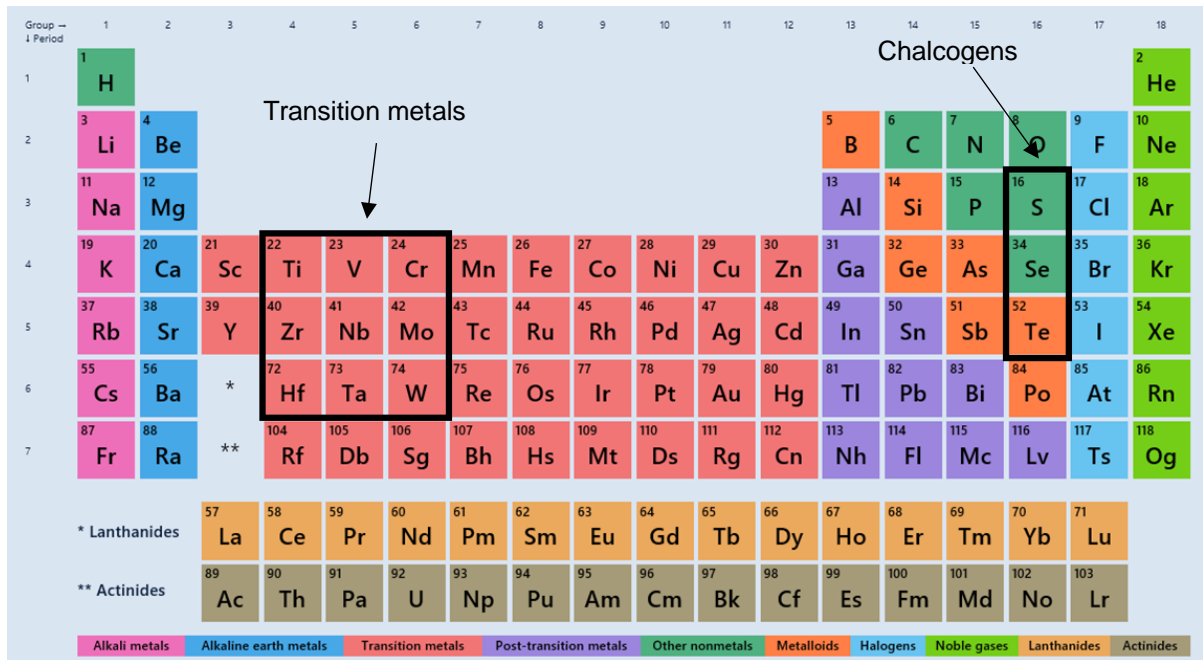


Figure 2.1: Periodic table showing the transition metals and chalcogen atoms found in transition metal dichalcogenides [9].

2.2. Electronic and structural properties of TMDs

The layered structures of TMDs make them attractive to use for electronic applications as they exhibit diverse characteristics [6] [10]. The electronic structure of these materials is a result of the distinctive distribution of electronic states across their 2D plane [11]. The electronic structure of TMDs can be studied through computational methods like density functional theory (DFT) which is first principles calculations as well as various spectroscopy techniques [12]. The electronic structure of the active center is heavily influenced by the coordination configuration, which in turn affects the material's properties for various applications [13]. TMDs can crystallize in either octahedral or trigonal prismatic coordination phases, which are commonly known as the 1T and 2H phases, respectively [4].

Since TMDs form layered structures, each layer can exhibit any of the two coordination phases which can result in a variety of different properties [4]. The coordination around the central metal affects the d-electron count which is the electronic structure. As a result, diverse properties are observed depending on the ligand field splitting of the

non-bonding group 4 to group 10 d-orbitals and the filling of these orbitals [11]. Group 6 compounds with two non-bonding d-electrons tend to exhibit trigonal prismatic coordination (2H) with filled dz^2 orbitals giving rise to semiconducting band gap [14]. As the thickness of TMD materials decreases from bulk layers to monolayers, the band structure of these compounds can transition from an indirect to a direct band gap [3]. The band gap of bulk TMDs decreases with increasing valence band splitting. Usually, the band structures of TMDs exhibit valence band maxima situated at the center (Γ) and corners (K') of the Brillouin zone, while the conduction band minima are located at the K and Λ points [11] [15]. As a result, the direct band gap means the materials exhibit higher quantum efficiency and more light emission in the visible frequency region making group 6 TMDs suitable candidates for optical and electronic applications [15].

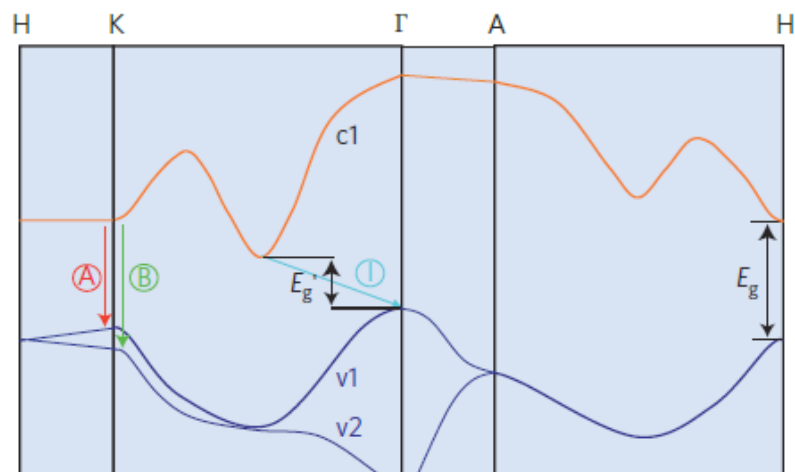


Figure 2.2: Simplified electronic structure of group 6 TMDs showing the coexistence of the split direct band gap and the indirect band gap [16].

2.3. Tungsten diselenide

Tungsten diselenide (WSe_2) is a 2D material belonging to the group of TMD compounds, with tungsten (W) located at the center of the transition metal sandwiched between two selenium (Se) chalcogen atoms. WSe_2 exhibits versatile properties that are enabled by the polymorphism of its layers. WSe_2 can display various metal coordination configurations, including trigonal prismatic (2H phase), octahedral (1T phase), and distorted octahedral (1T' phase) [17]. The 2H phase is the

thermodynamically stable phase that is favourable for semiconducting properties and related applications such as electrocatalytic hydrogen evolution and energy storage [17] [18]. The 1T and 1T' phases are metastable, and they exhibit metallic properties with promising use in catalysis applications [18]. In general, the 1T phase of TMDs tends to easily relax into the 1T' phase, resulting in the formation of the distorted octahedral phase [19]. Sokolikova *et al.* found that the 1T' polymorph has faster charge-transfer kinetics in the metallic phase of WSe₂ in comparison to the semiconducting 2H phase which is difficult to achieve [17]. The properties of WSe₂ differ depending on the thickness. Generally, WSe₂ is known to have semiconducting properties as it has a band gap range of 1-2 eV, indicating high optical absorptions [20]. This is desirable for optoelectronic applications such as photoelectrochemical reactions. Doping can be utilized to control the p-type or n-type semiconducting behavior of bulk WSe₂, which is initially an indirect semiconductor [21] [22].

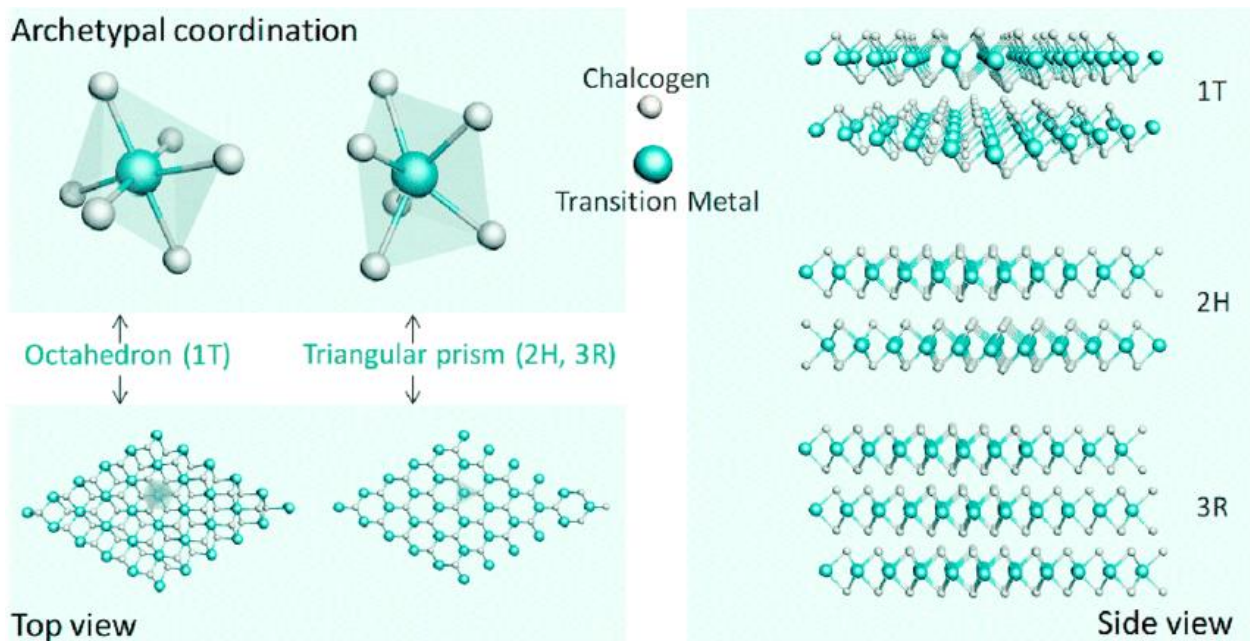


Figure 2.3: Crystal structure and stacking sequence of 1T, 2H and 3R WSe₂ phases [23].

2.4 Synthesis of TMDs

TMD synthesis methods are commonly categorized as top-down or bottom-up. The top-down approach involves methods such as exfoliation, intercalation, and

sonication, while the bottom-up approach uses deposition techniques with molecular compounds as initial reagents [24].

2.4.1. Top-down approach

This method is an exfoliation technique that entails the transformation of bulk materials into layered materials.

i) Mechanical exfoliation

The top-down method of mechanical exfoliation involves using physical forces, such as shearing, peeling, and compression delamination, to produce monolayers from bulk materials. This is a widely used approach for producing 2D materials [25]. Van der Waals forces are the key to this technique, as they are relatively weak and easily broken, allowing individual layers to be separated from the bulk material. The Scotch Tape method is a frequently used mechanical exfoliation technique that involves using a piece of cello tape to peel off thin films from bulk materials, thereby obtaining high-purity monolayer or few-layer structures [26]. Li *et al* employed the mechanical exfoliation technique to produce MoS₂ and WSe₂ nanosheets [27]. This method involved using freshly cleaved thin crystals on Scotch Tape, which resulted in the separation of one layer and multilayer TMD nanosheets, leaving them on the substrate [27]. They were successful in obtaining MoS₂ and WSe₂ nanosheets using this technique however they experienced challenges as the method requires large sized TMD bulk crystals. Mechanical exfoliation produces high quality nanosheets, but it is hard to regulate the thickness and has a low rate of production [26]. Therefore, mechanical exfoliation is considered a time-consuming method and cannot be scaled up for industrial applications [28].

ii) Liquid phase exfoliation

Liquid exfoliation, also known as sonication-assisted exfoliation is a technique that uses ultrasonication with a suitable solvent [26]. Ultrasonication waves generate cavitation bubbles that fall apart, separating layered crystallites and resulting in ultras-small nanoflakes in the solvent [29]. The underlying principle of this method is that

sonication breaks the weak van der Waals forces between the layers, leaving behind strong covalent bonds. The use of a solvent aids in the preservation of the exfoliated nanosheets by preventing their aggregation and reassembly. The choice of solvent is critical as it can enhance the efficiency of the exfoliation process. Organic solvents are commonly employed in this technique due to their high adsorption energy, which favours exfoliation [26]. Liquid exfoliation is a scalable method, but large-scale production tends to result in obscure nanosheets being deposited onto the substrate [28].

iii) Chemical exfoliation

Chemical exfoliation is a method that involves the use of chemical intercalators to weaken the van der Waals forces between the layers of bulk crystals. This is typically achieved by ultrasonication in solvents such as water or ethanol, which helps the intercalators penetrate the interlayer regions and expand the space between the layers. This results in the exfoliation of the bulk material into thin layers or nanosheets [26]. Lithium ions usually obtained from n-butyllithium (n-BuLi) is commonly used as an intercalating agent. Kim *et al* utilized n-BuLi to induce a phase transition from the bulk 2H-phase to few-layered 1T-phase TMD nanosheets. In this method, electron transfer from n-BuLi to TMD weakens the coordination of the metal atom, resulting in a more flexible and easily deformable structure that can be exfoliated into nanosheets [30]. This results in the rearrangement of the lattice causing phase transition to occur. This method can be used in bulk scale production however there are disadvantages associated with it as it can become highly toxic due to the highly explosive lithium compounds [31].

2.4.2. Bottom-up approach

Bottom-up approach is an approach that involves growing TMD nanocrystals from suitable transition metal and chalcogen precursors under specific conditions. It has several advantages such as high-purity and high-quality production, fast reaction times, simple operation technique that produces homogenous nanocrystals [32]. Therefore, it is crucial to have a clear understanding of both the energetics and kinetics involved in the process since they have a significant impact on the resulting products.

As with top-down approach, there are several bottom-up techniques such as gas phase synthesis, hydro and solvothermal synthesis, microwave, and colloidal synthesis.

i) Gas phase synthesis

Gas phase synthesis is also commonly referred to as chemical vapour deposition (CVD) and it is the most used bottom-up technique. For this method, metal and chalcogen precursors are brought into contact with the substrate under conditions of elevated pressure and temperature then reacted in gas phase [26]. Very high temperatures and low pressures is necessary to volatilize the metal and chalcogen precursors for deposition to occur on the substrate to form the crystalline product [3]. The interaction that takes place on the substrate influences the resultant TMDs. The molecules used act as promoting agents during the formation of TMDs. Mohl *et al* found that to produce WSe_2 by selenization of WO_3 , hydrogen gas can serve as an activating agent to promote the formation of the desired product [3]. It has been found that using halide or metal-organic precursor improves the scalability of CVD method [28].

ii) Hydro/solvothermal synthesis

This technique involves reacting precursors in an aqueous or non-aqueous solution in an autoclave at high temperatures and pressures for several hours. TMDs can be obtained using this technique under specific conditions of solvent and reaction time [26]. Hydro- and solvothermal methods are alike whereby similar precursors can be used for both methods. The main difference between the two methods is that the hydrothermal method employs water as the solvent, whereas the solvothermal method uses organic solvents with high boiling points. Although the hydro/solvothermal method requires the use of fairly high temperatures, the temperature is still lower than that of the CVD method. However, the disadvantage of this technique is the long reaction time that ranges from 10-48 hours along with high pressure requirements. This was observed Yi *et al* prepared 1T- WS_2 through the solvothermal method for 24 h at 200 °C [33].

iii) Microwave-assisted synthesis

Microwave-assisted method is a technique that is both rapid and energy-efficient and can be used to synthesize TMDs. The benefit of using this method versus other conventional heating methods is that it can heat the reagents rapidly and uniformly [31]. This method is commonly used for the synthesis of metal and metal oxide nanoparticles as opposed to layered TMDs. Harpeness *et al* implemented microwave-assisted method to produce MoSe₂ however they found that it was difficult to obtain single layer MoSe₂ as the nanocrystals were difficult to separate as they were highly agglomerated [34]. The same method was also used by Panigrahi and Pathak to synthesize WS₂ nanowires, they also experienced difficulties associated with agglomeration as they obtained amorphous nanoparticles [35].

iv) Colloidal synthesis

Colloidal synthesis is a solution-based technique that uses high boiling point organic solvents to react metal and chalcogen precursors, which can also act as a capping agent. The method thermally or chemically converts the solubilized reagents into nanostructures that are stabilized by the capping agent [1]. Generally, colloidal synthesis reactions are carried out at elevated temperatures (± 300 °C) with shorter reaction times (1 – 2 h) in comparison to the hydro/solvothermal method. Another advantage of this technique is that it is a scalable and controllable method [24]. This can be accomplished by regulating the experimental parameters such as the precursors, capping ligands, and temperatures [36]. Controlling the reaction parameters can modify the TMDs obtained as well as their properties. The capping ligand used can affect the binding affinities of the TMDs which can influence the morphology and thickness of the nanostructures obtained [37]. This stabilizes the particles and prevents agglomeration. Generally, colloidal TMDs layers have a strong tendency to aggregate by forming nanostructures and nanoflower-like morphologies whereby capping ligands can adjust the inter nanosheet interactions resulting in different levels of aggregation [1].

2.5. Colloidal growth mechanism

There are two types of growth mechanisms that can be used to describe how nanocrystals grow in colloidal synthesis: The classical nucleation theory (CNT) and LaMer's theory. The classical nucleation theory is a theoretical framework that describes the nucleation process and the Gibbs free energy barrier that must be overcome for nucleation to occur [38]. During colloidal synthesis, nucleation occurs when the nucleus increases and reaches a critical radius (r_c) that allows it to grow into stable nuclei. When this occurs, Gibbs free energy also increases until it reaches its maximum, once the nuclei have reached the critical radius that prevents dissolution of the nuclei. This is the minimum size a particle can remain in solution without being redissolved [39]. Thereafter, the free energy begins to decrease as the stable nuclei grows **Figure 2.4**. This process is considered a thermodynamic process as CNT is prone to reduce its Gibbs free energy [40].

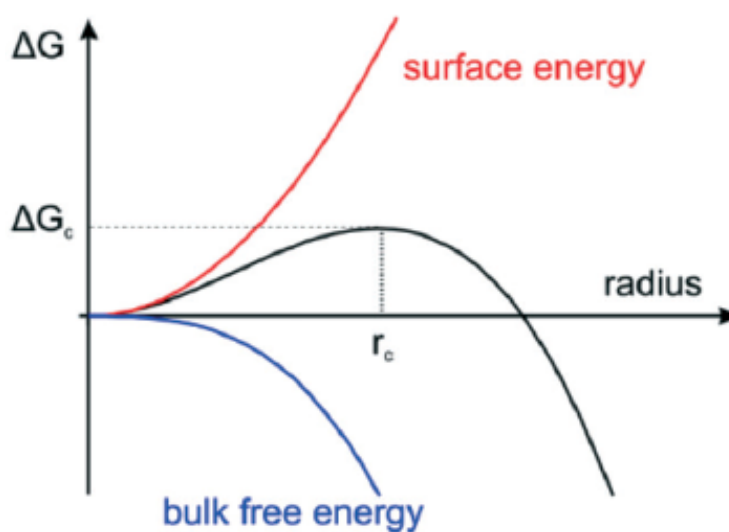


Figure 2.4: Diagram of the classical nucleation theory showing the relationship of the free energy (ΔG) and the radius (r) of the nuclei [41].

LaMer's theory is based on the partition of nucleation and growth of colloidal particles in solution [42]. According to LaMer's theory, the formation of monomers occurs in two distinct stages nucleation and growth [39]. The following is the general mechanism of the colloidal synthesis process: (i) The concentration of monomers in the solution

gradually increases until it reaches a state of super-saturation or critical nucleation [C_{max}]. (ii) Saturation continues to increase, reaching "burst-nucleation," which is the point where the monomer concentration reaches the critical supersaturation threshold [C_m]. This process reduces the concentration of free monomers in the solution due to the formation of nuclei. (iii) Subsequently, the nucleation growth occurs through the diffusion of monomers in the solution, leading to the growth of larger and more stable nuclei. [37], [40]. Based on these theories, there are certain parameters that can control the growth mechanism of nanoparticles. These parameters include reaction time, initial concentration of precursors as well as capping agents [36], [43].

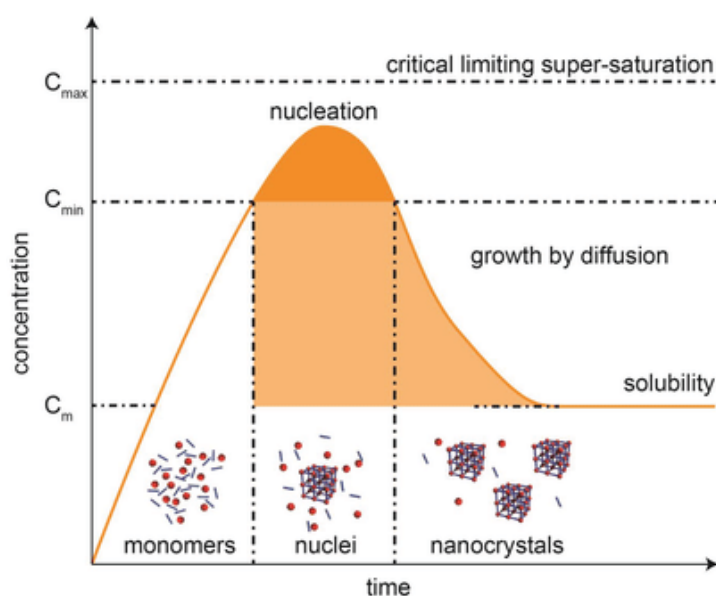


Figure 2.5: Diagram summarising LaMer's theory based on the separation of nucleation and growth [44].

Nucleation and kinetics influence the anisotropic growth of nanosheets. In colloidal synthesis, anisotropic growth is influenced by the capping ligand used as it can effectively control the surface energies of the exposed facets of the nanoparticles which determines the growth direction of nanosheets [1] [36]. Therefore, TMDs with varying morphologies can be obtained via colloidal synthesis. There are two types of nanomaterials: nano-objects and nanostructures. Nano-objects can be described as materials that have one dimension at nanoscale whereas nanostructures are materials that comprises of nanoscale structures to form larger nanoscale material.

2.6. Photoelectrochemical water splitting

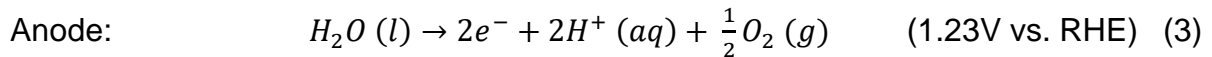
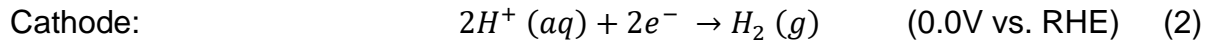
The utilization of renewable energy resources to meet our energy needs has become increasingly popular in recent years. This is mostly driven by several factors such as climate change, energy security, and the negative impact of burning fossil fuels towards the environment [45]. Fossil fuels are considered non-renewable resources as they are used for energy production, yet they are not renewable. However, they are not considered ideal candidates for energy production as they are considered pollutants and have a detrimental effect on mankind and the environment [46]. Thus, a greater emphasis on finding alternative energy sources that are considered clean, safe, and sustainable has increased. Hydrogen (H_2) has gained attention as a potential energy vector that can be used as fuel as it produces a high energy yield, it is clean and can easily be stored [47]. Hydrogen fuel is based on the use of molecular hydrogen obtained from hydrogen containing compounds to produce fuel that can be converted into energy for daily use [48]. H_2 is an efficient energy carrier with the highest energy density among all chemical fuels (142 MJ/kg), it is clean and renewable therefore it is a suitable candidate for alternative energy sources [49]. There are various ways of generating H_2 such as natural gas reforming which uses fossil fuels therefore not ideal [50]. Whereas photoelectrochemical (PEC) reaction is considered a clean method that can be used for H_2 production. Electrochemical water splitting can result in molecular hydrogen and oxygen through the decomposition of water caused by an electric current. The process can be divided into two half reactions, namely the hydrogen evolution reaction (HER) and the oxygen evolution reaction (OER). PEC water splitting presents a viable method to produce H_2 with lower environmental impacts, making it a promising solution for industrial-scale applications [51].

PEC water splitting process takes place in a PEC cell that contains two electrodes submerged in aqueous electrolyte solution as seen in **Figure 2.6**. A PEC cell comprises of an anode electrode containing the photocatalyst, a cathode electrode supporting an electrocatalyst, and an electrolyte solution that facilitates internal ionic conductivity [52]. The electrolyte solution can be either acidic or alkaline, and the chemical reactions can be represented using the following equations:

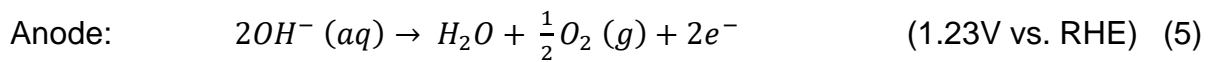
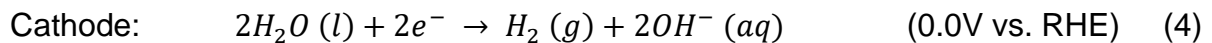
Total Reaction:



Acidic media: HER



Alkaline/neutral media: OER



The cathodic and anodic half reactions show a thermodynamic total voltage of 1.23 V (25 °C, 1 atm) is required for water splitting to occur.

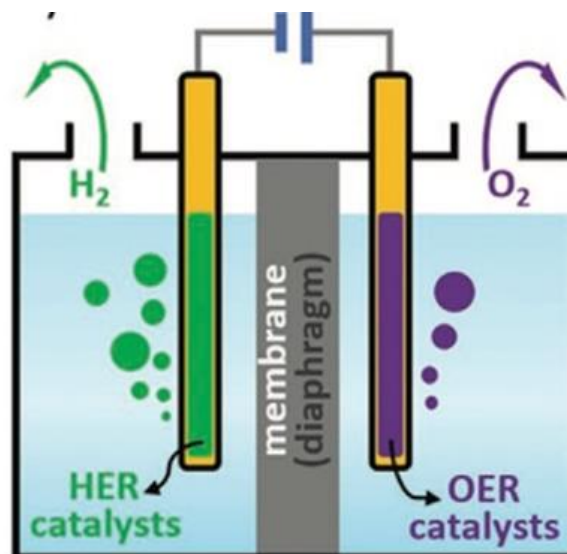


Figure 2.6: Diagram showing basic electrochemical cell [53].

Fujishima and Honda were the pioneers of the PEC water splitting reaction which employs a low-cost semiconducting material with high efficiency [51]. The fundamental principle of PEC water splitting is to convert solar energy into environmentally friendly and storable H₂ fuel [54]. This is accomplished by submerging a photoelectrode in an electrolyte solution, which induces electron transfer between the semiconductor and the electrolyte solution, resulting in the Fermi level equilibrating with the redox potential

of the electrolyte solution [51]. The water splitting process occurs in three stages: (i) generation of electron-hole pairs in photoelectrodes following the absorption of photons, (ii) transport and separation of charges to the catalyst surface, and (iii) redox reactions of absorbed species to produce oxygen and hydrogen from water [54].

An effective PEC water splitting process requires the use of semiconductors, both p-type and n-type, to convert water into hydrogen and oxygen [54]. The PEC water splitting process relies on the use of semiconductors, both p-type and n-type, to effectively convert water into hydrogen and oxygen. When the rate of electron transfer is faster than that of holes, the cathodic photocurrent takes place in p-type semiconductors. Conversely, the anodic photocurrent (n-type semiconductor) occurs when there is hole transport to the electrolyte, resulting in anodic PEC water splitting. This means that a p-type cathode, electrically connected to an oxygen-evolving method cathode, can be used to achieve the hydrogen evolution reaction (HER). On the other hand, an n-type anode is used to achieve the oxygen evolution reaction (OER) [55]. Semiconductors possess a unique ability to act as photocatalysts, enabling them to activate the chemical reduction and oxidation process in the presence of light. Photoelectrodes can capture light energy for these reactions, and additional voltage is required to carry out the reaction [56]. Light-absorbing materials, such as semiconductors, can capture photons and convert them into excited electron-hole pairs, as depicted in **Figure 2.7** [57].

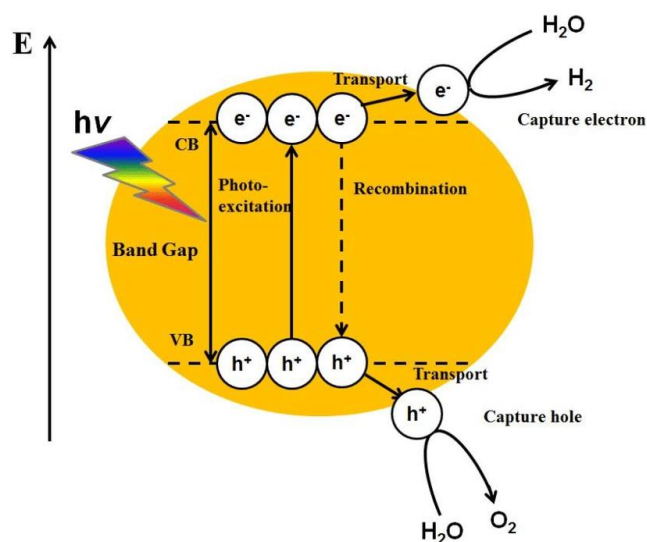


Figure 2.7: Diagram showing the mechanism of the electron-hole pair [58].

2.7. Hydrogen evolution reaction (HER)

Electrochemical HER is a prospective, less-adverse way of generating hydrogen and as with other electrochemical reactions, it needs a catalyst that will enhance the reaction kinetics and reduce the overpotential [59]. An electrocatalyst with excellent reaction interfaces is required to promote electrocatalytic kinetics and reduce the overpotential [60]. There are several parameters that are deemed important when evaluating the electrocatalytic activity of water-splitting electrocatalysts. These parameters include overpotential, Tafel slope, Faradaic efficiency etc. Overpotential (η) is described as the extra potential that exceeds the theoretical potential of an electrochemical reaction and it is considered the main factor that overcomes difficulties during the catalytic conversion process [13]. It can be described as the distinction between the equilibrium potential and the applied potential and a lower overpotential is favourable towards better catalytic activity [49]. Lower reaction overpotential can effectively lower the activation energy of the reaction [49].

The exchange current density is a parameter commonly used to evaluate the catalytic activity of HER catalysts, as it is directly related to the onset overpotential. This is due to the fact that the kinetics of most HER catalysts exhibit similar behaviour [13]. As the kinetics of HER surpasses the overpotential of the catalysts, as a result current density can be used as a parameter to determine the electrocatalytic activity of a catalyst [13]. Current density is measured during cyclic voltammetry (CV), it should not change as the number of scanning cycles increases [49]. By plotting the logarithmic current density ($\log J$) as a function of the voltage (V) of the electrocatalytic electrode, it is possible to determine the current density [61].

The Tafel slope is described as the increase in overpotential required to affect a significant rise in current density [62]. The Tafel slope can also be used to identify the rate-limiting step and potential reaction pathways. At low overpotentials and current densities, the Tafel slopes for the Volmer, Heyrovsky, and Tafel steps are typically around 120, 40, and 30 mV/dec, respectively [49]. The Tafel slope depends on overpotential and current density as it is used to influence the extent at which current

would simultaneously increase with an increase in potential at the cathode [62] [63]. Therefore, a small Tafel slope is required for faster kinetics.

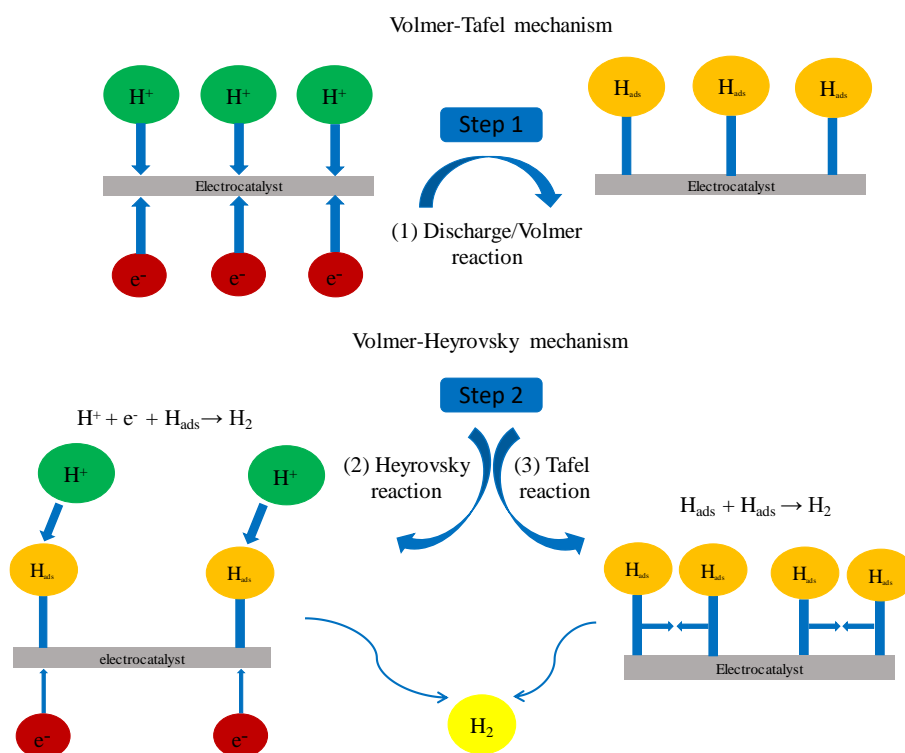


Figure 2.3: HER mechanism that takes place on the surface of the electrocatalyst [64].

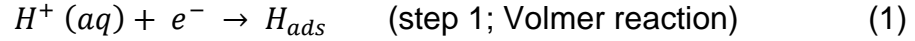
To calculate the Tafel slope, one can use Tafel plots that are obtained by replotting the linear sweep voltammetry (LSV) as a plot of $\log(J)$ versus overpotential [13]. The Tafel slope is the linear portion of the plot:

$$\eta = b \log(j/j_0)$$

where b is the Tafel slope, j is the current density and j_0 is the exchange current density. A smaller Tafel slope indicates that the overpotential required to achieve a certain current density is lower, which suggests that the charge transfer kinetics of the electrocatalyst are faster [65].

HER mechanism starts with the adsorption of H on the electrocatalyst surface, this is known as the Volmer reaction. A voltage is applied which causes an electron to

migrate to the cathode surface and captures a proton (H^+) in the solution, generating an adsorbed atom (i.e., intermediate state) on the active site of the catalytic cathode surface.



$$b_{1,v} = \frac{2.3 RT}{\alpha F} \quad (2)$$

Where $b_{1,v}$ is the Tafel slope, α is the symmetry coefficient which is 0.5, F is the Faraday constant, R is the ideal constant, and T is the absolute temperature. The next step can take place via two different pathways to produce H_2 . The first pathway is called the Heyrovsky reaction:



$$b_{1,T} = \frac{2.3 RT}{(1 + \alpha)F} \quad (4)$$

When the H_{ads} is low, an electrochemical desorption reaction can occur, leading to the new creation of H_2 through the interaction of H_{ads} with a new electron and another H^+ in the solution (3). The Tafel reaction or chemical desorption step is observed when the H_{ads} coverage is high, and the recombination between adjacent H_{ads} species becomes the predominant process.



$$b_{1,T} = \frac{2.3 RF}{2F}$$

The process shown above is a thermodynamic process that can be described as continuous adsorption and desorption of H_{ads} species from the catalytically active sites. For a catalyst to be considered efficient, it should find a balance between binding strongly to H_{ads} species to allow the formation of the $H_{ads} - H_{ads}$ bond but it should permit fast desorption of the generated H_2 on the surface of the catalyst [66] [67]. The type of electrocatalyst used effects hydrogen production resulting from electrocatalyst reduction of protons (H^+) into molecular (H_2).

2.8. Transition metal doping

WSe₂ belongs to a class of materials known as transition metal dichalcogenides (TMDs). These materials possess unique electronic and optical properties that make them attractive for a variety of applications. These properties are attributed to the 2D layered structures of WSe₂ forms, results in higher surface area and desirable characteristics [68]. WSe₂ also has semiconductor characteristics which makes it a potential candidate for photoelectrocatalytic applications. However, its electrocatalytic activity is not as good as noble metal. Therefore, transition metal doping of WSe₂ can be done to influence the electrocatalytic activity of the TMD by decorating WSe₂ with a noble metal. Platinum (Pt) is known to be the most efficient electrocatalyst however it is expensive. Pt-group metals are considered excellent electrocatalyst for HER due to their capability of producing high current densities at low overpotential [69] [70]. For that reason, Pt can be decorated onto the surface of WSe₂ to boost the electrocatalytic activity of the material. This would ultimately decrease the band gap and improve the semiconducting characteristics of the Pt/WSe₂ nanohybrid [68]. There are two types of methods that can be used for transition metal doping: in-situ and ex-situ. In-situ doping is when the dopant is added directly during the deposition process. Whereas in ex-situ doping, the dopant is added after producing the support material. Lin *et al* used a one-step hydrothermal reaction process to reduce (NH₄)₂MoS₄ and H₂PtCl₆ simultaneously to form MoS₂-PtNP nanohybrids where PtNPs was decorated onto the surface of MoS₂ nanoflowers [71]. They found that their method was simple, efficient, and economical when compared to previous reports. Generally, small amounts of PtNPs can effectively improve the electrocatalytic efficiency of WSe₂ [72]. Therefore, Pt/WSe₂ nanohybrids can be used as electrodes in photoelectrochemical reactions.

2. 9 References

- [1] Y. Sun, M. Terrones and R. E. Schaak, "Colloidal Nanostructures of Transition-Metal Dichalcogenides," *Accounts of Chemical Research*, vol. 54, pp. 1517-1527, 2021.
- [2] A. Giri, H. Yang, W. Jang, J. Kwak, K. Thiyagarajan, M. Pal, D. Lee, R. Singh, C. Kim, K. Cho, A. Soon and U. Jeong, "Synthesis of Atomically Thin Transition Metal Ditelluride Films by Rapid Chemical Transformation in Solution Phase," *Chemistry of Materials*, vol. 30, pp. 2463-2473, 2018.
- [3] M. Mohl, A.-R. Rautio, G. Asres, M. Wasala, P. Patil, T. Saikat and K. Kordas, "2D Tungsten Chalcogenides: Synthesis, Properties and Applications," *Advanced Materials Interface*, vol. 7, p. 2000002, 2020.
- [4] X. Chia, A. Y. Eng, A. Ambrosi, S. M. Tan and M. Pumera, "Electrochemistry of Nanostructure Layered Transition-Metal Dichalcogenides," *Chemical Reviews*, vol. 115, pp. 11941-11966, 2015.
- [5] X. Chia, Z. Sofer, J. Luxa and M. Pumera, "Layered Noble Metal Dichalcogenides: Tailoring Electrochemical and Catalytic Properties," *Applied Materials & Interfaces*, vol. 9, pp. 25587-25599, 2017.
- [6] M. Mattinen, M. Leskela and M. Ritala, "Atomic Layer Deposition of 2D Metal Dichalcogenides for Electronics, Catalysis, EnergyStorage, and Beyond," *Advanced Materials Interfaces*, p. 2001677, 2021.
- [7] S. Quereshi, E. Ahmad, K. K. Pant and S. Dutta, "Insights into Microwave-Assisted Synthesis of 5-Ethoxymethylfurfural and Ethyl Levulinate Using Tungsten Disulfide as a Catalyst," *ACS Sustainable Chemistry & Engineering*, vol. 8, pp. 1721-1729, 2020.
- [8] Z. Lin, B. Carvalho, E. Kahn, R. Lv, R. Rao, H. Terrones, M. Pimenta and M. Terrones, "Defect engineering of two-dimensional transition metal dichalcogenides," *2D Materials*, vol. 3, p. 022002, 2016.
- [9] S. Manzeli, D. Ovchinnikov, D. Pasquier, O. Yazyev and A. Kis, "2D transition metal dichalcogenides," *Nature Reviews Materials*, vol. 2, p. 17033, 2017.
- [10] H. Terrones and M. Terrones, "Electronic and vibrational properties of defective transition metal dichalcogenide Haeckelites: new 2D semi-metallic systems," *2D Materials*, p. 011003, 2014.
- [11] W. Zhao, R. Ribeiro and G. Eda, "Electronic Structure and Optical Signatures of Semiconducting Transition Metal Dichalcogenide Nanosheets," *Accounts of Chemical Research*, vol. 48, pp. 91-99, 2015.

- [12] F. Yang, J. Shang, L. Kou, C. Li and Z. Deng, "Computational Investigation of Orderly Doped Transition Metal Dichalcogenides: Implications of Nanoscale Optoelectronic Devices," *ACS Applied Nano Materials*, vol. 5, pp. 3824-3831, 2022.
- [13] L.-M. Cao, D. Lu, D.-C. Zhong and T.-B. Lu, "Prussian blue analogues and their derived nanomaterials for electrocatalytic water splitting," *Coordination Chemistry Reviews*, vol. 407, p. 213156, 2020.
- [14] M. Jana, A. Singh, D. Late, C. Rajamathi, K. Biswas, C. Felser, U. Waghmare and C. Rao, "A combined experimental and theoretical study of the structural, electronic and vibrational properties of bulk and few-layer Td-WTe₂," *Journal of Physics: Condensed Matter*, vol. 27, p. 285401, 2015.
- [15] G.-B. Liu, D. Xiao, Y. Yao, X. Xu and W. Yao, "Electronic structures and theoretical modelling of two-dimensional group-VIB transition metal dichalcogenides," *Chem Soc Rev*, vol. 44, p. 2643, 2015.
- [16] B. Han and Y. H. Hu, "MoS₂ as a co-catalyst for photocatalytic hydrogen production from water," *Energy Science and Engineering*, vol. 4, no. 5, pp. 285-304, 2016.
- [17] M. S. Sokolikova, P. C. Sherrell, P. Palczynski, V. L. Bemmer and C. Mattevi, "Direct solution-phase synthesis of 1T' WSe₂ nanosheets," *Nature Communications*, vol. 10, p. 712, 2019.
- [18] J. H. Geisenhoff, A. K. Tamura and A. M. Schimpf, "Using ligands to control reactivity, size and phase in the colloidal synthesis of WSe₂ nanocrystals," *Chem Communication*, vol. 55, p. 8856, 2019.
- [19] P. Zhou, P. Schiettecatte, M. Vandichel, A. Rousaki, P. Vandenabeele, Z. Hens and S. Singh, "Synthesis of Colloidal WSe₂ Nanocrystals: Polymorphism Control by Precursor-Ligand Chemistry," *Crystal Growth & Design*, vol. 21, pp. 1451-1460, 2021.
- [20] S. M. Delphine, M. Jayachandran and C. Sanjeeviraja, "Pulsed electrodeposition and characterisation of tungsten diselenide thin films," *Materials Chemistry and Physics*, vol. 81, pp. 78-93, 2003.
- [21] P. Antunez, D. Webber and R. Brutchey, "Solution-Phase Synthesis of Highly Conductive Tungsten Diselenide Nanosheets," *Chemistry of Materials*, vol. 25, pp. 2385-2387, 2013.
- [22] A. Tedstone, D. Lewis and P. O'Brien, "Synthesis, Properties, and Applications of Transition Metal-Doped Layered Transition Metal Dichalcogenides," *Chemistry of Materials*, vol. 28, pp. 1965-1974, 2016.

- [23] C. Meng, X. Chen, Y. Gao, Q. Zhao, D. Kong, M. Lin, X. Chen, Y. Li and Y. Zhou, "Recent Modification Strategies of MoS₂ for Enhanced Electrocatalytic Hydrogen Evolution," *Molecules*, vol. 25, p. 1136, 2020.
- [24] V. Brune, M. Grosch, R. Weißing, F. Hartl, M. Frank, S. Mishra and S. Mathur, "Influence of the choice of precursors on the synthesis of two-dimensional transition metal dichalcogenides," *Dalton Transactions*, vol. 50, no. 1, p. 12365, 2021.
- [25] Sonam Rani, "Two-dimensional transition metal dichalcogenides and their heterostructures: Role of process parameters in top-down and bottom-up synthesis approaches," *Materials Science in Semiconductor Processing*, vol. 139, no. 1, p. 106313, 2022.
- [26] D. Monga, S. Sharma, N. P. Shetti, S. Basu, K. R. Reddy and T. M. Aminabhavi, "Advances in transition metal dichalcogenide-based two-dimensional nanomaterials," *Materials Today Chemistry*, vol. 19, no. 1, p. 100399, 2021.
- [27] H. Li, J. Wu, Z. Yin and H. Zhang, "Preparation and Applications of Mechanically Exfoliated Single-Layer and Multilayer MoS, and WSe, Nanosheets," *Accounts of Chemical Research*, vol. 47, no. 1, pp. 1067-1075, 2014.
- [28] M. Mattinen, M. Leskelä and M. Ritala, "Atomic Layer Deposition of 2D Metal Dichalcogenides for Electronics, Catalysis, Energy Storage, and Beyond," *Advanced Materials Interfaces*, pp. 1-47, 2021.
- [29] B. L. Li, M. I. Setyawati, H. L. Zou, J. X. Dong, H. Q. Luo, N. B. Li and D. T. Leong, "Emerging 2D Transition-Metal Dichalcogenides for Sensors, Biomedicine, and Clean Energy," *Advanced Science News*, vol. 13, no. 1700527, p. 1, 2017.
- [30] T. I. Kim, J. Kim, I.-J. Park, K.-O. Cho and S.-Y. Choi, "Chemically exfoliated 1T-phase transition metal dichalcogenide nanosheets for transparent antibacterial applications," *2D Materials*, pp. 1-14, 2018.
- [31] D. J. Late, C. S. Rout, D. Chakravarty and S. Ratha, "Emerging Energy Applications of Two-Dimensional Layered Materials," *Canadian Chemical Transactions*, vol. 3, no. 2, pp. 118-157, 2015.
- [32] H. Li, X. Jia, O. Zhang and X. Wang, "Metallic Transition-Metal Dichalcogenide Nanocatalysts for Energy Conversion," *Chem*, vol. 4, no. 1, pp. 1510-1537, 2018.
- [33] J. Yi, X. She, Y. Song, M. Mao, K. Xia, Y. Xu, Z. Mo, J. Wu, H. Xu and H. Li, "Solvothermal synthesis of metallic 1T-WSe₂: A supporting co-catalyst on carbon

nitride nanosheets toward photocatalytic hydrogen evolution," *Chemical Engineering Journal*, vol. 335, no. 1, pp. 282-289, 2018.

- [34] R. Harpeness, A. Gedanken, A. M. Weiss and M. A. Slifkin, "Microwave-assisted synthesis of nanosized MoSe₂," *Journal of Materials Chemistry*, vol. 13, no. 1, pp. 2603-2606, 2003.
- [35] P. K. Panigrahi and A. Pathak, "Microwave-assisted synthesis of WS₂ nanowires through tetrathiotungstate precursors," *Science and Technology of Advanced Materials*, vol. 9, no. 1, p. 6, 2008.
- [36] Y. Cho, T. A. Le, H. Kim, Y. Hong, H. Hwang, H. Park, S. Seo and H. Lee, "Unveiling surface charge on chalcogen atoms toward the high aspect-ratio colloidal growth of two-dimensional transition metal dichalcogenides," *Nanoscale*, vol. 13, p. 1291, 2021.
- [37] W. Jung, S. Lee, D. Yoo, S. Jeong, P. Miro, A. Kuc, T. Heine and J. Cheon, "Colloidal Synthesis of Single-Layer MSe₂ (M =Mo, W) Nanosheets via Anisotropic Solution-Phase Growth Approach," *Journal of the American Society*, vol. 137, pp. 7266-7269, 2015.
- [38] J. W. Schmelzer, "On the determination of the kinetic pre-factor in classical nucleation theory," *Journal of Non-Crystalline Solids*, vol. 356, no. 1, pp. 2901-2907, 2010.
- [39] N. T. K. Thanh, N. Maclean and S. Mahiddine, "Chemical Reviews," *Mechanisms of Nucleation and Growth of Nanoparticles in Solution*, vol. 114, no. 1, pp. 7610-7630, 2014.
- [40] B. Mokross, "Entropic nucleation theory," *Journal of Non-Crystalline Solids*, vol. 284, no. 1, pp. 91-98, 2001.
- [41] M. Nasilowski, B. Mahler, E. Lhuillier, S. Ithurria and B. Dubertret, "Two-Dimensional Colloidal Nanocrystals," *Chemical Reviews*, vol. 116, pp. 10934-10982, 2016.
- [42] C. d. M. Donegá, P. Liljeroth and D. Vanmaekelbergh*, "Physicochemical Evaluation of the Hot-Injection Method, a Synthesis Route for Monodisperse Nanocrystals," *Small*, vol. 12, no. 1, pp. 1152-1162, 2005.
- [43] A. Azam, J. Yang, W. Li, J.-K. Huark and S. Li, "Tungsten diselenides (WSe₂) quantum dots: Fundamental, properties, synthesis and applications," *Progress in Materials Science*, vol. 132, no. 1, pp. 1-32, 2023.
- [44] Y. Luo, M. Ahmad, A. Schug and M. Tsotsalas, "Rising Up: Hierarchical Metal-Organic Frameworks in Experiments and Simulations," *Advanced Materials*, vol. 31, p. 1901744, 2019.

- [45] N. Fajrina and M. Tahir, "A critical review in strategies to improve photocatalytic water splitting towards hydrogen production," *International Journal of Hydrogen Energy*, vol. 44, pp. 540-577, 2019.
- [46] Z. Wu, Y. Zhao, W. Jin, B. Jia, J. Wang and T. Ma, "Recent Progress of Vacancy Engineering for Electrochemical Energy Conversion Related Applications," *Advanced Functional Materials*, vol. 31, p. 2009070, 2021.
- [47] H. Ahmad, S. Kamarudin, L. Minggu and M. Kassim, "Hydrogen from photocatalytic water splitting process: A review," *Renewable and Sustainable Energy Reviews*, vol. 43, pp. 599-610, 2015.
- [48] K. Khan, A. Tareen, M. Aslam, Y. Zhang, R. Wang, Z. Ouyang, Z. Gou and H. Zhang, "Recent advances in two-dimensional materials and their nanocomposites in sustainable energy conversion applications," *Nanoscale*, 2019.
- [49] Q. Zhu, Y. Qu, D. Liu, K. W. Ng and H. Pan, "Two-dimensional Layered Materials: High-Efficient Electrocatalysts for Hydrogen Evolution Reaction," *ACS Applied Nano Materials*, vol. 3, pp. 6270-6296, 2020.
- [50] H. Kwon, D. W. Bae, H. Kim, G. Kim, J. Cho, H. J. Park, H. Baik, A. R. Jeong, C.-H. Lin, C.-Y. Chiang, C.-S. Ku, H. Yang and S. Cho, "Nanoporous Silver Telluride for Active Hydrogen Evolution," *ACS Nano*, 2021.
- [51] X. Chen, Z. Zhang, L. Chi, A. Nair, W. Shanguan and Z. Jiang, "Recent Advances in Visible-Light-Driven Photoelectrochemical Water Splitting: Catalyst Nanostructures and Reaction Systems," *Nano-Micro Letter*, vol. 8, no. 1, pp. 1-12, 2016.
- [52] M. Antoniadou, S. Sfaelou, V. Dracopoulos and P. Lianos, "Platinum-free photoelectrochemical water splitting," *Catalysis Communications*, vol. 43, pp. 72-74, 2014.
- [53] Z. Zhang, P. Li, X. Zhang, C. Hu, Y. Li, B. Yu, N. Zeng, C. Lv, J. Song and M. Li, "Recent Advances in Layered-Double-Hydroxides Based Noble Metal Nanoparticles Efficient Electrocatalysts," *Nanomaterials*, vol. 11, p. 2644, 2021.
- [54] N. Rosman, R. Yunus, L. Minggu, K. Arifin, M. Salehmin, M. Mohamed and M. Kassim, "Photocatalytic properties of two-dimensional graphene and layered transition-metal dichalcogenides based photocatalyst for photoelectrochemical hydrogen generation: An overview," *International Journal of Hydrogen Energy*, vol. 43, pp. 18925-18945, 2018.
- [55] J. Ke, F. He, H. Wu, S. Lyu, J. Liu, B. Yang, Z. Li, Q. Zhang, J. Chen, L. Lei, Y. Hou and K. Ostrikov, "Nanocarbon-Enhanced 2D Photoelectrodes: A New Paradigm in Photoelectrochemical Water Splitting," *Nano-Micro Letters*, vol. 13, p. 24, 2021.

- [56] J. Joy, J. Mathew and S. George, "Nanomaterials for photoelectrochemical water splitting - review," *International Journal of Hydrogen Energy*, vol. 43, pp. 4804-4817, 2018.
- [57] A. Kudo and Y. Miseki, "Heterogeneous photocatalyst materials for water splitting," *The Royal Society of Chemistry*, vol. 38, pp. 253-278, 2009.
- [58] S. Jiulong, "Development of inorganic-organic hybrid materials for waste water treatment," December 2014. [Online]. Available: <https://www.researchgate.net/publication/314081363>. [Accessed March 2023].
- [59] X. Jin, T.-H. Gu, K.-G. Lee, M. J. Kim, M. S. Islam and S.-J. Hwang, "Unique advantages of 2D inorganic nanosheets in exploring high-performance electrocatalysts: Synthesis, application, and perspective," *Coordination Chemistry Reviews*, vol. 415, p. 213280, 2020.
- [60] B. You and Y. Sun, "Innovative Strategies for Electrocatalytic Water Splitting," *Accounts of Chemical Research*, vol. 51, pp. 1571-1580, 2018.
- [61] R. Maathew, C.-P. Lee, C.-A. Tseng, P. Chand, Y.-J. Huang, H.-T. Chen, K.-C. Ho, A. Anbalagan, C.-H. Lee and Y.-T. Chen, "Stoichiometry-Controlled MoxW1-xTe2 Nanowhiskers: A Novel Electrocatalyst for Pt-Free Dye-Sensitized Solar Cells," *ACS Applied Materials & Interfaces*, vol. 12, pp. 34815-34824, 2020.
- [62] X. Chia, A. Adriano, P. Lazar, Z. Sofer, J. Luxa and M. Pumera, "Layered Platinum Dichalcogenides (PtS₂, PtSe₂, and PtTe₂) Electrocatalysis: Monotonic Dependence on the Chalcogen Size," *Advanced Functional Materials*, vol. 26, pp. 4306-4318, 2016.
- [63] M. Chhowalla, H. Shin, G. Eda, L.-J. Li, K. Loh and H. Zhang, "The chemistry of two-dimensional layered transition metal dichalcogenide nanosheets," *Nature Chemistry*, vol. 5, pp. 263-275, 2013.
- [64] S. Nkabinde, "Colloidal synthesis and characterization of molybdenum and tungsten-based phosphide electrocatalysts for hydrogen evolution reaction," 2022. [Online]. Available: <https://hdl.handle.net/10539/34593>. [Accessed 2023].
- [65] J. Tian, W. Wu, Z. Tang, Y. Wu, R. Burns, B. Tichnell, Z. Liu and S. Chen, "Oxygen Reduction Reaction and Hydrogen Evolution Reaction Catalyzed by Pd-Ru Nanoparticles Encapsulated in Porous Carbon Nanosheets," *Catalysts*, vol. 8, p. 329, 2018.
- [66] A. Eftekhari, "Electrocatalysts for hydrogen evolution reaction," *International Journal of Hydrogen Energy*, vol. 42, pp. 11053-11077, 2017.
- [67] H. Yang, Q. He, Y. Liu, H. Li, H. Zhang and T. Zhai, "On-chip electrocatalytic microdevice: an emerging platform for expanding the insight into electrochemical processes," *Chem Soc Rev*, vol. 49, pp. 2916-2936, 2020.

- [68] X. Lu, L. Guo, P. Wang, M. Cui, D. Kanghong and W. Peng, "Theoretical investigation of the adsorption of gas molecules on WSe₂ monolayers decorated with Pt, Au nanoclusters," *Applied Surface Science*, vol. 513, p. 145860, 2020.
- [69] M. S. Dehcheshmeh and A. Kiani, "Synthesis of Pt nano catalyst in the presence of carbon monoxide: Superior activity towards hydrogen evolution reaction," *International Journal of Hydrogen Energy*, vol. 44, pp. 23969-23974, 2019.
- [70] Y. Fu, J. Li and J. Li, "Photo-improved hydrogen evolution reaction activity of the Pt/CdS electrocatalyst," *Progress in Natural Science: Materials International*, vol. 29, pp. 379-383, 2019.
- [71] D. Lin, Y. Li, P. Zhang, W. Zhang, J. Ding, J. Li, G. Wei and Z. Su, "Fast preparation of MoS₂ nanoflowers decorated with platinum nanoparticles for electrochemical detection of hydrogen peroxide," *RSC Advances*, vol. 6, pp. 52739-52745, 2016.
- [72] P. S. Toth, G. B. Szabo, G. Samu, K. Rajeshwar and C. Janaky, "Peeling off the surface: Pt-decoration of WSe₂ nanoflakes results in exceptional photoelectrochemical HER activity," *Sus Mat*, vol. 86, pp. 1-12, 2022.
- [73] J. Polte, "Fundamental growth principles of colloidal metal nanoparticles - a new perspective," *CrystEngComm*, vol. 17, no. 1, p. 6809, 2015.

Chapter 3

Synthesis of WSe₂ nanostructures with varying reaction parameters

3.1. Introduction

Two-dimensional nanomaterials have attractive chemical and physical properties due to their compositions and crystal structures which makes them appealing to use for various applications [1] [2]. To utilize these materials for applications, it is necessary to determine their physicochemical properties such as thickness, composition, crystalline phase, and surface chemistry [1]. The manipulation of reaction conditions such as time, temperature, concentration, precursors, and capping agents can allow for control over the size and shape of NPs [3] [4]. One approach to controlling the size, shape, and crystallinity of nanomaterials is to use solution-based synthesis methods, where the reaction parameters can be varied. This includes adjusting the mole ratios of precursors used, as well as the reaction time and temperature. By manipulating these parameters, it is possible to achieve precise control over the properties of the resulting nanomaterials.

Previously, chemical vapour deposition (CVD) or bulk exfoliation has been predominately used to synthesize transition metal dichalcogenides (TMDs) nanostructures with the capability of controlling the properties of the material, however these methods have limitations in scaling up the synthesis [5]. Therefore, solution-based methods have been developed and are considered suitable alternate with controllable reaction parameters that affect the morphology, composition, and crystallinity of TMD nanostructures [3]. An alternative method for effectively synthesizing TMDs is colloidal synthesis which offers solutions to various drawbacks, such as limited scalability and the production of TMDs not firmly attached to the substrate [1]. Colloidal synthesis can result in ordinarily metastable TMD phases with interesting properties depending on the choice of precursor, capping ligand, concentration, temperature, and other reaction parameters that affect nucleation growth [4]. By controlling the ratio of the reaction parameters, we can modify the formation of WSe₂ to obtain different nanostructures [6].

TMD structures are made up of strong covalent bonds between M-X (M: transition metal, X: chalcogen) atoms that forms X-M-X sandwiched layers due to weak van der Waals forces [7]. WSe₂ crystallizes in a layered structure and forms hexagonal layers that influences the coordination of transition metals and stacking order of the atoms [8].

Varying the reaction conditions result in different nanostructures being formed with different surface properties and chemical activities [9]. In the synthesis of WSe₂ nanostructures, the primary concept for controlling morphology is to separate the nucleation and growth processes and regulate the growth rate of various phases [9]. Therefore, the size and shape of WSe₂ can be tuned by varying the molar ratio of the reactants.

The concentration of the reactants affects the growth rate of the nanostructures which sequentially changes the morphology [10]. Metals precursors that contain strong C-Se bonds tend to favour slow nucleation growth rate that influences the final crystal phase formed [4]. Ostwald's rules for crystallization suggest that crystallization occurs from a solution when the Gibbs free energy is high. Nucleation occurs when the growth rate is greater than the dissolution rate, as the reaction kinetics influence the phase control during crystal growth [7]. The process of solution synthesis of TMD nanostructures typically begins with the decomposition of metal and chalcogen precursors into monomer complexes, which then react to create small nuclei [1]. The process is then followed by nucleation growth to form nanocrystals.

Nucleation growth is also strongly influenced by the reaction temperature. The optimal temperature for nucleation and growth depends on the specific materials and reaction conditions. At higher temperatures, the formation of vapours increases, which can lead to a higher nucleation density and a larger number of nuclei being formed. The temperature also affects the rate of diffusion, which can impact the growth rate of the nuclei. Therefore, the temperature must be carefully controlled to achieve the desired size and morphology of the TMD nanostructures [8]. Sokolikova *et al.* reported that synthesis temperature of ~300 °C is the optimal reaction temperature for nucleation growth is one that avoids boiling of the solvent at higher temperatures and prevents inhibition of nucleation growth at lower temperatures [11]. In addition, high growth temperatures improve the crystallinity of the material.

3.2. Method and materials

3.2.1. Chemicals

Tungsten (VI) chloride (WCl_6 , $\geq 99.9\%$), selenium powder ($\geq 99.9\%$), oleyl alcohol (85% technical grade) and toluene (99%).

3.2.2. Experimental procedure

The typical synthesis procedure involved the addition of WCl_6 and Se in a mole ratio of 1:4 to a three-neck round bottom flask containing 10 mL of oleyl alcohol. After degassing the solution under N_2 gas for 30 minutes with magnetic stirring, the mixture was heated to 320 °C for 120 minutes. The resulting nanoparticles were washed multiple times with toluene, collected by centrifugation, air-dried, and prepared for characterization. To prevent solvent boiling or inhibition of nucleation growth, the reaction temperature was carefully controlled. The specific reaction conditions for each experiment are listed in Table 3.1.

Table 3.1: Summary of experimental conditions.

Parameter	Temperature (°C)	Time (min)	Mole ratio (W:Se)
Concentration	320	120	1:4
	320	120	1:3
	320	120	1:2
Temperature	320	60 and 120	1:4
	250	60 and 120	1:4
	150	60 and 120	1:4

3.2.3. Characterization

The nanostructures produced in the experiment were subjected to various characterization techniques. The powder X-ray diffraction (PXRD) analysis was performed on a Bruker MeasSrv D2-205530 diffractometer with Cu-K α radiation ($\lambda = 1.54060 \text{ \AA}$) at 30 kV/10 mA, using a glancing angle of incidence detector and a

temperature of 25 °C. The sample morphologies were determined using FEI Technai T12 Transmission Electron Microscope (TEM) in TEM mode, after dispersing the samples in ethanol and sonicating them for 30 min. The absorption measurements were carried out using a SPECORD 210 Plus Analytik Jena UV-vis spectrophotometer, while Raman spectra were obtained using the HORIBA MacroRaman spectrophotometer with a 785 nm excitation laser. The samples were dispersed in ethanol and placed in a quartz cuvette (1 cm path length) for the UV-vis analysis, while for Raman analysis, the sample was placed on a Raman holder.

3.3. Results

3.3.1. Effect of concentration

The resultant nanostructures obtained were characterised using PXRD to confirm the crystalline phase and purity of the materials. The diffractograms are shown in **Figure 3.1**. All the diffraction patterns were matched with PDF card number 01-089-5257. that correspond to the hexagonal prismatic phase (2H) of WSe₂ with varying degrees of purity. The 1:2 W:Se mole ratio showed the most impurities, indicated by * and it attributed to WO₃. As the selenium concentration was increased, the impurity peaks disappeared. This is due to the excess selenium outcompeting the atmospheric oxygen. The (002) plane attributed to the c-axis of the material is indicative of the number of WSe₂. The more prominent the peak, the more layers are present. As a monolayer will result in the disappearance of the peak. The (002) is only observed in the 1:3 and 1:4 W:Se mole ratios. In addition to the (002), the diffraction peaks obtained at (100) and (110) confirmed that the materials are 2D structures [14].

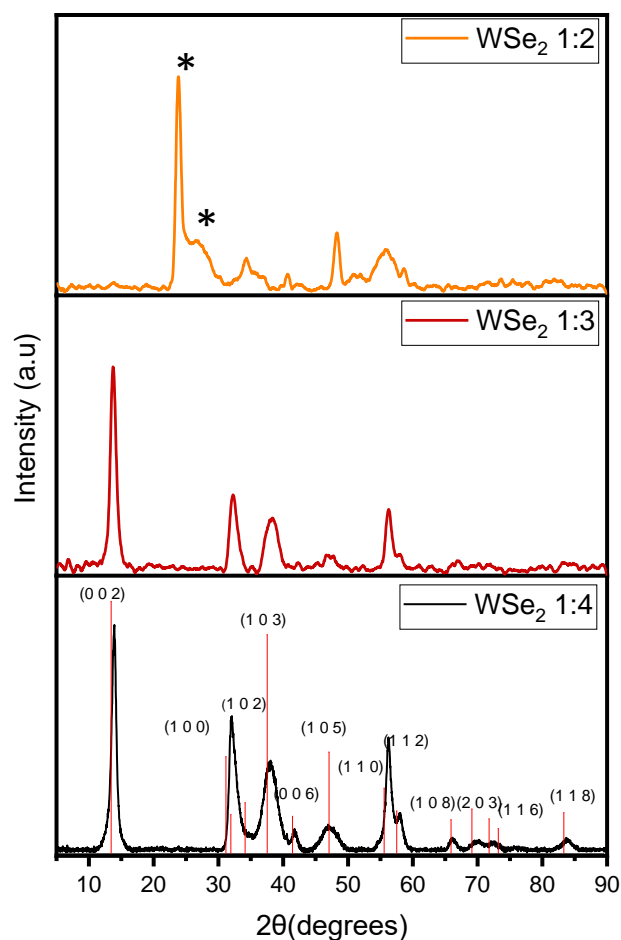


Figure 3.1: PXR D patterns of WSe₂ nanoparticles synthesized at various mole ratios (*) indicates WO₃.

The number of layers in TMD nanomaterials can be identified using Raman spectroscopy [15]. The Raman spectrum in **Figure 3.2** indicates two characteristic peaks that can be identified as A_{1g} which is caused by the chalcogen atoms moving out of plane in opposing directions and the metal atoms in-between stay fixed in position; and the E_{2g}¹ peak attributed to the metal and chalcogen atoms moving in opposite directions within the plane. **Table 3.2** shows the Raman frequencies of the materials and their corresponding vibrational assignments. A blue shift was observed due to an increase in wavenumber which indicates a decrease in particle size occurred as the mole ratio decreased. Interlayer interaction affects the Raman peak shift whereby the frequency of A_{1g} mode decreases when the number of layers decreases while in contrast, the E_{2g}¹ mode increases [21][22]. The number of layers not only

affects the peak shift but also the shape and intensity of the peaks as seen in **Figure 3.2**.

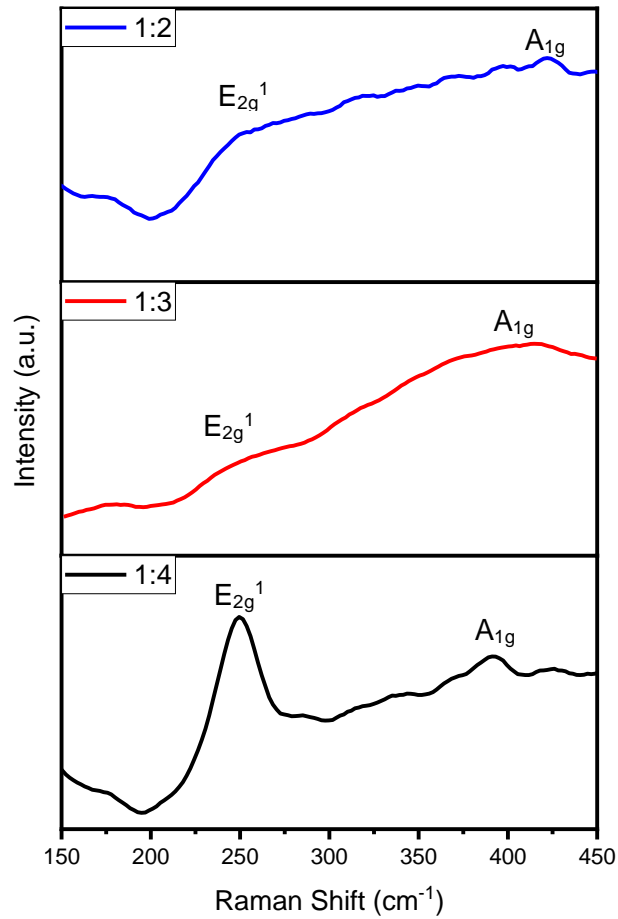


Figure 3.2: Raman spectroscopy of WSe₂ nanoparticles synthesized at various mole ratios.

Table 3.2: Raman frequencies and their vibrational assignment.

WSe ₂	E _{2g} ¹	A _{1g}
1:4	~245 cm ⁻¹	~395 cm ⁻¹
1:3	~255 cm ⁻¹	~410 cm ⁻¹
1:2	~260 cm ⁻¹	~420 cm ⁻¹

The optical properties of the nanomaterials were analysed using UV-vis spectroscopy shown in **Figure 3.3**. Four excitons were observed which corresponds with the 2H

WSe₂ phase that was observed on the PXRD spectra as well. Excitons A and B, at 935 nm and 915 nm respectively appear due to direct transitions gap of point K [16]. The absorption peaks of A' and B' were observed in the UV-vis spectra, which resulted from the ground and excited states of the two transitions of A and B. These peaks were observed to split due to the perturbation caused by d-electrons at the inter- and intra-level, which were affected by the Se p-orbitals [2].

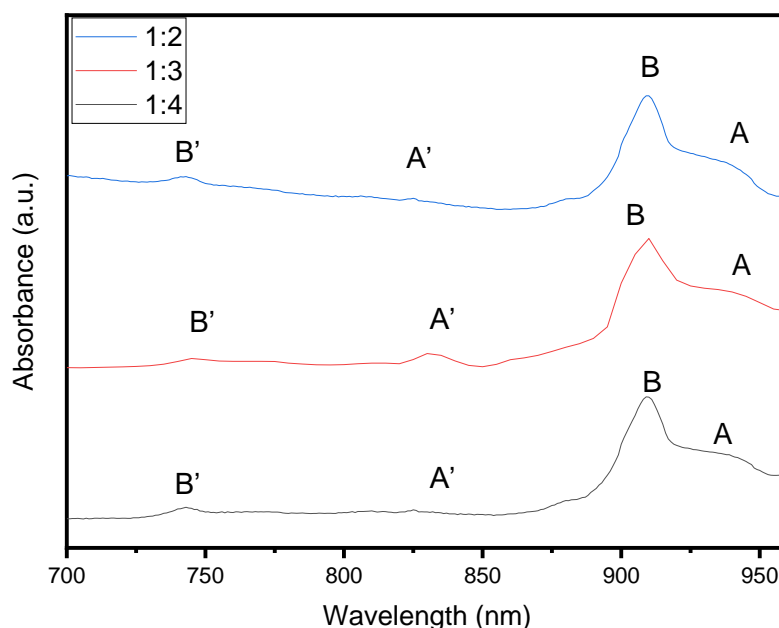


Figure 3.3: UV-vis absorption spectra of WSe₂ nanoparticles synthesized at various mole ratios.

Transmission electron microscopy (TEM) was utilised to visualise the structures and morphologies of the WSe₂ nanomaterial formed. The TEM micrograph in **Figure 3.4** shows that different nanostructures were produced based on the mole ratios. The 1:4 mole ratio produced defined nanoflower morphology with compact petals. The morphology observed could be the effect of continuous folding of nanosheets that are formed rapidly during synthesis, followed by concurrent lateral and vertical growth process that results in flower-like morphology [1]. Interestingly, when the mole ratio was reduced to 1:3 a co-existence of two morphologies was observed, nanoflowers and nanorods. Then at the 1:2 mole ratio, thin nanorods were observed.

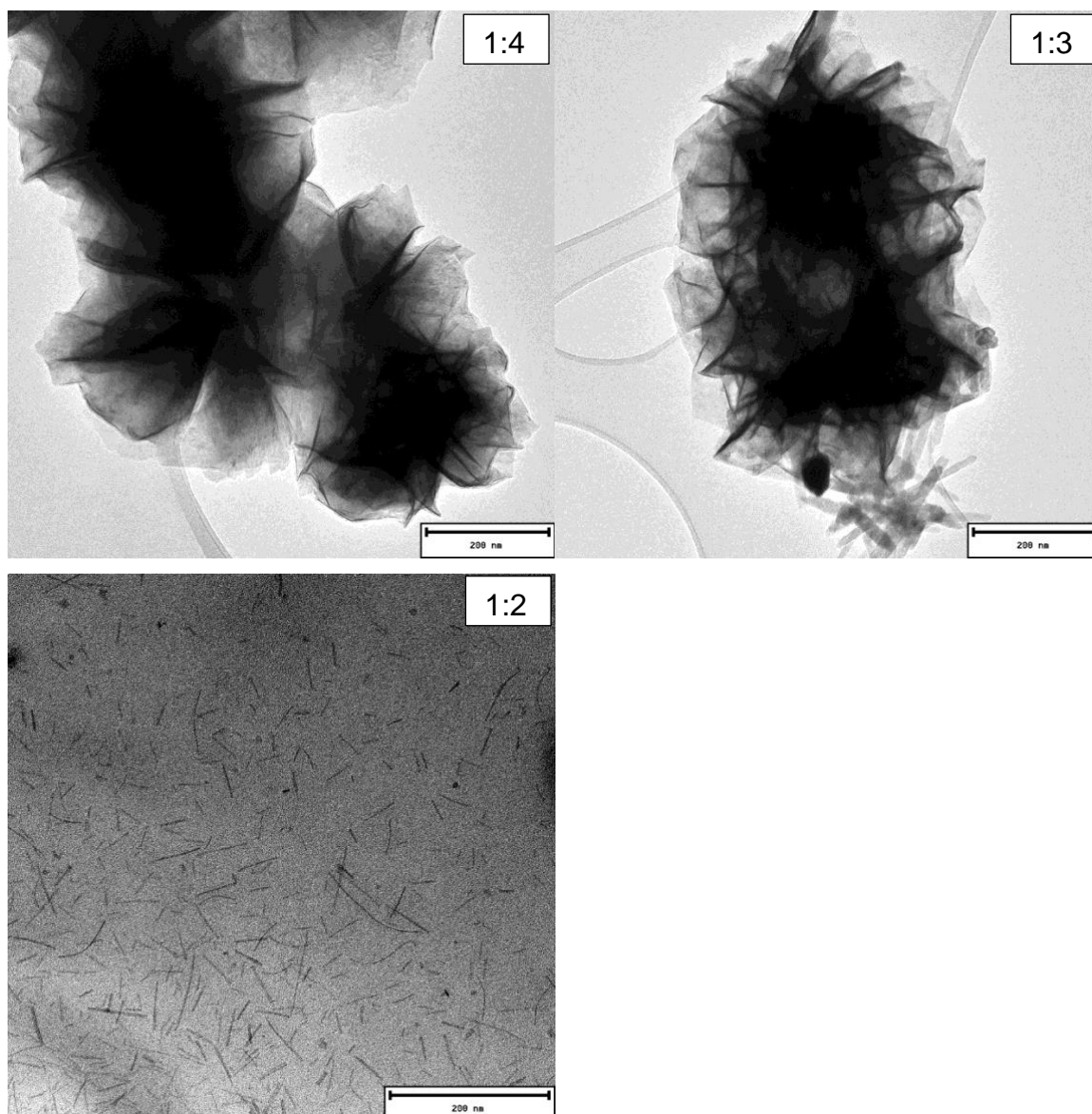
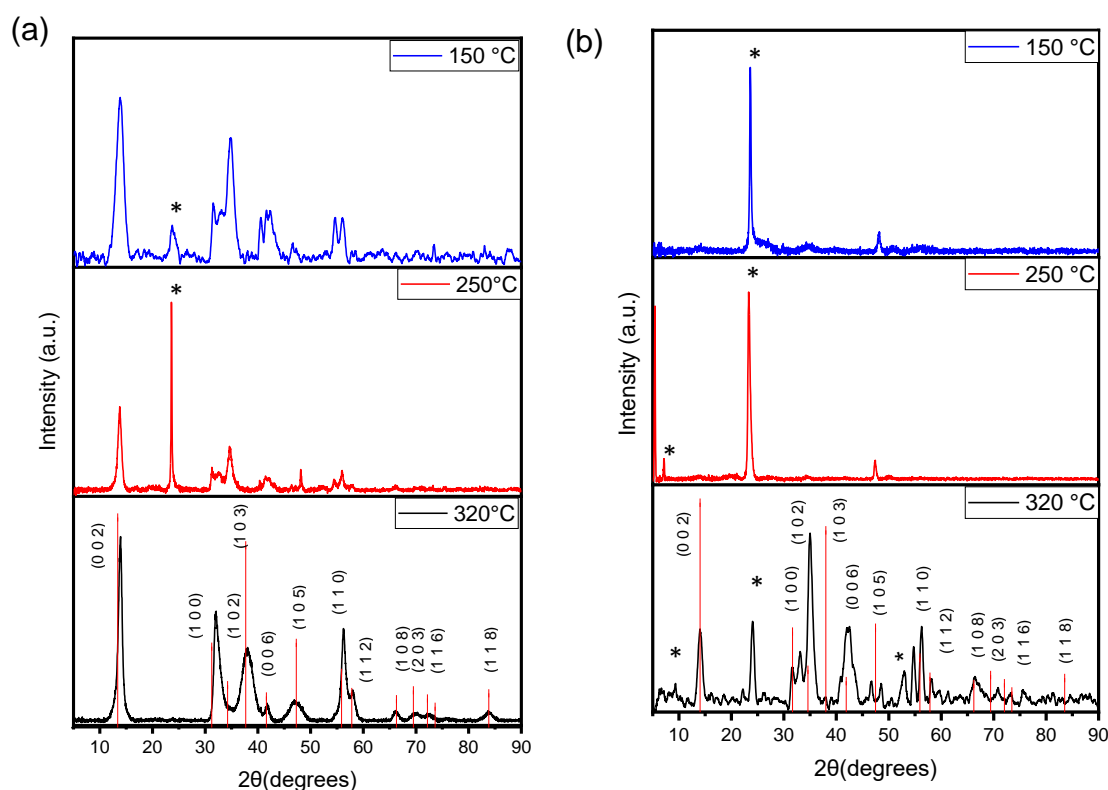


Figure 3.4: TEM images of WSe₂ nanoparticles synthesized at various mole ratios.

3.3.2. Effect of temperature and time

The resultant nanoparticles were characterized using PXRD to confirm their crystal phase and purity in **Figure 3.5**. The diffraction patterns obtained were matched to PDF card number 01-089-5257. The 320 °C temperature at 120 min matched well with WSe₂. However, when the temperature decreased, there were less diffraction peaks matching with WSe₂ and the materials contained impurities (WO₃) indicated by (*). When the reaction times were decreased to 60 min, less diffraction peaks were observed that match with WSe₂ including impurities indicated by (*). This suggests

that at the lower temperatures and reduced time of synthesis, the formation of WSe_2 was yet to be observed and only pronounced WO_3 peaks were observed.



3.5: PXRD patterns of WSe_2 nanoparticles synthesized at various temperatures for (a) 120 min and (b) 60 min (*) indicates WO_3 .

The Raman spectrum in **Figure 3.6** showed that the sample prepared at 320 °C for 120 min had an intense E_{2g}^1 peak. As the temperature decreased, this caused the peak intensities of the respective E_{2g}^1 peaks to decrease as well. However, the opposite was observed regarding the A_{1g} peak. For the 320 °C 120 min sample, the A_{1g} peak appeared to be less intense whereas when the temperature was decreased, the intensity increased for the other samples. A peak shift was also observed as the higher wavenumbers as the temperature was decreased. For the 60 min samples, they all have low intensity E_{2g}^1 peaks and increased intensity for the A_{1g} peaks with a shoulder. Unlike the 120 min samples, peak shift was not observed.

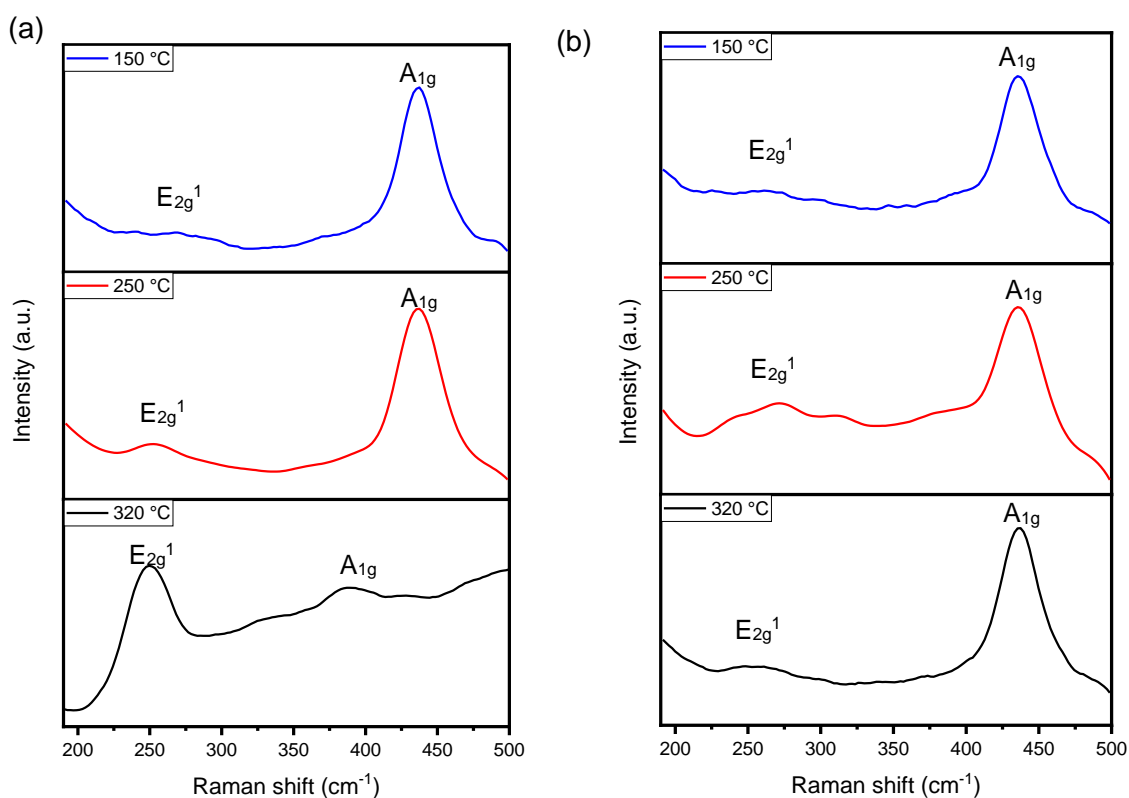


Figure 3.6: Raman spectra of WSe₂ nanoparticles synthesized at various temperatures for (a) 120 min and (b) 60 min.

The UV-vis spectra shown in **Figure 3.7** was used to determine the optical properties of the nanomaterials when time and temperature was varied. Four excitons were observed for each sample which indicates that the 2H phase of WSe₂ was formed. A blue shift was observed as the temperature decreased, from 320 °C to 250 °C, for both times.

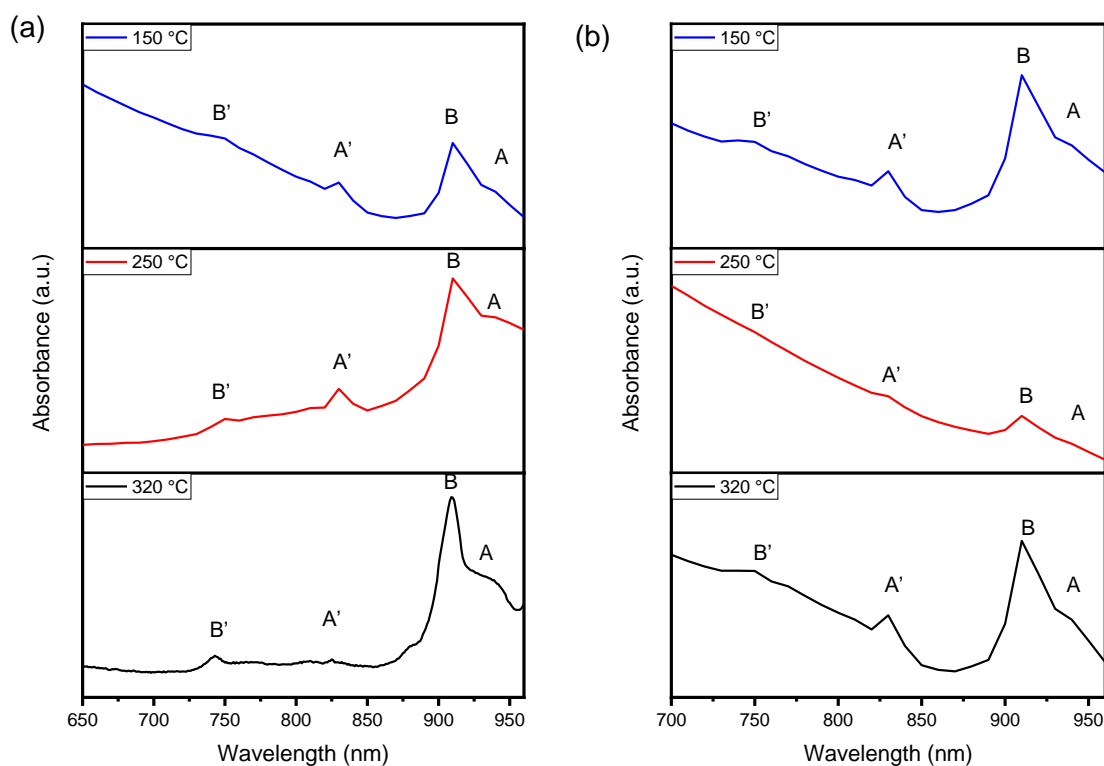


Figure 3.7: UV-vis spectra of WSe₂ nanoparticles synthesized at various temperatures for (a) 120 min and (b) 60 min.

TEM images were analysed to study the effects of temperature and time variations of the as synthesized nanoparticles and the results are shown in **Figure 3.8**. When the nanoparticles were synthesized for 120 min, high temperatures 250 – 320 °C resulted in defined nanoflower-like morphologies. When the temperature decreased to 150 °C, less defined nanoflowers were observed. Then when the time was decreased to 60 min, at 320 °C monodispersed nanoflowers were observed. At 250 °C, the cloud-like structures were observed. When the temperature decreased to 150 °C, this resulted in the formation of nanorods.

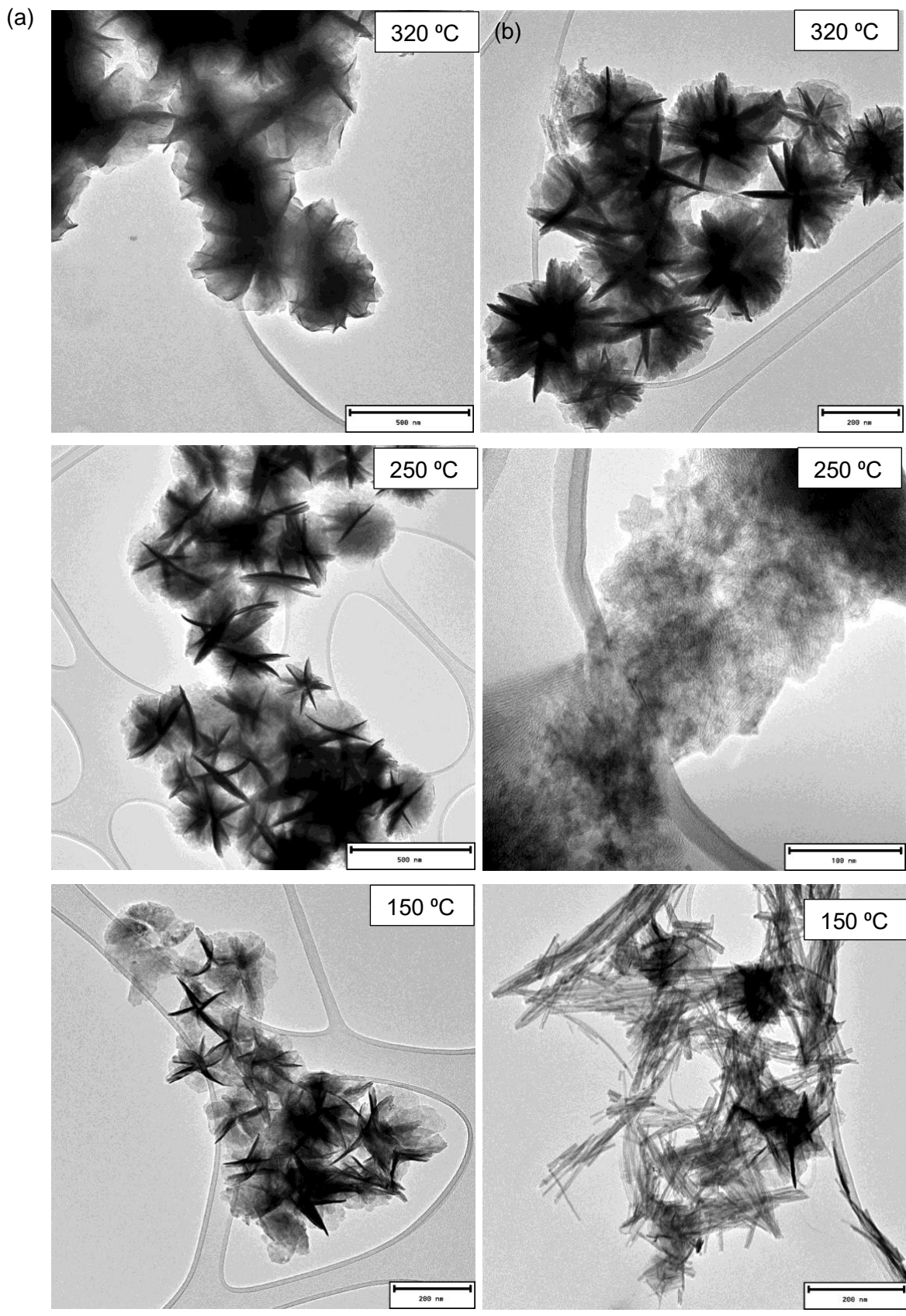


Figure 3.8: UV-vis spectra of WSe₂ nanoparticles synthesized at various temperatures for (a) 120 min and (b) 60 min

3.5. Conclusion

To summarize, this study demonstrated that the synthesis of WSe_2 nanoparticles can be achieved through the precise control of reaction parameters, including precursor concentration, temperature, and reaction time. These parameters were found to impact the nucleation and growth rate of the nanoparticles, which in turn affected their morphology and properties. Specifically, increasing the precursor concentration was found to promote the formation of WSe_2 nanoflowers by influencing the size and morphology of the nuclei during growth. This study highlights the importance of carefully controlling reaction conditions in the synthesis of TMD nanomaterials to achieve desired properties and morphologies. An increase in temperature affects the composition and morphology of nanoparticles as it resulted in more defined nanoflower-like structures. An increase in reaction time affects nucleation growth resulting in monodispersed nanoparticles. Other researchers have also found that varying the reaction parameters affects the morphological and structural properties of WSe_2 nanomaterials. Therefore, the reaction thermodynamics and kinetics influences the nucleation growth by providing insight into the growth mechanism in relation to the number of layers formed.

3.5 References

- [1] Y. Sun, M. Terrones and R. Schaak, "Colloidal Nanostructures of Transition-Metal Dichalcogenides," *Accounts of Chemical Research*, vol. 10, pp. 284-293, 2020.
- [2] A. Sierra-Castillo, E. Haye, S. A'costa, C. Bittencourt and J.-F. Colomer, "Synthesis and Characterization of Highly Crystalline Vertically Aligned WSe₂ Nanosheets," *Applied Sciences*, vol. 10, p. 874, 2020.
- [3] Y. Cho, T. Anh, H. Kim, Y. Hong, H. Hwang, H. Park, S. Seo and H. Lee, "Unriling surface charge on chalcogen atoms toward the high aspect-ratio colloidal growth of two-dimensional transition metal chalcogenides," *Nanoscale*, vol. 13, pp. 1291-1302, 2021.
- [4] J. Q. Geinshoff, A. K. Tamura and A. Schimpf, "Using ligands to control reactivity, size and phase in the colloidal synthesis of WSe₂ nanocrystals," *ChemComm*, vol. 55, pp. 8856-8859, 2019.
- [5] D. Rossi, J. H. Han, W. Jung, J. Cheon and D. H. Son, "Orientational Control of Colloidal 2D-Layered Transition Metal Dichalcogenide Nanodiscs via Unusual Electrokinetic Response," *ACS Nano*, vol. 9, no. 8, pp. 8037-8043, 2015.
- [6] W. Guo, Y. Chen, L. Wang, J. Xu, D. Zeng and D.-L. Peng, "Colloidal synthesis of MoSe₂ nanonetworks and nanoflowers with efficient electrocatalytic hydrogen-evolution activity," *Electrochimica Acta*, vol. 231, pp. 69-76, 2017.
- [7] P. Zhou, G. Collins, Z. Hens, K. M. Ryan, H. Geaney and S. Singh, "Colloidal WSe₂ nanocrystals as anodes for lithium-ion batteries," *Nanoscale*, vol. 12, pp. 22307-22316, 2020.
- [8] S. Rani, M. Sharma, D. Verma, A. Ghanghas, R. Bhatia and I. Sameera, "Two-dimensional transition metal dichalcogenides and their heterostructures: Role of process parameters in top-down and bottom-up synthesis approaches," *Materials Science in Semiconductor Processing*, vol. 139, p. 106313, 2022.
- [9] H. Zhu, H. Zhang, J. Liang, G. Rao, J. Li, G. Liu, Z. Du, H. Fan and J. Luo, "Controlled Synthesis of Tellurium Nanostructures from Nanotubes to Nanorods and Nanowires and Their Template Applications," *The Journal of Physical Chemistry C*, vol. 115, pp. 6375-6380, 2011.

- [10] F. Gao, Q. Lu and S. Komanneni, "Gluconate controls one-dimensional growth of tellurium nanostructures," *Journal of Materials Research*, vol. 21, no. 2, pp. 343-348, 2006.
- [11] M. S. Sokolikova, P. C. Sherrell, P. Palczynski, V. L. Bemmer and C. Mattevi, "Direct solution-phase synthesis of 1T' WSe₂ nanosheets," *Nature Communications*, vol. 10, p. 712, 2019.
- [12] Y. Hwang and N. Shin, "Colloidal Synthesis of MoSe₂/WSe₂ Heterostructure Nanoflowers via Two-Step Growth," *Materials*, vol. 14, p. 7294, 2021.
- [13] S. M. Eichfeld, V. O. Colon, Y. Nie, K. Cho and J. A. Robinson, "Controlling nucleation of monolayer WSe₂ during metal-organic chemical vapor deposition growth," *2D Materials*, vol. 3, p. 025015, 2016.
- [14] S. Quereshi, E. Ahmad, K. K. Pant and S. Dutta, "Insights into Microwave-Assisted Synthesis of 5-Ethoxymethylfurfural and Ethyl Levulinate Using Tungsten Disulfide as a Catalyst," *ACS Sustainable Chemistry & Engineering*, vol. 8, pp. 1721-1729, 2020.
- [15] M. Mohl, A.-R. Rautico, G. A. Asres, M. Wasala, P. D. Patil, S. Talapatra and K. Kordas, "2D Tungsten Chalcogenides: Synthesis, Properties and Applications," *Advanced Materials Interfaces*, vol. 7, p. 2000002, 2020.
- [16] W. Jung, S. Lee, D. Yoo, S. Jeong, Miro, Pere, A. Kuc, T. Heine and J. Cheon, "Colloidal Synthesis of Single-Layer MSe₂ (M = Mo, W) Nanosheets via Anisotropic Solution-Phase Growth Approach," *Journal of the American Chemical Society*, Vols. 7266-7269, p. 137, 2015.
- [17] J. You, M. D. Hossain and Z. Luo, "Synthesis of 2D transition metal dichalcogenides by chemical vapor deposition with controlled layer number and morphology," *Nano Convergence*, vol. 5, p. 26, 2018.
- [18] S. Jeon and K. Yong, "Morphology-controlled synthesis of highly adsorptive tungsten oxide nanostructures and their application to water treatment," *Journal of Materials Chemistry*, vol. 20, pp. 10146-10151, 2010.
- [19] F. Zhang, K. Momeni, M. AlSaud, A. Azizi, M. Hainey, J. Redwing, L.-Q. Chen and N. Alem, "Controlled synthesis of 2D transition metal dichalcogenides: from vertical to planar MoS₂," *2D Materials*, vol. 4, p. 025029, 2017.

- [20] H. Li, J. Zou, S. Xie, X. Leng, D. Gao and X. Mao, "Effect of selenization parameters on hydrogen evolution reaction activity of WSe₂ electrodes," *Applied Surface Science*, vol. 425, pp. 622-627, 2017.
- [21] J. Tai, B. Wang, D. Hu, P. Xu and Z. Zhang, "Ultraviolet-Visible-Near-infrared photodetector based on exfoliated Tungsten Selenide," *Materials Letters*, vol. 287, p. 129247, 2021.
- [22] Q. H. Wang, K. Kalantar-Zadeh, A. Kis, J. N. Coleman and M. S. Strano, "Electronics and Optoelectronics of two-dimensional transition metal dichalcogenides," *Nature Nanotechnology*, vol. 7, pp. 699-712, 2012.

Chapter 4

Synthesis of WSe₂ nanostructures by varying the tungsten precursor and capping ligand

4.1. Introduction

Colloidal synthesis is a technique that allows versatility in the production of nanoparticles by manipulating the properties of the nanoparticles. The morphologies and properties of the resulting nanoparticles can be influenced by varying the reaction parameters, such as the type of precursors and capping agents. The choice of metal precursor and capping agent can have a significant impact on the final shape and properties of the nanoparticles [1]. This is because they can determine the rate of nucleation that can promote large amounts of nanosized nuclei that happens fast whereby decoupling of the nucleation and growth stages occurs in order to reduce the polydispersity of the particles [2]. Therefore, the type of precursor used can influence nucleation and growth rates of nanoparticles in colloidal synthesis.

Metal oxides and metal chlorides are commonly used as precursors for the synthesis of TMDs via colloidal synthesis because they have relatively low decomposition temperatures, making it easier to form nuclei in solution. The decomposition of precursors releases metal and chalcogen species, which can react to form nuclei and subsequently grow into TMD nanostructures under appropriate reaction conditions [2]. Three different tungsten precursors were used in this study: WCl₆ (tungsten hexachloride), W(CO)₆ (tungsten hexacarbonyl) and H₂WO₄ (tungstic acid). Halide metal precursors such as WCl₆ typically, the decomposition of TMD precursors necessitates high temperatures and the presence of a reducing agent [3]. WCl₆ is also air and moisture sensitive, and it decomposes fast due to the presence of weak W-Cl bonds therefore it is more reactive than W(CO)₆ [4]. W(CO)₆ is less active, however stable in air and decomposes at low temperatures [3] [4]. Subsequently, H₂WO₄ is a hydrated form of tungsten trioxide, WO₃.

The decomposition of metal and chalcogen precursors results in the formation of monomer complexes whereby their reaction in solution forms small nuclei covered by organic capping ligands [5]. Capping ligands are useful in controlling the shape and size of nanocrystals by steric stabilization which prevents aggregation of nanoparticles. Alkylamines and carboxylic acid groups on ligands can influence the

reaction outcome of nanoparticles [1]. Herein, two different organic capping ligands were used: oleyl alcohol (OA) and oleylamine (OLA). OA and OLA are both considered classical ligands due to having one alkyl chain as a tail group which results in steric effects that change the growth mechanism of the nanoflowers by controlling the surface energy of the facets [6]. OLA is usually used as a capping ligand and mild reducing agent in colloidal synthesis of nanoparticles [7].

4.2. Method and materials

4.2.1. Chemicals

Tungsten (VI) chloride (WCl_6 , $\geq 99.9\%$), tungsten hexacarbonyl ($W(CO)_6$, 97%), tungstic acid (H_2WO_4), selenium powder ($\geq 99.9\%$), oleyl alcohol (OA, 85% technical grade), oleylamine (OLA, 70% technical grade and toluene (99%). All chemicals were purchased at Sigma Aldrich and used without further processing or purification.

4.2.2. Experimental Procedure

The tungsten precursor (WCl_6 or $W(CO)_6$ or H_2WO_4) was mixed with Se at a 1:4 mole ratio and added to a three-neck round bottom flask containing the capping ligand (OA or OLA). The three-neck round bottom flask was subjected to magnetic stirring under N_2 gas after degassing for 30 minutes. The mixture was then heated to $\sim 320^\circ C$ and maintained for 120 minutes before being cooled to room temperature. The resulting nanoparticles were washed multiple times with toluene by centrifugation to remove by-products, air dried, and prepared for further analysis.

WCl_6 - WSe_2 indicates WSe_2 synthesized using WCl_6 as the precursor.

$W(CO)_6$ - WSe_2 indicates WSe_2 synthesized using $W(CO)_6$ as the precursor.

H_2WO_4 - WSe_2 indicates WSe_2 synthesized using H_2WO_4 as the precursor.

4.2.3. Characterization

The synthesized nanostructures were characterized using various techniques.

Powder X-ray diffraction (PXRD) was performed using a Bruker MeasSrv D2-205530 diffractometer with Cu-K α radiation ($\lambda = 1.54060 \text{ \AA}$), operating at 30 kV/10 mA and a glancing angle of incidence detector at an angle of 2° . The measurements were taken for 2θ values between 10 - 90° with a step time of 37 s at room temperature.

The sample morphologies were examined using FEI Technai T12 Transmission Electron Microscope (TEM) operated at 120 kV in TEM mode. For the TEM analysis,

the samples were dispersed in ethanol, sonicated for 30 min, and then placed on a lacey-carbon copper grid to dry at room temperature. The optical properties of the nanoparticles were analysed using a SPECORD 210 Plus Analytik Jena UV-vis spectrophotometer, after dispersing the nanoparticles in ethanol and placing them in a quartz cuvette with a path length of 1 cm. Raman spectra were obtained using the HORIBA MacroRaman spectrophotometer with 785 nm excitation laser, by placing the sample on a holder.

4.2. Results

4.2.1. Capping ligand: OA

PXRD was used to confirm the crystalline phase and purity of the nanomaterials. The diffraction peaks shown in **Figure 4.1** were matched with PDF card number 01-089-5257 which is the 2H phase of hexagonal WSe_2 . Both the WCl_6 - WSe_2 and $W(CO)_6$ - WSe_2 nanoparticles matched well with the reference peaks. Whereas the H_2WO_4 - WSe_2 sample had an additional peak at 25° indicated by * suggested that the material is not purely WSe_2 as it contained tungsten oxide WO_3 . The three samples all had the (002) plane which suggested that they all formed layered structures. The PXRD patterns were found to have sharp peaks which indicated that the samples were highly crystalline [8]. It was observed that some of the reflected peak intensities differed for each sample. This could be attributed to the crystallite size of each material as a high intensity suggests that the thickness of the WSe_2 layer and crystallite size increases [9].

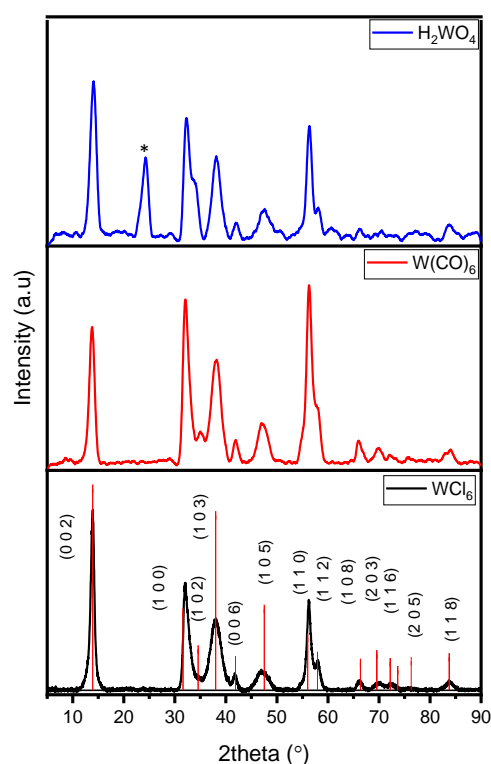


Figure 4.1: PXR D patterns of WSe₂ nanoparticles synthesized using different tungsten precursors, (*) indicates WO₃.

Raman spectra in **Figure 4.2** revealed that all three precursors exhibit one sharp peak at $\sim 250\text{ cm}^{-1}$ which is the in-plane E_{2g}^1 vibrational mode. Then a shoulder peak was observed at $\sim 285\text{ cm}^{-1}$ which was attributed to the out-of-plane A_{1g} vibrational mode. The intensity of the E_{2g}^1 peak was higher than the A_{1g} peak. The different materials exhibited slightly different wavenumbers for each mode. WCl_6 -WSe₂, E_{2g}^1 was at 250 cm^{-1} and A_{1g} was at 286 cm^{-1} . $W(CO)_6$ -WSe₂, E_{2g}^1 was at 250 cm^{-1} and A_{1g} was at 282 cm^{-1} . H_2WO_4 -WSe₂, E_{2g}^1 was at 255 cm^{-1} and A_{1g} peak was at 290 cm^{-1} . The peak positions could have been influenced by the crystallinity of the materials which was observed on the PXR D patterns [10]. The H_2WO_4 -WSe₂ material exhibited higher wavenumbers than the other samples which suggested that a blue shift occurred. The blue shift observed suggests that the shifts were size-dependent as the particle size decreased when the wavenumber increased [11].

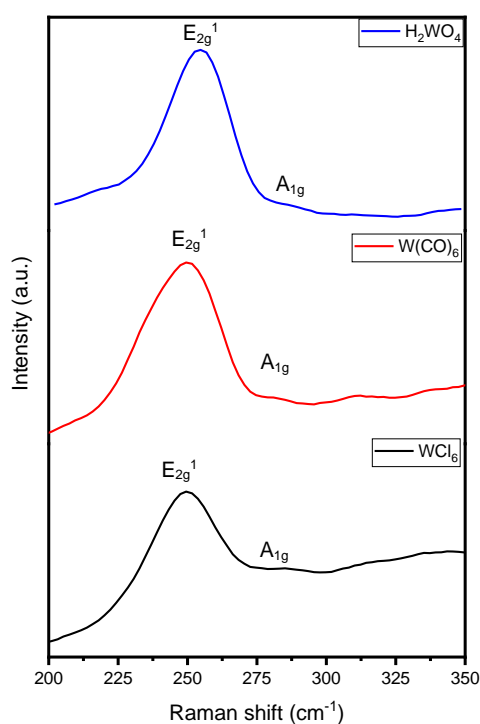


Figure 4.2: Raman spectroscopy of WSe₂ nanoparticles synthesized with different tungsten precursors.

The optical properties of the WSe₂ nanostructures were determined by UV-vis spectroscopy shown in **Figure 4.3**. Four absorption peaks were observed for the WSe₂ synthesized nanostructures which is characteristic of 2H-WSe₂. This also confirmed the presence of two or more layers due to four excitons: B', A', B and A being observed on the spectra. A and B which is located around 933 nm and 908 nm respectively, are the direct transition gap of point K of the Brillouin zone which is situated between the conduction band and the split valence band [12] [13] Then A' and B' located at 825 nm and 743 nm respectively represent the ground and excited states of the A and B transition split that occurs when the d-electron is perturbed by the Se p-orbital [14]. A blue shift of excitonic peaks, A and B, was observed which suggested that the thickness of the WSe₂ nanoparticles was reduced when the metal precursor was changed from WCl₆ to W(CO)₆ to H₂WO₄ [15]. The optical band gap was measured based on the longest wavelength absorption of each material which was found to be 1.316 eV, 1.322 eV and 1.330 eV for WCl₆-WSe₂, W(CO)₆-WSe₂ and H₂WO₄-WSe₂ respectively. This indicated a blue shift occurred based on the experimental band gap of bulk WSe₂ value of 1.20 eV [16].

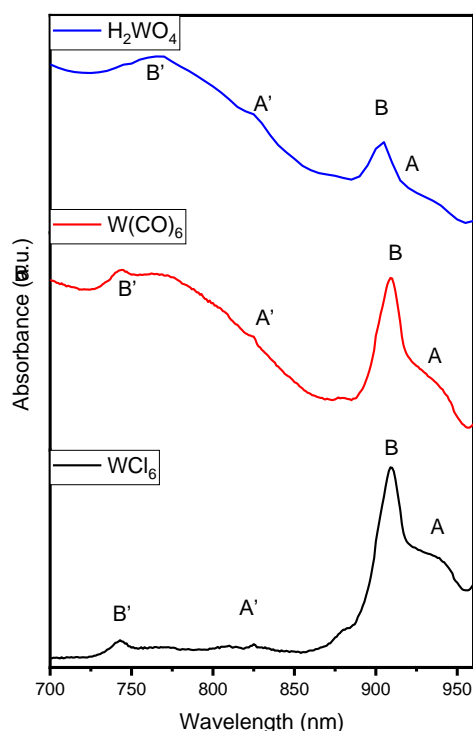


Figure 4.3: UV-vis absorption spectra of WSe₂ nanoparticles synthesized using different tungsten precursors.

The TEM images in **Figure 4.4** show that the different tungsten precursors all formed flower-like WSe₂ nanostructures. The nanoflower morphology was caused by the formation of few layered nanosheets that formed from one central point [17]. However, from the images it was observed that the thickness of the nanosheets varied depending on the metal precursor used. WCl₆-Wse₂ **Figure 4.4 (a)** appeared to form more agglomerated nanoflowers due to densely packed layers of the nanosheets [17]. W(CO)₆-Wse₂ **Figure 4.4 (b)** appeared to have less layers than WCl₆-Wse₂, however H₂WO₄ **Figure 4.4 (c)** had the least layers as the nanoflower-like structure appeared to have thin edges. This observation correlates with the blue shift observed on UV-vis spectra suggesting that the thickness of the nanoparticles was reduced. TEM study also revealed that the average particle size decreased as the number of layers decreased. The average lateral sizes of WCl₆-WSe₂, W(CO)₆-WSe₂ and H₂WO₄-WSe₂ was 450 nm, 362 nm, and 310 nm respectively. This suggests that the type of precursor used influences the morphology of WSe₂ nanoparticles.

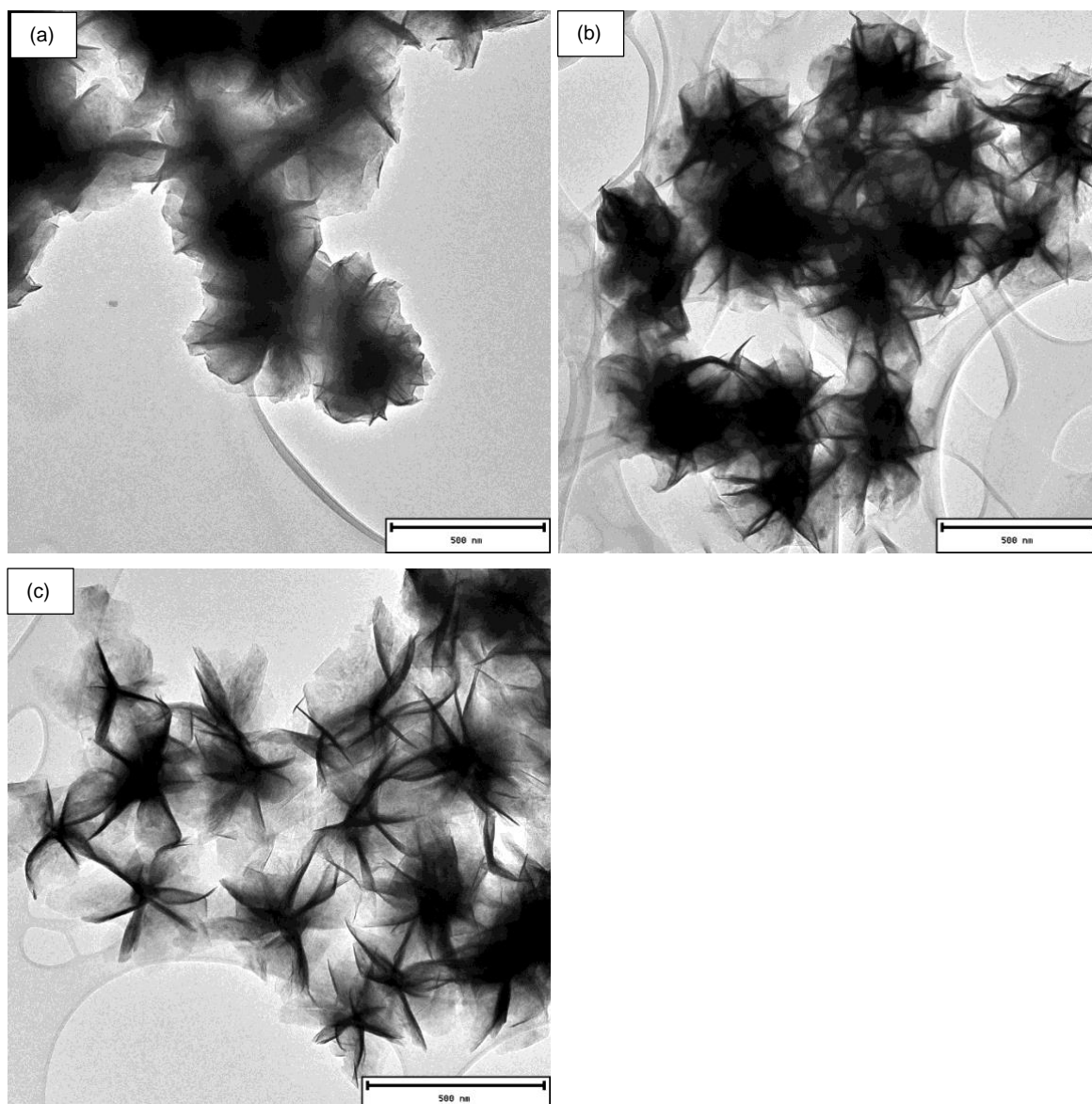


Figure 4.4: TEM images of WSe₂ nanoparticles synthesized with different tungsten precursors (a) WCl₆-WSe₂, (b) W(CO)₆-WSe₂, (c) H₂WO₄-WSe₂.

FTIR spectroscopy was used to confirm the presence of the capping agents on the surface of the nanoparticles. OA served as the capping agent whereby the pure capping agent was analysed alongside the WSe₂ nanoparticles in **Figure 4.5**. All three WSe₂ samples displayed the vibrational features of OA including the symmetric and asymmetric vibrations of -C-H at 725 cm⁻¹, -C-OH at 1043 cm⁻¹, -C=C at 1464 cm⁻¹, -CH₂ at 2918 cm⁻¹, -CH₂- at 3008 cm⁻¹ and -OH at 3350 cm⁻¹ [18]. These vibrational modes are important as they may give an indication as to how the capping agent is bounded onto the nanoparticles. The -CH bend at 725 cm⁻¹ appeared to have disappeared from the H₂WO₄-WSe₂ spectra, instead a broad absorption band at 800-600 cm⁻¹ was observed. This could have been caused by the presence of the hydroxyl

(-OH) compound at 3350 cm^{-1} [19]. This suggests that the hydrogen bond formed through the hydroxyl groups of oleyl alcohol molecules because of OH stretching [20]. However, the -OH stretch at 3350 cm^{-1} seemed to have disappeared on the H_2WO_4 - WSe_2 spectra. The WCl_6 - WSe_2 sample appeared to have more pronounced OA vibrational modes which suggests that oleyl alcohol served as a good capping agent for this sample. Whereas for the $\text{W}(\text{CO})_6$ - WSe_2 and the H_2WO_4 - WSe_2 samples the peaks were not as distinct therefore suggesting that OA may be chemisorbed onto the WSe_2 .

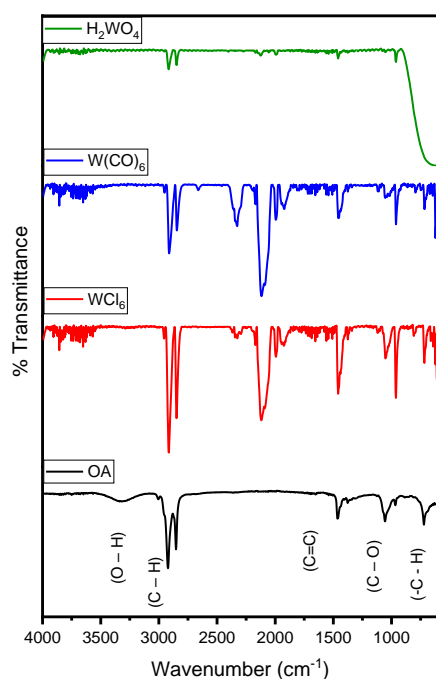


Figure 4.5: FTIR spectra of pure OA capping agent and capped- WSe_2 nanoparticles synthesized using different tungsten precursors.

4.2.2. Capping ligand: OLA

PXRD was used to investigate the crystallinity and structural properties of the OLA synthesized nanoparticles and the results are shown in **Figure 4.6**. The nanoparticles formed from the different tungsten precursors were indexed to the hexagonal phase of WSe_2 card number 01-089-5257. However, the samples did not match well with the reference peaks as additional peaks are observed between 18° - 29° range. This implied that the particles were not pure and contained tungsten oxide. The H_2WO_4 - WSe_2 pattern showed a high-intensity peak at 13.8° that corresponds with the (002) plane. This plane was attributed to the c-axis of the nanoparticles and implied that the

WSe₂ sample had a well stacked layered structure [12]. Peak broadening was observed which affected the intensity of the peaks, this implied that the crystallinity of the particles was poor. This also suggested that the particles formed amorphous structures.

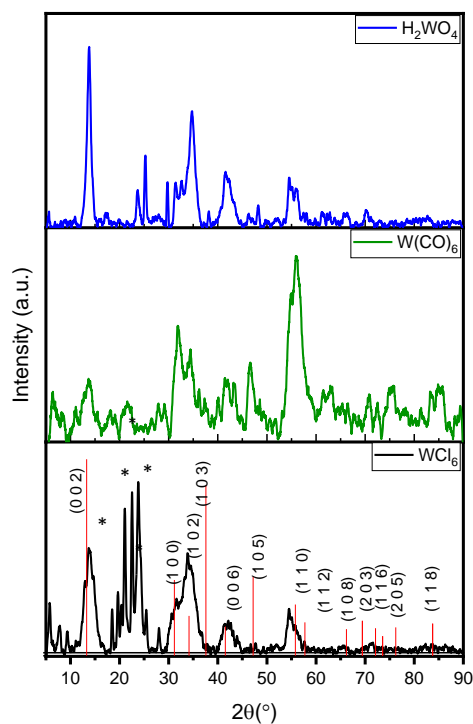


Figure 4.6: PXR D patterns of WSe₂ nanoparticles synthesized using different tungsten precursors, (*) indicates WO₃.

The Raman spectra in **Figure 4.7** revealed the presence of one distinct peak at ~ 233 cm^{-1} . At this position it was assumed to be the E_{2g}^1 mode that is usually observed at ~ 250 cm^{-1} . This suggested that the peak position was red shifted as the wavenumber decreased because of a decrease in the average size of the nanoparticles or the thickness [21]. Raman red shift implies that the crystal quality of the materials became worse [22]. The A_{1g} mode however was a lot less distinct which could have resulted from it being closely located to the E_{2g}^1 mode therefore the two peaks tend to merge which resulted in one single observable peak [23] [24].

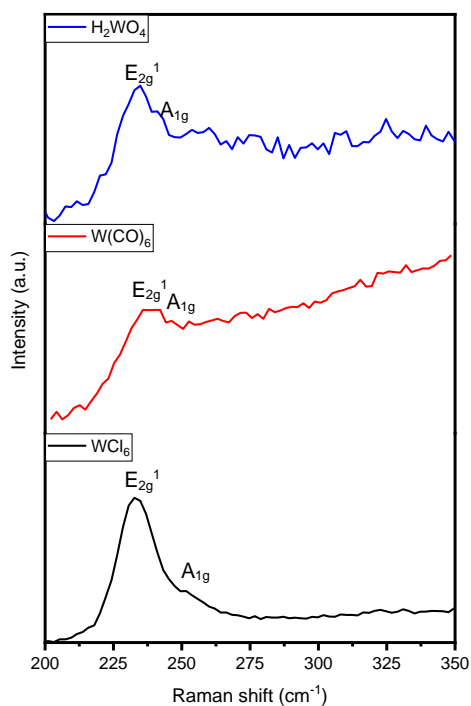


Figure 4.7: Raman spectroscopy of WSe₂ nanoparticles synthesized with different tungsten precursors.

Figure 4.8 presents the results of the analysis of the optical properties of the synthesized WSe₂ nanoparticles using UV-vis spectroscopy. For all the tungsten precursors used, four absorption peaks were observed. This suggested that each sample had two or more layers. The optical band gap was calculated and was found to be 1.364 eV for all of the OLA synthesized materials. The experimental band gap value is 1.20 eV, this indicated a blue shift occurred [16].

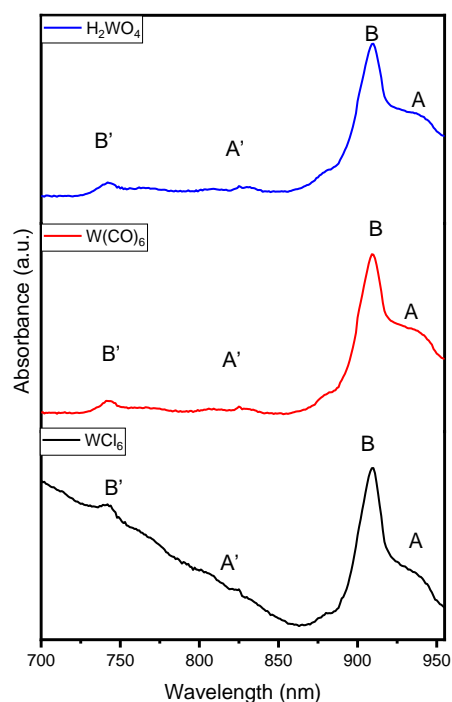


Figure 4.8: UV-vis absorption spectra of WSe₂ nanoparticles synthesized using different tungsten precursors.

The TEM images in **Figure 4.9** showed that the nanoparticles synthesized with OLA as the capping agent resulted in amorphous structures. This confirmed PXRD results as a decrease in crystallinity was observed. The WCl₆-WSe₂ appeared to be the least crystalline nanoparticles as the precursor produced more agglomerated nanoparticles. The capping agent could have also contributed to this observation. The W(CO)₆-WSe₂ nanoparticles displayed layered sheet-like morphology. The H₂WO₄-WSe₂ nanoparticles appeared to exhibit similar morphology, layered structures.

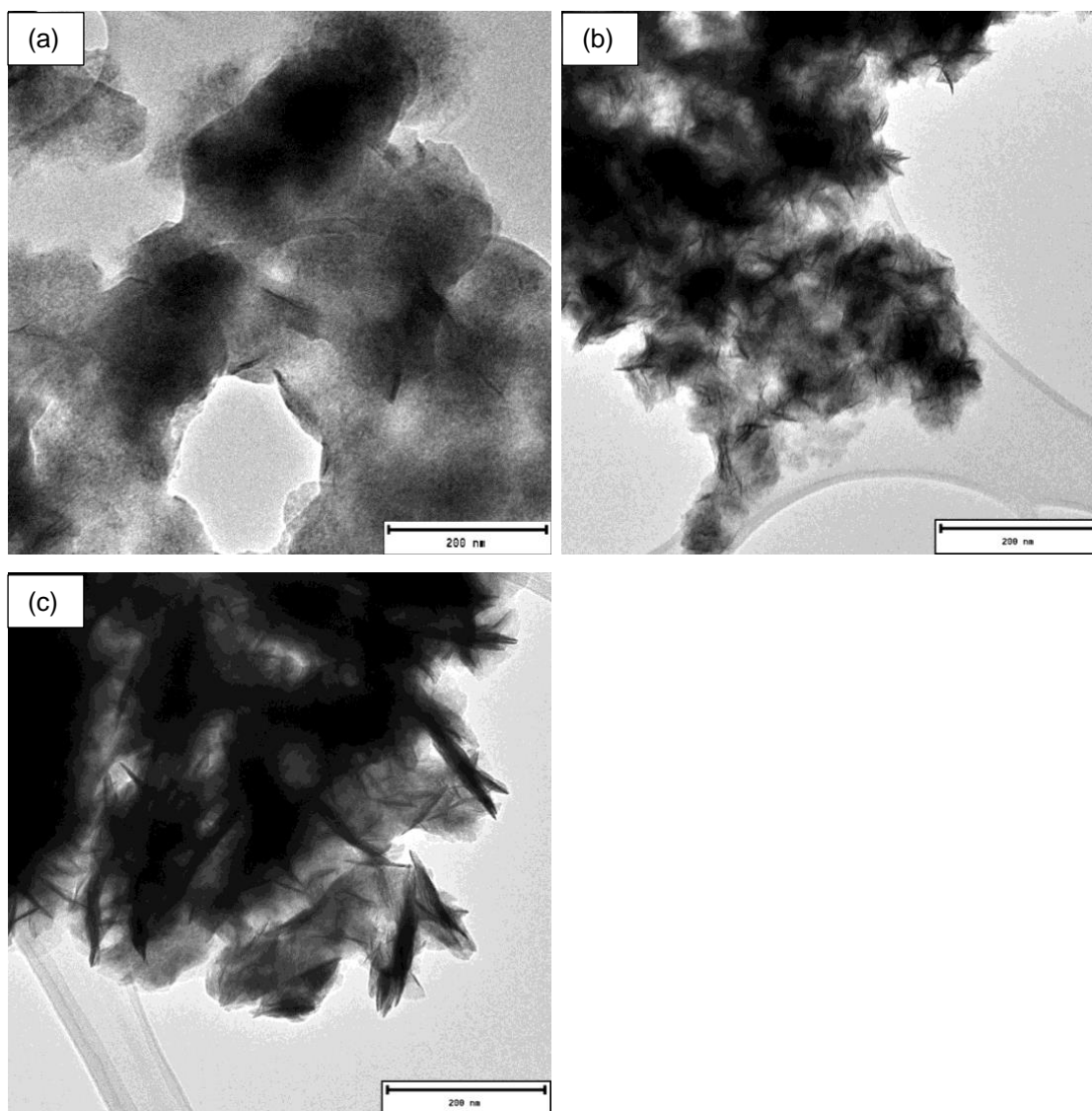


Figure 4.9: TEM images of WSe₂ nanoparticles synthesized with different tungsten precursors (a) WCl₆-WSe₂, (b) W(CO)₆-WSe₂, (c) H₂WO₄-WSe₂.

The FTIR spectra was used to analyse the effects of OLA being used as the capping agent for synthesized WSe₂ nanoparticles. The FTIR spectra of pure OLA and of the WSe₂ samples are depicted in **Figure 4.10**. The WSe₂ samples all displayed the vibrational modes of OLA were present within the materials. The -C-C at 729 cm⁻¹, NH₂ at 795 cm⁻¹, C=C at 963 cm⁻¹, C-N at 1085 cm⁻¹, C-H at 1390 cm⁻¹, CH₃ at 1456 cm⁻¹, NH₂ at 1625 cm⁻¹, C-H at 2845 cm⁻¹, =C-H at 3000 cm⁻¹, NH₂ at 3325 cm⁻¹. The amine head groups of OLA are important in determining how the capping agent is bounded onto the WSe₂ nanoparticles. The NH₂ bends at 795 cm⁻¹ and 1625 cm⁻¹, C-N bend at 1085 cm⁻¹ and the NH₂ stretch at 3325 cm⁻¹. The NH₂ bend at 795 cm⁻¹ was more pronounced on the WCl₆ and W(CO)₆ particles whereas the NH₂ bend at 1625 cm⁻¹ and the C-N bend at 1085 cm⁻¹ were present on all the particles. On all the

particles, the NH_2 stretch at 3325 cm^{-1} disappeared, this implied that OLA was chemisorbed onto the WSe_2 nanoparticles.

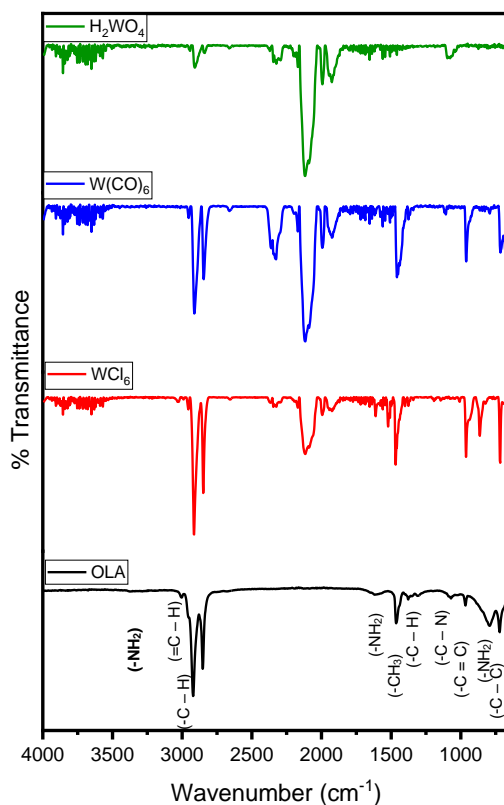


Figure 4.10: FTIR spectra of pure OLA capping agent and capped- WSe_2 nanoparticles synthesized using different tungsten precursors.

4.3. Conclusion

From the study, we could see that the type of tungsten precursor and capping agent used can influence the properties and morphology of WSe_2 formed. WCl_6 and $\text{W}(\text{CO})_6$ in OA produced WSe_2 with no impurities which could be due to their low decomposition temperatures in solution. Whereas H_2WO_4 is the hydrated form of WO_3 therefore making it difficult to convert it fully into WSe_2 without the presence of WO_3 in solution. However, when OLA was used as the capping agent the different precursors all formed WSe_2 nanoparticles containing WO_3 . WSe_2 tends to form nanoflowers but it requires the use of a well-suited capping agent in order to prevent agglomeration. Therefore, OA was found to be the best capping agent that can produce well dispersed flowerlike WSe_2 nanoparticles.

4.4. References

- [1] P. Zhou, P. Schiettecatte, M. Vandichel, A. Rousaki, P. Vandenabeele, Z. Hens and S. Singh, "Synthesis of Colloidal WSe₂ Nanocrystals: Polymorphophism Control by Precursor-Ligand Chemistry," *Crystal Growth & Design*, vol. 21, pp. 1451-1560, 2021.
- [2] T. Kolokoto, V. Mashindi, R. Kadzutu-Sithole, L. F. Machogo-Phao, Z. Ndala, N. Shumbula, S. Nkabinde, G. Ngubeni, S. Gqoba, K. Mubiayi and N. Moloto, "The effect of the metal and selenium precursors on the properties of NbSe₂ and Nb₂Se₉ nanostructures and their application in dye-sensitized solar cells," *RSC Advances*, vol. 11, p. 31159, 2021.
- [3] F. Reale, K. Sharda and C. Mattevi, "From bulk crystals to atomically thin layers of group VI-transition metal dichalcogenides vapour phase synthesis," *Applied Materials Today*, vol. 3, pp. 11-22, 2016.
- [4] M. S. Sokolikova, P. C. Sherrell, P. Palczynski, V. L. Bemmer and C. Mattevi, "Direct solution-phase synthesis of 1T' WSe₂ nanosheets," *Nature Communications*, vol. 10, p. 712, 2019.
- [5] Y. Sun, M. Terrones and R. E. Schaak, "Colloidal Nanostructures of Transition-Metal Dichalcogenides," *Accounts of Chemical Research*, vol. 54, pp. 1517-1527, 2021.
- [6] Y. Cho, T. A. Le, H. Kim, Y. Hong, H. Hwang, G. H. Park, S. Seo and H. Lee, "Unveiling surface charge on chalcogen atoms towards the high aspect-ratio colloidal growth of two-dimensional transition metal chalcogenides," *Nanoscale*, vol. 13, p. 1291, 2021.
- [7] G. Pippia, A. Rousaki, M. Barbone, J. Billet, R. Brescia, A. Polovitsyn, B. Martin-Garcia, M. Prato, F. P. M. De Boni, A. Mhenni, I. Van Driessche, P. Vandenabeele, K. Muller and I. Moreels, "Colloidal Continuous Injection Synthesis of Flourescent MoX₂ (X = S, Se) Nanosheets as a First Step Toward Photonic Applications," *ACS Applied Nano Materials*, vol. 5, pp. 10311-10320, 2022.

- [8] S. Jamil, F. Farooq, S. Khan and M. Janjua, "Synthesis of WSe₂ Nanorods by Selenium Powder Precursor for Photocatalytic Application and Fuel Additive," *Journal of Cluster Science*, vol. 32, pp. 1061-1073, 2021.
- [9] J. H. Nam, M. J. Jang, H. Y. Jang, W. Park, X. Wang, S. M. Choi and B. Cho, "Room-temperature sputtered electrocatalyst WSe₂ nanomaterials for hydrogen evolution reaction," *Journal of Energy Chemistry*, vol. 47, pp. 107-111, 2020.
- [10] G. Zhang and Y.-W. Zhang, "Thermoelectric properties of two-dimensional transition metal dichalcogenides," *Journal of Materials Chemistry C*, vol. 5, p. 7684, 2017.
- [11] R. A. Yadav, N. Padma, S. Sen, K. Chandrakumar, H. Donthula and R. Rao, "Anomalous vibrational behavior of two dimensional tellerium: Layer thickness and temperature dependent Raman spectroscopic study," *Applied Surface Science*, vol. 531, p. 147303, 2020.
- [12] P. Zhou, G. Collins, Z. Hens, K. M. Ryan, H. Geaney and S. Singh, "Colloidal WSe₂ nanocrystals as anodes for lithium-ion batteries," *Nanoscale*, vol. 12, p. 22307, 2020.
- [13] M. Chhowalla, H. S. Shin, G. Eda, L.-J. Li, K. P. Loh and H. Zhang, "The chemistry of two-dimensional layered transition metal dichalcogenide nanosheets," *Nature Chemistry*, vol. 5, pp. 263-275, 2013.
- [14] A. Sierra-Castillo, E. Haye, S. Acosta, C. Bittencourt and J. Colomer, "Synthesis and Characterization of Highly Crystalline Vertically Aligned WSe₂ Nanosheets," *Applied Sciences*, vol. 10, p. 874, 2020.
- [15] W. Jung, S. Lee, D. Yoo, S. Jeong, P. Miro, A. Kuc, T. Heine and J. Cheon, "Colloidal Synthesis of Single-Layer MSe₂ (M = Mo, W) Nanosheets via Anisotropic Solution-Phase Growth Approach," *Journal of the American Chemical Society*, vol. 137, pp. 7266-7269, 2015.
- [16] S. Kumar and U. Schwingenschlogl, "Thermoelectric Response of Bulk and Monolayer MoSe₂ and WSe₂," *Chemistry of Materials*, vol. 27, pp. 1278-1284, 2015.
- [17] Z. Ndala, N. Shumbula, S. Nkabinde, T. Kolokoto, O. Nchoe, P. Shumbula, Z. Tetana, E. Linganiso, S. Gqoba and N. Moloto, "Evaluating teh Effect of

Varying the Metal Precursor in the Colloidal Synthesis of MoSe₂ Nanomaterials and Their Application as Electrodes in the Hydrogen Evolution Reaction," *Nanomaterials*, vol. 10, p. 1786, 2020.

- [18] D. Caruntu, K. Yao, Z. Zhang, T. Austin, W. Zhou and C. O'Connor, "One-Step Synthesis of Nearly Monodisperse, Variable-Shaped In₂O₃ Nanocrystals in Long Chain Alcohol Solutions," *Journal of Physical Chemistry C*, vol. 114, pp. 4875-4886, 2010.
- [19] A. Nandiyanto and R. Ragadhita, "How to Read and Interpret FTIR Spectroscopy of Organic Material," *Indonesian Journal of Science & Technology*, vol. 4, no. 1, pp. 97-118, 2019.
- [20] R. Murakami, Y. Takata, A. Ohta, M. Suzuki, T. Takiue and M. Aratono, "Calorimetric Studies of Aggregate Formation of Oleyl Alcohol in Oil Solutions," *Journal of Physical Chemistry B*, vol. 106, pp. 6548-6553, 2002.
- [21] C. Yang and S. Li, "Size-Dependent Raman Red Shifts of Semiconductor Nanocrystals," *Journal of Physical Chemistry B*, vol. 112, pp. 14193-14197, 2008.
- [22] W. Shi, M.-L. Lin, Q.-H. Tan, X.-F. Qiao, J. Zhang and P.-H. Tan, "Raman and photoluminescence spectra of two-dimensional nanocrystallites of monolayer WS₂ and WSe₂," *2D Materials*, vol. 3, p. 025016, 2016.
- [23] H. Jin, M. Anh, S. Jeong, J. H. Han, D. Yoo, D. H. Son and J. Cheon, "Colloidal Single-Layer Quantum Dots with Lateral Confinement Effects on 2D Exciton," *Journal of the American Chemical Society*, vol. 138, pp. 13253-13259, 2016.
- [24] H. Li, J. Zou, S. Xie, X. Leng, D. Gao, H. Yang and X. Mao, "WSe₂ nanofilms grown on graphite as efficient electrodes for hydrogen evolution reactions," *Journal of Alloys and Compounds*, vol. 725, pp. 884-890, 2017.

Chapter 5

Pt nanocrystals decorated on WSe₂ to form Pt/WSe₂ nanohybrids.

5.1. Introduction

TMDs have gained considerable attention due to their exceptional catalytic, optical, electronic, and mechanical properties [1] [2]. These properties are attributed to their layered structure, which allows for anisotropic electronic and chemical properties, making them suitable for various electrochemical applications [3]. The versatility of TMDs is due to the polymorphism of their monolayers, where the metal coordination exhibits different phases [4]. TMDs have a crystalline structure consisting of repeating layers, which gives rise to their two-dimensional anisotropic properties. WSe₂ exists in the 1T, 1T' and 2H phases whereby the 2H phase is the semiconducting phase that is desirable for photoelectrocatalytic applications. The direct synthesis of WSe₂ generally results in the formation of the thermodynamically stable 2H phase [4]. Additionally, WSe₂ has a band gap in the 1-2 eV range and high optical absorption which makes it suitable to use as a catalyst for photoelectrochemical conversion reactions [5]. WSe₂ has potential application for catalysis of hydrogen evolution as the structure tends to provide active sites for a multitude of mechanisms to take place [3].

An efficient catalytic material is required for water splitting reaction to take place. At the moment, noble metals have been demonstrated to exhibit the highest level of efficiency and stability in various applications however they are expensive and rare therefore not suitable for commercialization [6]. Platinum (Pt) is a precious metal that exhibits excellent electrochemical activity although it is expensive. Therefore, to reduce the amount which will subsequently reduce the overall cost of Pt, a capping agent or support template can be used. This will increase the surface area and dispersion of the metal particles [7].

TMDs can be used as the support template of Pt nanoparticles (PtNPs) with functional catalytic properties as well. This can result in the hybridization of WSe₂ with PtNPs and serve as the anode material required for efficient electrocatalytic reactions to take place. The conductivity of cathode materials can be enhanced by combining TMDs with highly conductive materials, thereby increasing the efficiency of electrochemical activity [8]. The layered structures of TMDs nanosheets have edges that provide active sites for various applications. Morphology control can be used to increase the number

of active sites by transition metal doping [3]. PtNPs can be introduced onto the surface of WSe_2 as cocatalysts for HER. This is achieved by loading Pt onto the surface as the layered structure of WSe_2 has deficiencies that allows doping to take place to generate a p- or n-type material [9]. By controlling the layers of 2D layered nanomaterials, the performance optimization of the electrode catalyst can be achieved, with the loading amount playing a crucial role in determining the outcome [10].

5.2. Methods and Materials

Tungsten hexachloride (WCl_6), tungsten hexacarbonyl ($W(CO)_6$), tungstic acid (H_2WO_4), selenium powder (Se), oleyl alcohol, platinum tetrachloride ($PtCl_4$) and sodium borohydride ($NaBH_4$). All chemicals were purchased at Sigma Aldrich and used without further processing or purification.

WSe_2 nanoflowers were obtained from previous studies in Chapter 4 whereby WSe_2 was synthesised using different tungsten procedures and oleyl alcohol was used as the capping agent. $PtCl_4$ was dissolved in deionised H_2O then placed in a vial containing WSe_2 and sonicated for 15 minutes. Thereafter, $NaBH_4$ was added dropwise into the solution and left to stir at room temperature for 30 minutes. The product obtained was washed with deionised H_2O /ethanol v/v solution and dried in an oven overnight at $80^\circ C$.

5.2.2. Characterization

The Bruker D2 diffractometer was employed to conduct powder X-ray diffraction (PXRD) using $CuK\alpha$ radiation (λ 1.54184 Å) at 30 kV/30mA. UV-vis absorption spectra were obtained using the Varian Cary Eclipse (Cary 50) spectrophotometer within the 200-1100 nm wavelength range. The FEI Technai T12 was utilized to conduct transmission electron microscopy (TEM) at an acceleration voltage of 120 kV. X-ray photoelectron spectroscopy (XPS) measurements were carried out using the Thermo ESCALab 250Xi instrument with monochromatic Al $K\alpha$ (1486.7 eV) X-rays at a power of 300 W and a spot size of 900 μm .

5.3. Results and Discussion

The resultant Pt/ WSe_2 nanohybrids obtained were characterised using PXRD shown in **Figure 5.1**. The diffraction peaks were matched with PDF card numbers 00-001-

1194 Pt Platinum and 01-089-5257 WSe₂. This indicated that both Pt and WSe₂ was presented in the materials. The diffraction peaks observed were broad with most of the intensity being lost in the background noise [11]. The intense peak observed at 14° on the WCl₆ and W(CO)₆ Pt/WSe₂ nanohybrid samples indicate that WSe₂ was multi-layered. However, this peak was not observed on H₂WO₄ Pt/WSe₂ sample. Instead an intense peak at 24° was observed which indicates the presence of tungsten oxide (WO₃) which was observed in previous chapters as well. This is due to H₂WO₄ being the hydrated form of WO₃ therefore it is difficult to convert it completely into WSe₂. An amorphous peak is also observed at ~25° for all three samples which suggests Pt/WSe₂ nanohybrids were formed. The characteristic diffraction peaks at 39.6° and 46.6° correspond to the (1 1 1) and (2 0 0) planes of face-centred cubic (fcc) structure of Pt [7].

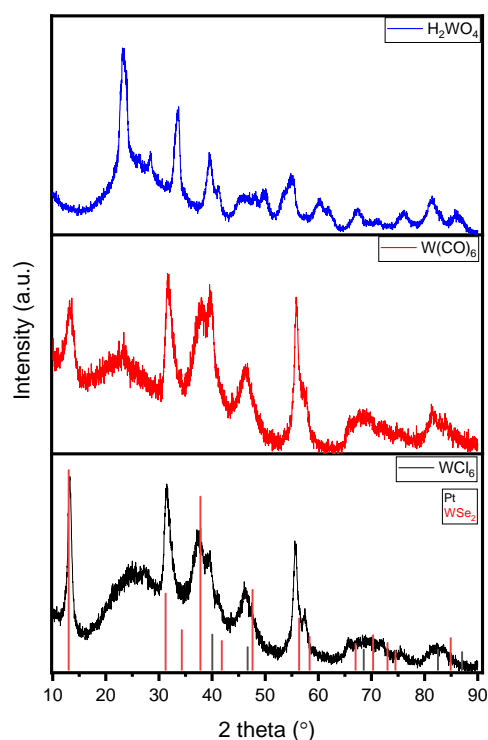


Figure 5.1: PXR D patterns showing the Pt/WSe₂ nanohybrids synthesized using different tungsten precursors.

UV-vis spectroscopy is a characterization technique used to measure the optical properties of Pt/WSe₂ nanohybrids shown in **Figure 5.2**. The Pt/WSe₂ nanohybrids have a wide absorption range with no distinct peaks observed from 300 – 700 nm [12]. UV-vis was also used to confirm the formation of PtNPs [12]. The synthesis of PtNPs was confirmed by absorption observed within the 200 – 300 nm range [14]. Thereafter,

there were no distinct peaks observed until ~ 700 nm whereby the four excitons confirming the 2H phase of WSe_2 were observed as mentioned in previous chapters.

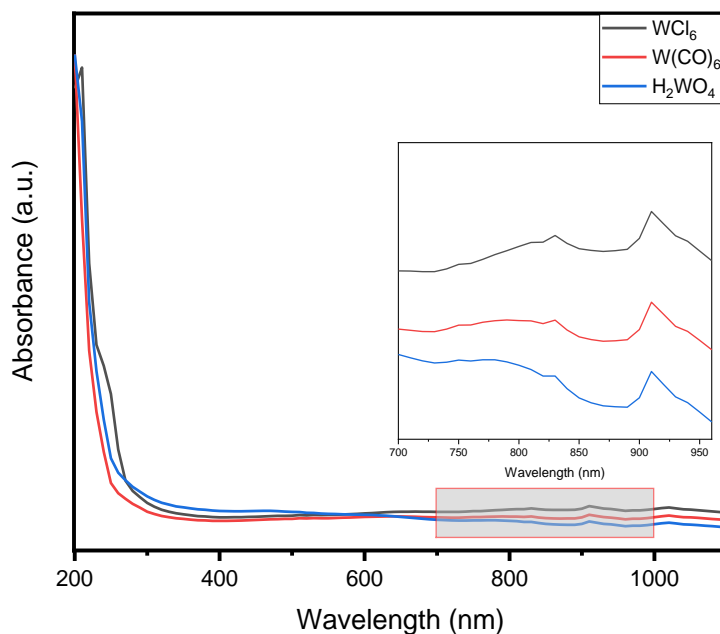


Figure 5.2: UV-vis absorption spectra showing the Pt/WSe₂ nanohybrids synthesized using different tungsten precursors.

The morphologies of the of the Pt/WSe₂ nanohybrids were characterized with TEM imaging and the images obtained are found in **Figure 5.3**. From the images, the WSe₂ nanoflowers were successfully decorated with PtNPs. The images show that the PtNPs are on the surface of the WSe₂ nanoflowers. The PtNPs obtained were spherical in structure and unevenly dispersed on the surface of WSe₂. Then uneven distribution of PtNPs could potentially affect the electrocatalytic activity of the nanohybrids. PtNPs tends to form spherical or near-spherical structures which was observed on the images [15]. The images also revealed a random distribution of the PtNPs on the surface of the WSe₂ nanoflowers which could result from post-synthetic agglomeration of the nanoparticles [7]. This observation could be related to the amorphous structure reported in the PXRD patterns of the nanohybrids. The surface of the nanoparticles being amorphous could result from not using a capping agent during the synthesis of PtNPs. The presence of a capping agent contributes to the surface reaction hence it could have prevented the surface of the NPs being

amorphous. As the purpose of a capping agent is to control the particle size and morphology of the Pt nanocrystals [16].

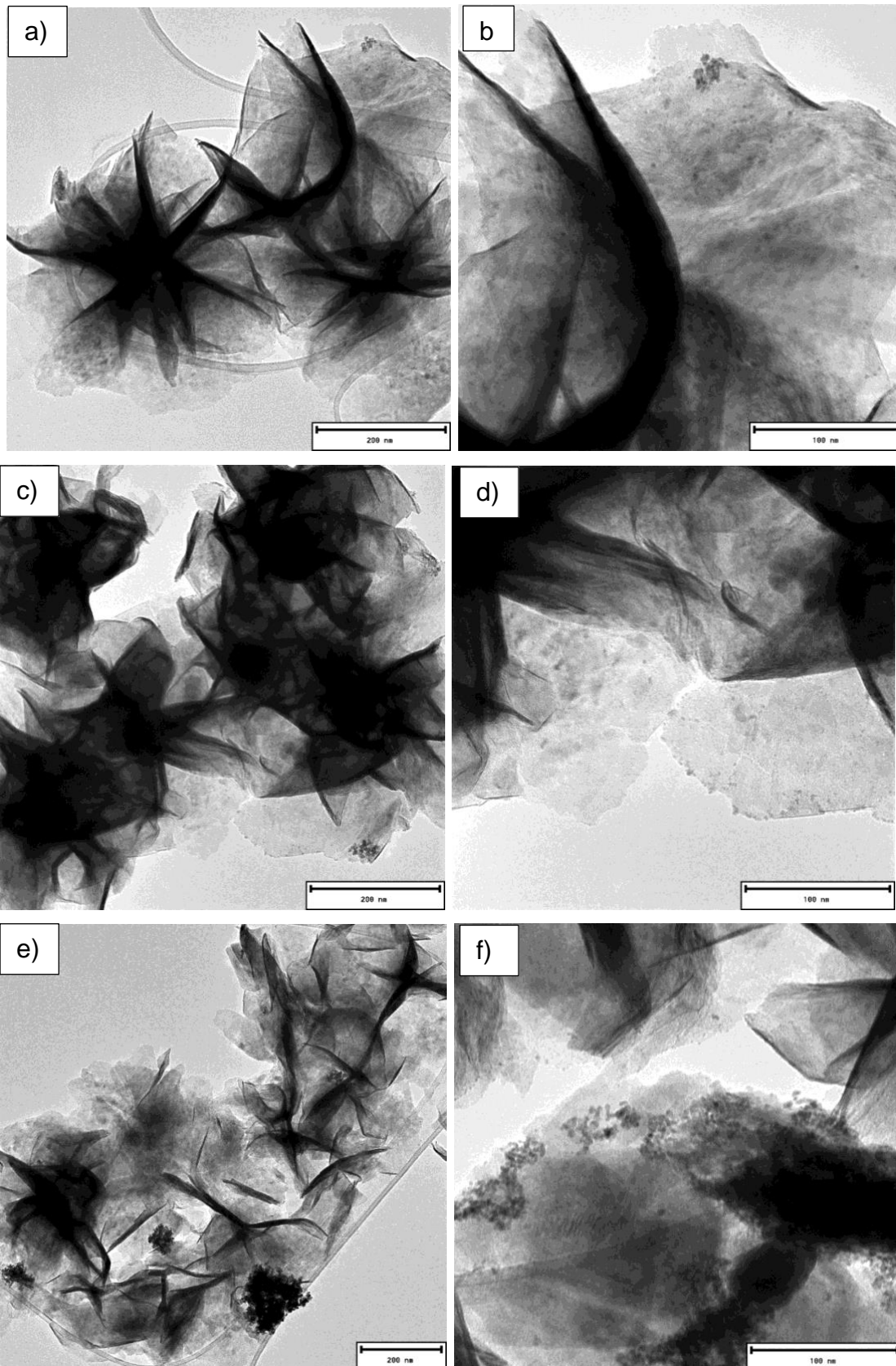


Figure 5.3: TEM images of Pt/WSe₂ synthesized with different tungsten precursors (a) WCl₆, (b) WCl₆, (c) W(CO)₆, (d) W(CO)₆, (e) H₂WO₄, (f) H₂WO₄.

Figure 5.4 shows the XPS spectrum of the Pt/WSe₂ (WCl₆) nano hybrids, which reveals the elemental compositions and corresponding binding energies of the sample. The spectrum indicates the presence of W, Se, Pt, C, and O. The carbon signal is attributed to the capping agent used for WSe₂, while the oxygen signal is also caused by the capping agent, oleyl alcohol. The percentage atomic composition shown in **Table 5.1** shows a high percentage of C, 66.5% attributed to oleyl alcohol. The next highest percentage observed is due to Se, at 16.4% which was used in excess relative to W at 9.2%. the percentage of O was relatively low at 4.9% which is attributed to the capping agent. The % atomic composition of Pt is relatively low at 3.0% due to a small loading amount being used.

The high resolution XPS spectra of WCl₆ depicted in **Figure 5.5** were used to examine the surface of the sample in greater detail, focusing on the C1s, Se3ds, W4f7, Pt4f7, and O1s core levels. The deconvoluted C–C peak observed in the C1s spectrum is attributed to oleyl alcohol, while the presence of C–O and O–C=O peaks indicates the oxidation of the capping agent. The O1s peak also suggests the oxidation of the capping agent as well as the presence of WO₃. The W4f7 core level spectrum is characterized by two components: W;WSe₂ at 31.5 eV and W4f7 (WO₃) at 35.1 eV. The Se 3ds core level spectrum shows one peak that is attributed to WSe₂. The Pt4f7 core level spectrum is characterized by two components Pt 71.1 eV and PtO₂ 75.4 eV.

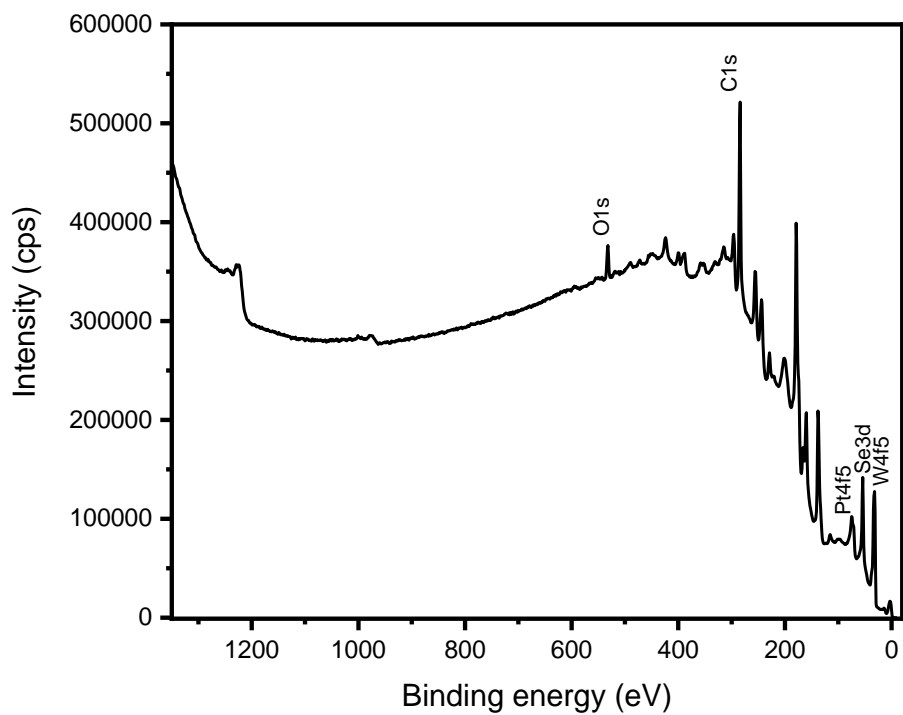
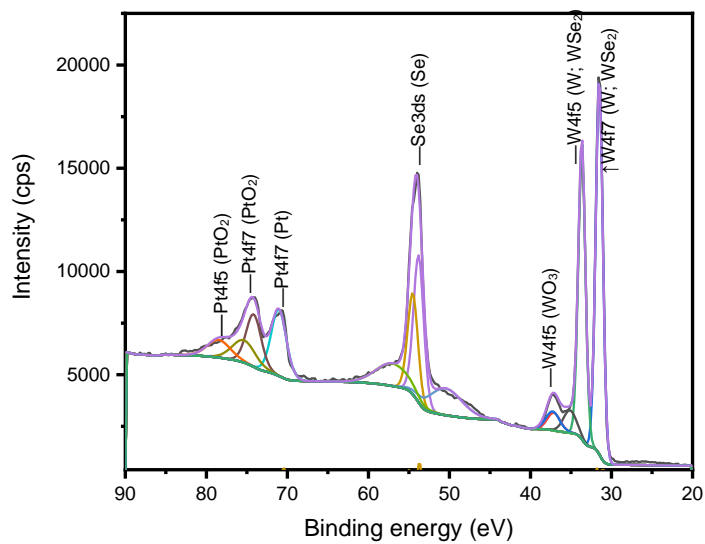


Figure 5.4: XPS survey spectra of Pt/WSe₂ synthesized using WCl₆ precursor.



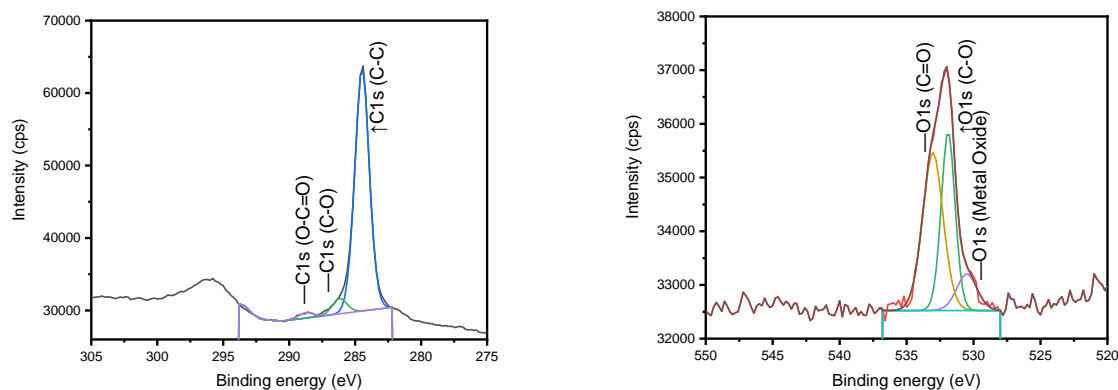


Figure 5.5: High resolution core level spectra of WCl_6 Pt/ WSe_2 nanohybrid with the focus on C1s, O1s, W4f7, Se3ds and Pt4f7.

Table 5.1: A summary of the stoichiometric assignments of the atomic composition, which were obtained from fitting the XPS spectra presented in Fig. 5.4 and 5.5.

Element	Atomic %	Peak Binding energy (eV)	Assignments	Assignment %
C	66.5	284.3	C-C	65.5
			C-O	4.2
			O-C=O	1.5
O	4.9	532.2	Metal Oxide	0.7
			C-O	2.3
			C=O	3.0
W4f5	9.2	32.4	W; WSe_2	4.4
			WO_3	0.4
Se3d	16.4	54.1	Selenide	16.4
Pt4f5	3.0	73.8	Pt	1.1
			PtO_2	0.6

The XPS spectrum presented in **Figure 5.6** of the Pt/ WSe_2 nanohybrids revealed the elemental composition and corresponding binding energies of the $W(CO)_6$ sample. The spectrum indicated the presence of W, Se, Pt, C, and O. The C originated from the capping agent, while the O was a result of the oxidation of the capping agent and the metal oxides found on the surface of the nanoparticles. **Table 5.2.** shows the %

atomic composition whereby C at 62.5% has the highest percentage due to the capping agent. The percentage of O is relatively low at 3.5% which is also attributed to the capping agent and the oxidation of oleyl alcohol as well as the metal oxides. The % atomic composition of Se was relatively high at 21.5% followed by W at 9.3%. The % atomic composition of Pt was relatively low at 3.2%.

High resolution XPS was performed for further analysis of C1s, O1s, Se3ds, W4f7 and Pt4f7 shown in **Figure 5.7**. The deconvoluted C–C peak observed in the C1s core level spectrum is attributed to the capping agent, while the presence of C–O is due to the oxidation of the capping agent, oleyl alcohol. The O1s peak also indicates that oxidation of the capping agent occurred. The W4f7 core level spectrum has three peaks assigned to W; WSe₂ (31.6 eV), WO₂ (32.1 eV) and WO₃ (35.4 eV). The Se3ds (54.3 eV) is due to WSe₂. The Pt4f7 core level spectrum peaks are caused by Pt (71.5 eV) and PtO₂ (75.6 eV).

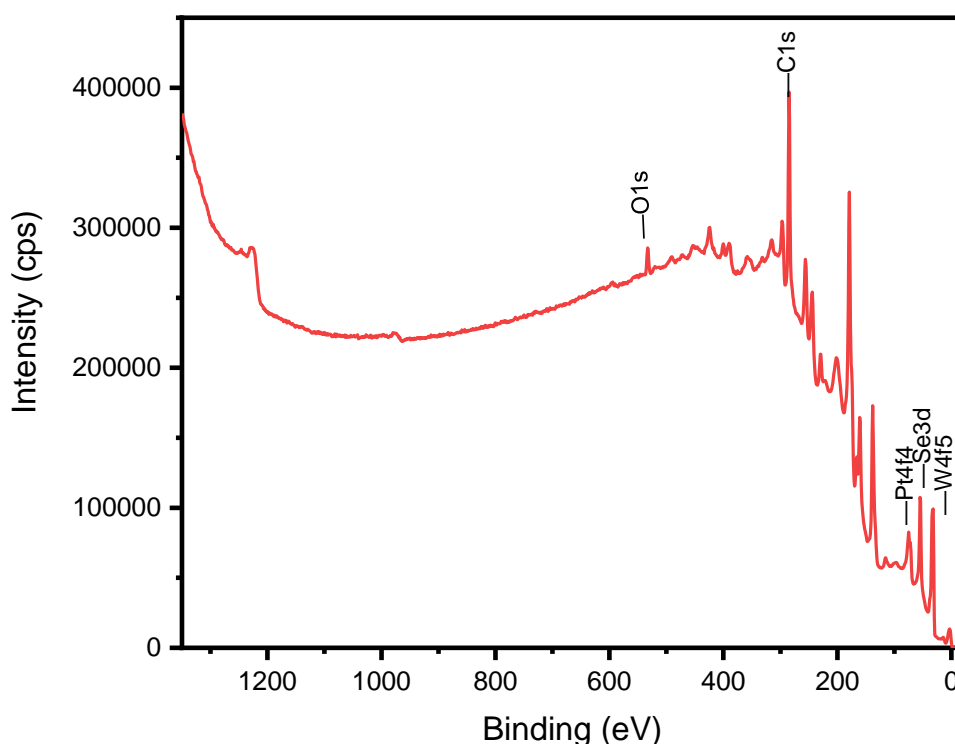


Figure 5.6: XPS survey spectra of Pt/WSe₂ synthesized using W(CO)₆ precursor.

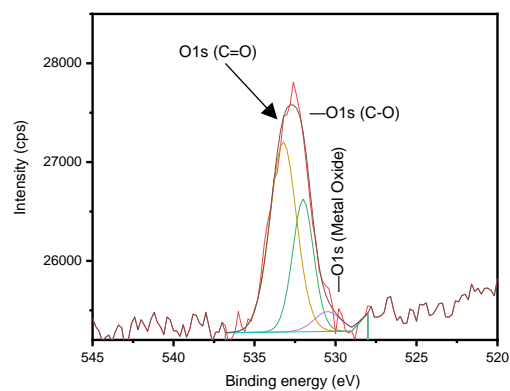
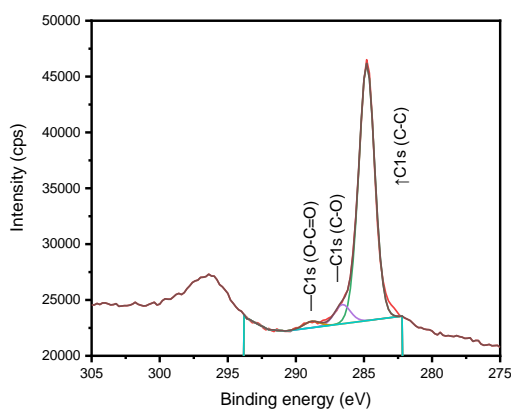
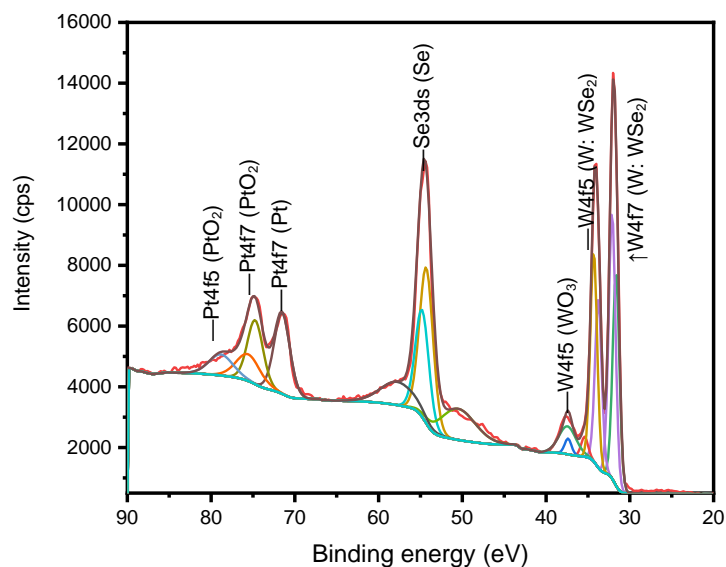


Figure 5.7: High resolution core level spectra of $W(CO)_6$ Pt/ WSe_2 nanohybrid with the focus on C1s.

Table 5.2: A summary of the stoichiometric assignments of the atomic composition, which were obtained from fitting the XPS spectra presented in Fig. 5.6 and 5.7.

Element	Atomic %	Peak Binding energy (eV)	Assignments	Assignment %
C	62.5	284.3	C-C	63.6
			C-O	4.8
			O-C=O	1.6
O	3.5	532.8	Metal Oxide	0.3

			C-O	1.5
			C=O	2.8
W4f5	9.3	32.8	W; WSe ₂	2.1
			WO ₂	2.6
			WO ₃	0.2
Se3d	21.5	54.4	Selenide	18.7
Pt4f5	3.2	74.5	Pt	1.2
			PtO ₂	0.6

The XPS spectrum of the Pt/WSe₂ (H₂WO₄) nanohybrids showed the presence of W, Se, Pt, C and O in **Figure 5.8**. The highest % atomic composition is attributable to C at 71.2% due to the capping agent. The percentage of C is fairly high at 9.8% and it is also attributed to the capping agent and the oxidation of the capping agent, oleyl alcohol. The % atomic composition of Se is considerably high at 10.6%. Whereas W and Pt are at 6.1% and 2.3% respectively.

Figure 5.9 shows the high resolution XPS spectrum that focuses on C1s, O1s, W4f7, Se3ds and Pt4f7. The core level spectrum shows the deconvoluted C–C peak caused by the capping agent C–O and O–C=O observed is due to the oxidation of the capping agent. The O1s peak is caused by the oxidation of the capping agent and the metal oxides found on the surface. The W4f7 is split into two components, W; WSe₂ (31.3 eV) and WO₃ (35.1 eV) which was observed on PXRD as well. The Se3ds core level spectrum has one peak caused by WSe₂. Then Pt4f7 has two peaks characterized by Pt (70.8 eV) and PtO₂ (72.5 eV).

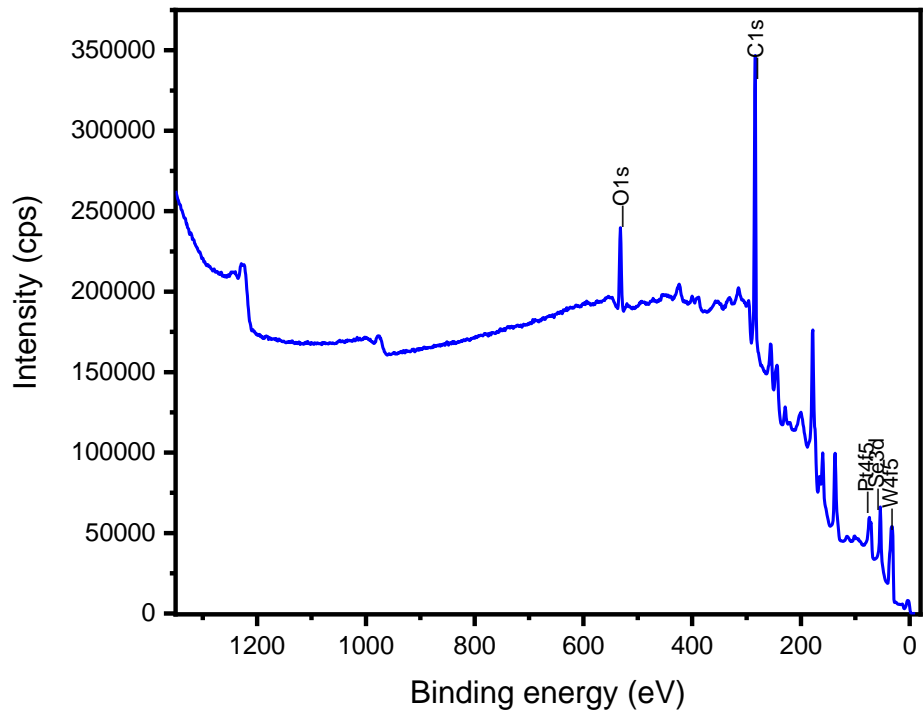
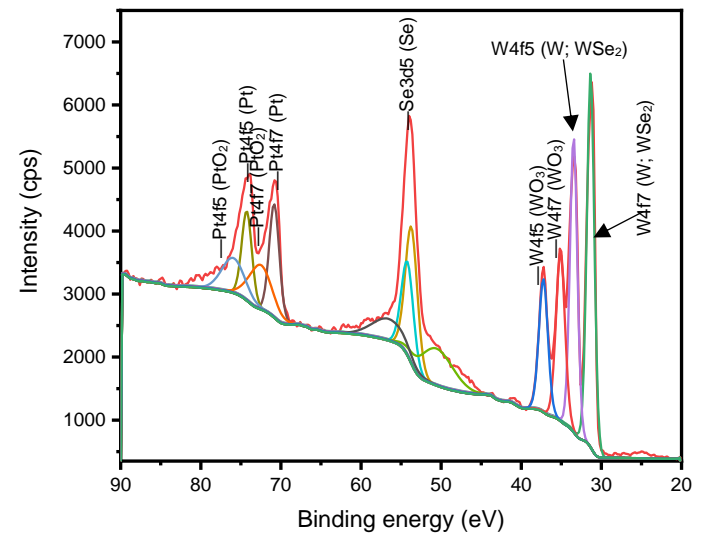


Figure 5.8: XPS survey spectra of Pt/WSe₂ synthesized using H₂WO₄ precursor.



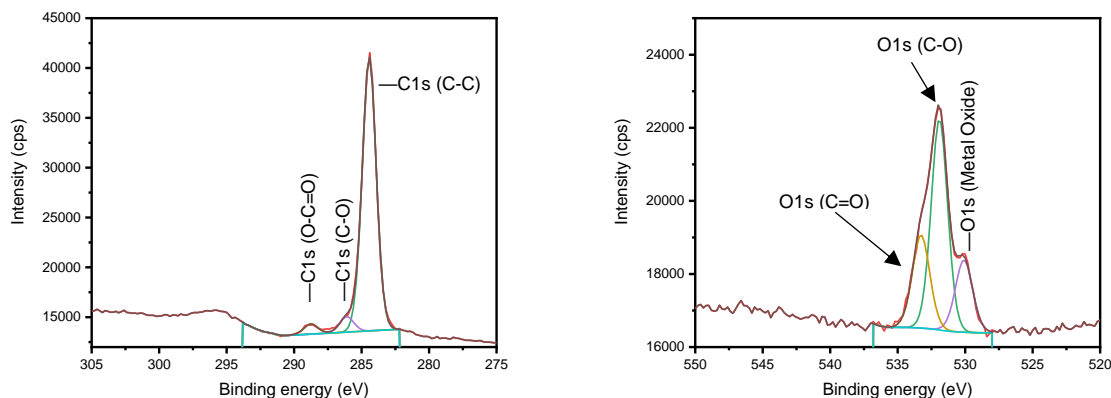


Figure 5.9: High resolution core level spectra of H₂WO₄ Pt/WSe₂ nano hybrid with the focus on C1s, O1s, W4f7, Se3ds and Pt4f7.

Table 5.3: A summary of the stoichiometric assignments of the atomic composition, which were obtained from fitting the XPS spectra presented in Fig. 5.8 and 5.9.

Element	Atomic %	Peak Binding energy (eV)	Assignments	Assignment %
C	71.2	284.3	C-C	69.0
			C-O	3.9
			O-C=O	2.6
O	9.8	532.0	Metal Oxide	2.3
			C-O	6.3
			C=O	3.0
W4f5	6.1	32.4	W; WSe ₂	2.5
			WO ₃	1.3
Se3d	10.6	53.9	Selenide	8.1
Pt4f5	2.3	72.9	Pt	0.6
			PtO ₂	0.5

5.4. Conclusion

Three tungsten precursors were used to synthesize WSe_2 nanoflowers thereafter the nanoflowers were decorated with Pt nanocrystals. This resulted in the formation of Pt/ WSe_2 nanohybrids. The nanohybrid were characterized using several techniques to analyse the compositional and structural properties of the nanomaterials. The multi-layered WSe_2 structures were successfully decorated with Pt nanocrystals however unevenly distributed on the surface. The H_2WO_4 precursor resulted in Pt/ WSe_2 containing impurities not observed in the other two precursors due to the high presence of oxygen observed on XPS. However, the presence of oxygen in the nanohybrids was observed in all three samples due to the oxidation of the capping agent oleyl alcohol. TEM showed that the amount of Pt decorated on the nanoflowers was small, XPS analysis verified the existence of Pt in the nanohybrids was relatively low due to a small loading.

5.5. References

- [1] J. Q. Geisenhoff, A. K. Tamura and A. M. Schimpf, "Using ligands to control reactivity, size and phase in the colloidal synthesis of WSe₂ nanocrystals," *Chem. Commun.*, vol. 55, pp. 8856-8859, 2019.
- [2] H. Jin, M. Ahn, S. Jeong, J. H. Han, D. Yoo, D. H. Son and J. Cheon, "Colloidal Single-Layer Quantum Dots with Lateral Confinement Effects on 2D Exciton," *Journal of the American Chemical Society*, vol. 138, pp. 13253-13259, 2016.
- [3] A. A. Tedstone, D. J. Lewis and P. O'Brien, "Synthesis, Properties, and Applications of Transition Metal-Doped Layered Transition Metal Dichalcogenides," *Chemistry of Materials*, vol. 28, pp. 1965-1974, 2016.
- [4] M. S. Sokolikova, P. C. Sherrell, P. Palczynski, V. L. Bemmer and C. Mattevi, "Direct solution-phase synthesis of 1T' WSe₂ nanosheets," *Nature Communications*, vol. 10, p. 712, 2019.
- [5] M. S. Delphine, M. Jayachandran and C. Sanjeeviraja, "Pulsed electrodeposition and characterization of tungsten diselenide thin films," *Materials Chemistry and Physics*, vol. 81, pp. 78-83, 2003.
- [6] M. D. Khan, M. Opallo and N. Revaprasadu, "Colloidal synthesis of metal chalcogenide nanomaterial from metal-organic precursors and capping ligand effect on electrocatalytic performance: progress, challenges and future perspectives," *Dalton Transactions*, vol. 50, pp. 11347-11359, 2021.
- [7] C. Huff, E. Biehler, Q. Quach, J. M. Long and T. M. Abdel-Fattah, "Synthesis of highly dispersive platinum nanoparticles and their application in a hydrogen generation reaction," *Colloids and Surfaces A: Physicochemical and Engineering Aspects*, vol. 610, p. 125734, 2021.
- [8] P. Zhou, G. Collins, Z. Hens, K. Ryan, H. Geaney and S. Singh, "Colloidal WSe₂ nanocrystals as anodes for lithium-ion batteries," *Nanoscale*, vol. 12, pp. 22307-22316, 2020.
- [9] P. D. Antunez, D. H. Webber and R. L. Brutchey, "Solution-Phase Synthesis of Highly Conductive Tungsten Diselenide Nanosheets," *Chemistry of Materials*, vol. 25, pp. 2385-2387, 2013.

- [10] J. H. Nam, M. Jang, H. Jang, W. Park, X. Wang, S. Choi and B. Cho, "Room-temperature sputtered electrocatalyst WSe₂ nanomaterials for hydrogen evolution reaction," *Journal of Energy Chemistry*, vol. 47, pp. 107-111, 2020.
- [11] P. Zhou, P. Schiettecatte, M. Vandichel, A. Rousaki, P. Vandenabeele, Z. Hens and S. Singh, "Synthesis of Colloidal WSe₂ Nanocrystals: Polymorphism Control by Precursor-Ligand Chemistry," *Crystal Growth & Design*, vol. 21, pp. 1451-1460, 2021.
- [12] L. Yuwen, F. Xu, B. Xue, Z. Luo, Q. Zhang, B. Bao, S. Su, L. Weng, W. Huang and L. Wang, "General synthesis of noble metal (Au, Ag, Pd, Pt) nanocrystal modified MoS₂ nanosheets and the enhanced catalytic activity of Pd-MoS₂ for methanol oxidation," *Nanoscale*, vol. 6, pp. 5762-5769, 2014.
- [13] R. Karthik, R. Sasikumar, S.-M. Chen, M. Govindasam, J. V. Kumar and V. Muthuraj, "Green Synthesis of Platinum Nanoparticles Using Quercus Glauca Extract and Its Electrochemical Oxidation of Hydrazine in Water Samples," *International Journal of Electrochemical Science*, vol. 11, pp. 8245-8255, 2016.
- [14] M. A. R. Khan, M. Mamun and M. Ara, "Review on platinum nanoparticles: Synthesis, characterization, and applications," *Microchemical Journal*, vol. 171, p. 106840, 2021.
- [15] S. Cheong, J. Watt, B. Ingham, M. Toney and R. Tilley, "In Situ and Ex Situ Studies of Platinum Nanocrystals: Growth and Evolution in Solution," *Journal of American Chemical Society*, vol. 131, pp. 14590-14595, 2009.
- [16] T. Tajerian, M. Monsefi and A. Rowan, "Simple chemistry drives controlled synthesis of platinum nanocrystal to micron size," *Journal of Nanostructure in Chemistry*, vol. 9, pp. 197-202, 2019.

Chapter 6

Pt/WSe₂ nanohybrids as the electrode in electrocatalytic HER

6.1. Introduction

Electrochemical water splitting reaction is a promising technique that can be used to produce clean H₂ [1]. Water splitting refers to the process of breaking down water into its constituent parts H₂ and O₂. Electrochemical reaction takes place in a cell that is made up of an anode, cathode, and electrolyte solution for internal ionic conductivity [2]. This reaction requires the use of a highly efficient semiconducting material [3]. Semiconductors possess the property to act as photocatalysts that can initiate the chemical reduction and oxidation processes under light irradiation [3]. Semiconducting material is the key component that boosts redox reactions [1]. When a water-splitting cell is operated, two reactions occur at the electrodes: the anodic oxygen evolution reaction (OER) and the cathodic hydrogen evolution reaction (HER)[4]. The overall result is the production of oxygen and hydrogen gas.

Electrocatalytic generation of H₂ from water is an electrochemical process that takes place in either acidic conditions or alkaline media [5]. Highly catalytic electrodes play a critical role in HER. The HER process requires an efficient electrode with a high catalytic surface area, and platinum (Pt) has been found to be the most effective due to its ability to provide a large surface area with low metal weight [6]. Other electrocatalytic properties that make Pt a suitable candidate for HER include, high exchange current density, low overpotential and low Tafel slope [7]. However, Pt is a noble metal which makes it expensive with low abundance in nature [8]. Therefore, two strategies have been proposed to address this issue. The first is to discover new electrocatalysts that have similar HER properties to Pt but are made from inexpensive and abundant elements. The second approach is to decrease the amount of Pt utilized in the electrocatalytic HER process [9].

Transition metal dichalcogenide (TMDs) such as WSe₂ have gained significant attention as potential catalysts for the HER process due to their unique physical and chemical properties, such as sizable bandgaps and crystalline structures [10] [11]. WSe₂ has been recognized as a potent electrocatalyst for HER due to the edge sites of the nanosheets which provide abundant charge transfer that can increase the electrocatalytic performance [11]. However, WSe₂ on its own is not as efficient as Pt

which is why we propose decorating WSe₂ with Pt to improve its electrocatalytic activity.

Herein, Pt/WSe₂ nanohybrids obtained in the previous chapter were investigated as potential electrocatalysts for electrocatalytic HER. The nanomaterials were characterised through electrochemical reactions such as cyclic voltammetry (CV), linear sweep voltammetry (LSV), and electrochemical impedance spectroscopy (PEIS). The electrochemistry experiments were conducted via a three-electrode system consisting of a counter, reference and working electrode. Certain characteristics of these experiments help with determining the electrocatalytic activity of the materials.

6.2. Experimental

6.2.1. Chemicals

The Pt/WSe₂ nanohybrids, which were previously discussed in the previous chapter, were prepared using different precursors such as WCl₆, W(CO)₆, and H₂WO₄, as well as sulfuric acid (H₂SO₄, ≥ 99.9%), Nafion (5 wt%), isopropanol (≥ 99.9%), commercial Pt/C (Tanaka Kikinzoku Kogyo K.K., 20 wt%), and carbon black-Vulcan (XC 72R). The 0.5 M H₂SO₄ solution was prepared using deionized water purified using a Millipore system. All chemicals were used as received without any further purification.

6.2.2. Electrochemical measurements and preparation of the working electrode

The electrochemical tests were performed utilizing a Biologic SP300 potentiostat with a 3-electrode setup in 0.5 M H₂SO₄. The working electrode was a glass carbon coated with Pt/WSe₂ nanohybrid (surface area = 0.196 cm²) obtained from WCl₆, W(CO)₆, or H₂WO₄, and potentials were recorded with respect to the reversible hydrogen electrode (RHE). The reference electrode was an Ag/AgCl electrode, and the counter electrode was a Pt wire. The working electrode was prepared by combining Pt/WSe₂ with carbon black, Nafion, isopropanol, and ultrapure H₂O. The Ag/AgCl reference electrode was adjusted with respect to the reference hydrogen electrode (RHE) by adding a value of (0.197 + 0.059 pH), and all potentials were measured against RHE. All measurements were conducted under ambient conditions, and the catalyst ink was sonicated for 30 min at room temperature (RT) before a 10 μL aliquot was pipetted onto the glassy carbon electrode and allowed to dry at room temperature.

6.3. Results and Discussion

Figure 6.1(a) shows the results of the LSV experiment conducted using a conventional 3-electrode configuration system to determine the electrocatalytic HER activity of the nano hybrids in a 0.5 M H₂SO₄ solution at a scan rate of 10 mVs⁻¹. For comparison, Pt/C (20 wt%) was also tested and was found to display excellent HER activity based on its onset potential. The LSV polarisation curves showed that nano hybrids from W(CO)₆ performed better than the other two nano hybrids. The curves also revealed that WCl₆, W(CO)₆ and H₂WO₄ derived nano hybrids required overpotentials of 344, 281 and 494 mV to produce a current density of 10 mA.cm⁻¹, respectively. In acid media, HER is characterised by three potential reactions namely, Volmer, Heyrovsky and Tafel reaction.

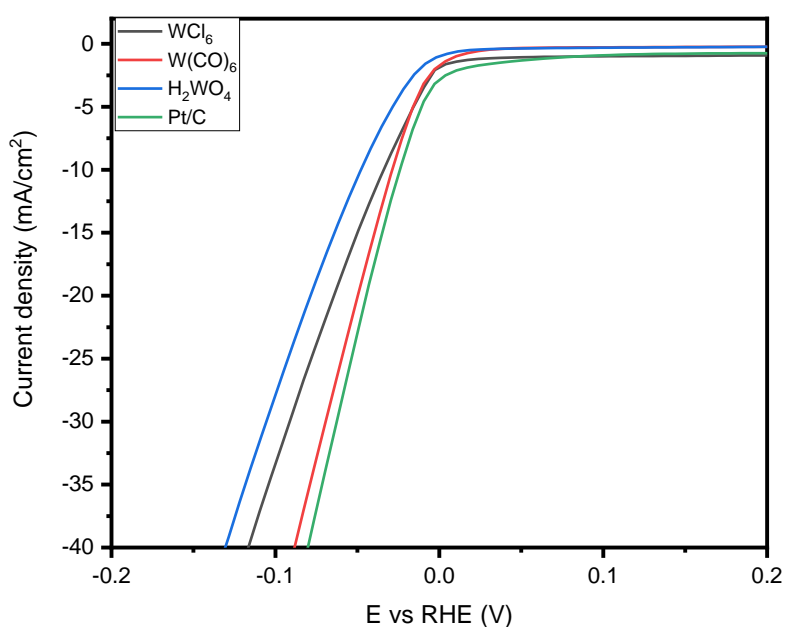


The calculated Tafel slopes were obtained for the aforementioned reactions, at 25 °C is 120, 40 and 30 mV.dec⁻¹, respectively [12]. The Tafel slope, which can be determined from the Tafel equation, is a crucial parameter for electrocatalysts, as it provides information about the reaction mechanism and the rate-determining step. A Tafel slope of 120 mV.dec⁻¹ indicates that the rate-determining step is the Volmer reaction. On the other hand, Tafel slopes of 40 mV.dec⁻¹ and 30 mV.dec⁻¹ suggest that the Heyrovsky or Tafel reaction is the rate-determining step, respectively. In this study, the Tafel slopes were obtained by extrapolating the LSV curves (η vs log(j)) using the Tafel equation in order to investigate the mechanisms of the Pt/WSe₂ nano hybrids (eq. 4).

$$\eta = b \log j + a \quad \text{eq. 4}$$

The overpotential is represented by η , b represents the Tafel slope and j relates to the current density and 'a' is the intercept which is generally assumed to be log(j₀) at $\eta = 0$. The Tafel slopes of Pt/C and Pt/WSe₂ nano hybrids are shown in **Figure 6.1(b)**. The Pt/C electrocatalyst had the smallest Tafel slope of 39.96 mV.dec⁻¹ which indicates faster transfer kinetics [13]. Then the Tafel slopes of the Pt/WSe₂ nano hybrids were 92.42, 64.20 and 80.03 mV.dec⁻¹ for WCl₆, W(CO)₆ and H₂WO₄ respectively. Since the calculated Tafel slopes of the Pt/WSe₂ nano hybrids lie within the 40-120 mV.dec⁻¹ range, this indicates that the Volmer-Heyrovsky mechanism was the common

pathway for the electrocatalysts. This means the reaction between H_{ads} , H^+ and e^- to generate hydrogen is the rate determining step [12]. The $W(CO)_6$ electrocatalyst has the smaller Tafel slope compared to the WCl_6 and H_2WO_4 electrocatalyst therefore this implies that it has faster kinetics with high H_2 generating rates. Previous studies have reported the Tafel slope of WSe_2 to be $137\text{ mV}\cdot\text{dec}^{-1}$, this implies that the Pt/WSe_2 nanohybrids have a smaller Tafel slope therefore more favourable HER reaction kinetics [14]. The overpotentials required to reach $10\text{ mA}/\text{cm}^2$ and corresponding Tafel slopes obtained in this study are comparable to those of other WSe_2 electrocatalysts (summarized in **Table 6.1**).



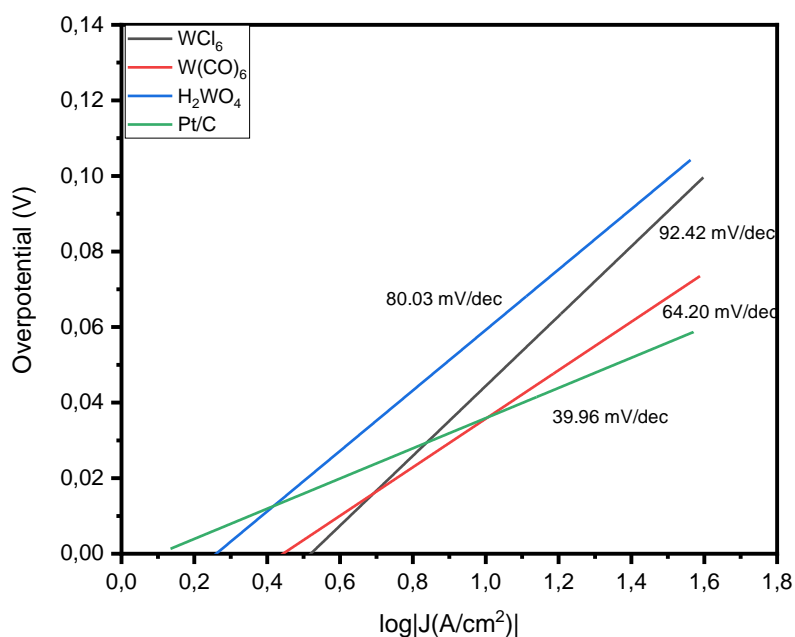


Figure 6.1: (a) LSV polarization curves of Pt/C, WCl₆, W(CO)₆ and H₂WO₄ Pt/WSe₂ nano hybrids at a scan rate of 10 mV/s; (b) corresponding Tafel plots for Pt/C, WCl₆, W(CO)₆ and H₂WO₄ Pt/WSe₂ nano hybrids.

Table 6.1: Comparison of catalytic activity of WSe₂ electrocatalysts in 0.5 M H₂SO₄.

HER catalyst	η_{10} (mV)	Tafel slope (mV/dec)	Ref
WCl ₆	-33.6	92.4	This work
W(CO) ₆	-28.1	64.2	This work
H ₂ WO ₄	-48.6	80.0	This work
WSe ₂	-239	80	[10]
WSe ₂	650	178	[15]
2H WSe ₂	640	232	[16]

CV was used to determine the catalytic activity of the Pt/WSe₂ nano hybrids shown in **Figure 6.2** with a scan rate of 10 mV.s⁻¹. The redox peaks were observed had varying peak intensities for the different Pt/WSe₂ nano hybrids. The anodic peak observed at 1.06 V and the cathodic peak was observed at 0.44 V. The peak voltage values (E_p) for the forward scan were constant for the nano hybrids at 1.06 V but the peak current density values (J_p) varied at 0.96, 2.4 and 0.27 mA.cm⁻² for WCl₆, W(CO)₆ and H₂WO₄

respectively. The same was observed on the reverse scan whereby E_p was constant at 0.44 V and J_p was -0.57, -2.03 and -0.19 mA.cm⁻² for WCl_6 , $W(CO)_6$ and H_2WO_4 . For all three samples, the cathodic current peak was more intense than the anodic peak which suggests better catalytic capability of the electrocatalysts towards the reduction of H^+ to H_2 . Of the three nanohybrids, $W(CO)_6$ had the highest current density which suggest that $W(CO)_6$ Pt/WSe₂ has better catalytic activity therefore faster kinetics [17]. High current density indicates high catalytic activity whereby the performance of the nanocatalyst strongly depends on the surface structure of the nanomaterial [18]. In chapter 5, the Pt/WSe₂ nanohybrids exhibited nanoflower-like WSe₂ structures decorated with Pt nanocrystals. This structure provides a high surface area that improves the catalytic activity of the materials observed above.

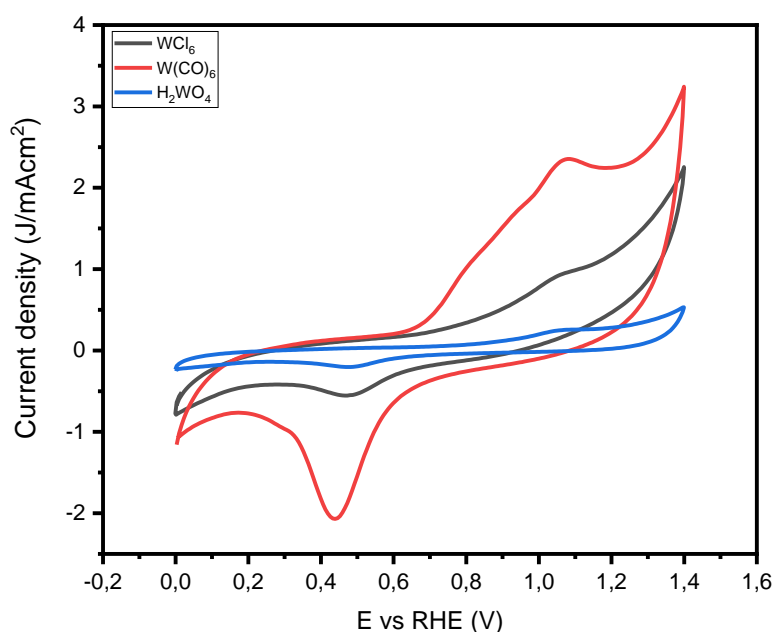


Figure 6.2: Cyclic voltammograms of WCl_6 , $W(CO)_6$ and H_2WO_4 - derived Pt/WSe₂ nanohybrids at a scan rate of 10 mV/s.

The ability of the nanohybrids to transfer charge to the electrolyte was evaluated using EIS. **Figure 6.3** shows the Nyquist plots of WCl_6 , $W(CO)_6$ and H_2WO_4 - derived Pt/WSe₂ nanohybrids. $W(CO)_6$ (10.2 Ω) has the smallest semicircle which indicates a small transfer resistance. The resistance measured in EIS is related to the ability of the electrode material to transfer electrons to the ions present in the solution [19]. This

suggests that this precursor is more effective at facilitating the transfer of electrons between the electrode material and the electrolyte. The impedance of H_2WO_4 (17.9 Ω) was also relatively smaller than WCl_6 (33.3 Ω). Based on this observation, $\text{W}(\text{CO})_6$ is the most conductive material followed by H_2WO_4 lastly, WCl_6 . The values obtained were significantly lower than previous studies done on WSe_2 nanoflowers which implies that the Pt decorated WSe_2 nanoflowers were more conductive [15].

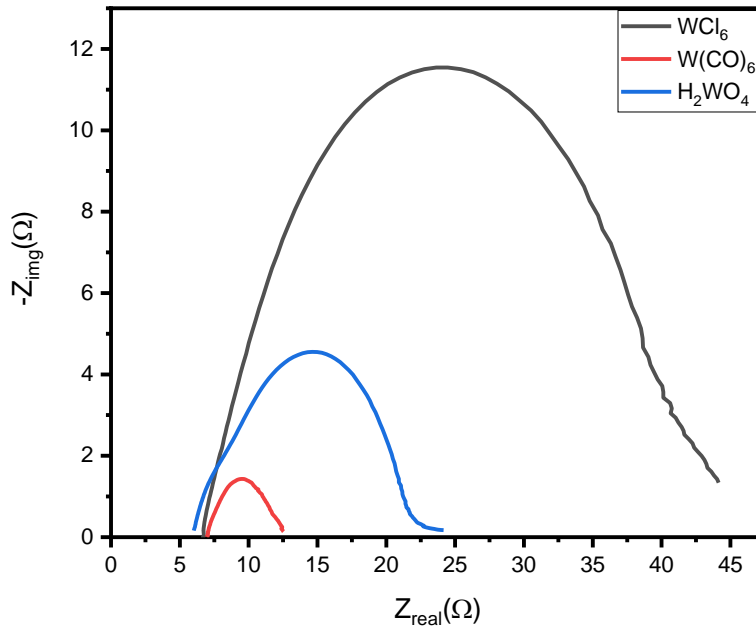


Figure 6.3: Nyquist plots of WCl_6 , $\text{W}(\text{CO})_6$ and H_2WO_4 Pt/ WSe_2 nanohybrids.

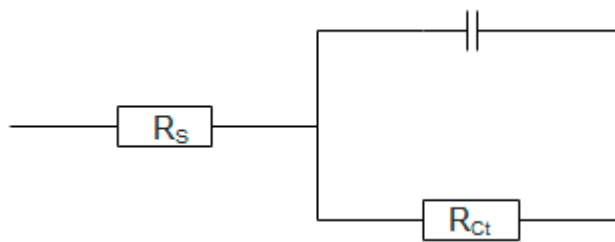


Figure 6.4: Equivalent circuit of the measured impedance spectra.

Table 6.2: Electrocatalytic parameters of the Pt/WSe₂ nanohybrids using different tungsten precursors.

Electrocatalytic parameters	WCl₆	W(CO)₆	H₂WO₄
Onset potential	54.4 mV	33.1 mV	17 mV
η_{10}	-33.6 mV	-28.1 mV	-49.4 mV
Tafel slope	92.4 mV/dec	64.2 mV/dec	80.0 mV/dec
J_0	-1.565 mA/cm ²	-1.256 mA/cm ²	-0.436 mA/cm ²
R_{ct}	33.3 Ω	10.2 Ω	17.9 Ω

6.4. Conclusion

In conclusion, Pt/WSe₂ nanohybrids were evaluated as electrode materials for HER. Three tungsten precursors were used to determine the electrocatalytic efficiency of Pt decorated WSe₂ nanostructures. The samples were examined displayed good catalytic activity where W(CO)₆ Pt/WSe₂ was found to be the better performing electrocatalyst for HER. The electrocatalytic efficiency of the nanohybrids could be attributed to the morphology of WSe₂, nanoflower-like morphology provides high surface area for electrochemical reactions to take place. Based on previous studies on WSe₂ nanostructures, Pt nanocrystals noticeably improved the electrocatalytic efficiency of Pt/WSe₂ nanohybrids. As the nanohybrids were comparable to Pt/C in particular W(CO)₆. These results indicate that Pt/WSe₂ nanohybrids could be an alternative to noble metal Pt as HER electrode material.

6.5. References

- [1] J. Ke, F. He, H. Wu, S. Lyu, J. Liu, B. Yang, Z. Li, Q. Zhang, J. Chen, L. Lei, Y. Hou and K. Ostrikov, "Nanocarbon-Enhanced 2D Photoelectrodes: A New Paradigm in Photoelectrochemical Water Splitting," *Nano-Micro Letters*, vol. 13, p. 24, 2021.
- [2] M. Antoniadou, S. Sfaelou, V. Dracopoulos and P. Lianos, "Platinum-free photoelectrochemical water splitting," *Catalysis Communications*, vol. 43, pp. 72-74, 2014.
- [3] J. Joy, J. Mathew and S. C. George, "Nanomaterials for photoelectrochemical water splitting - review," *International Journal of Hydrogen Energy*, vol. 43, pp. 4804-4817, 2018.
- [4] Z. Wu, Y. Zhao, W. Jin, B. Jia, J. Wang and T. Ma, "Recent Progress of Vacancy Engineering for Electrochemical Energy Conversion Related Applications," *Advanced Functional Materials*, vol. 31, p. 2009070, 2021.
- [5] B. You and Y. Sun, "Innovative Strategies for Electrocatalytic Water Splitting," *Accounts of Chemical Research*, vol. 51, pp. 1571-1580, 2018.
- [6] C. Coutanceau, P. Urchaga, S. Brimaud and S. Baranton, "Colloidal Syntheses of Shape- and Size-Controlled Pt Nanoparticles for Electrocatalysis," *Electrocatal*, vol. 3, pp. 75-87, 2012.
- [7] M. S. Dehcheshmeh and A. Kiani, "Synthesis of Pt nano catalyst in the presence of carbon monoxide: Superior activity towards hydrogen evolution reaction," *International Journal of Hydrogen Energy*, vol. 44, pp. 23969-23974, 2019.
- [8] H. Li, J. Zou, S. Xie, X. Leng, D. Gao and X. Mao, "Effect of selenization parameters on hydrogen evolution reaction activity of WSe₂ electrodes," *Applied Surface Science*, vol. 425, pp. 622-627, 2017.
- [9] Y. Fu, J. Li and J. Li, "Photo-improved hydrogen evolution reaction activity of the Pt/CdS electrocatalyst," *Progress in Natural Science: Materials International*, vol. 29, pp. 379-383, 2019.

- [10] H. Li, J. Zou, S. Xie, X. Leng, D. Gao and H. Yang, "WSe₂ nanofilms grown on graphite as efficient electrodes for hydrogen evolution reactions," *Journal of Alloys and Compounds*, vol. 725, pp. 884-890, 2017.
- [11] N. Rosman, R. Yunus, L. Minggu, K. Arifin, M. Salehmin, M. Mohamed and M. Kassim, "Photocatalytic properties of two-dimensional graphene and layered transition-metal dichalcogenide based photocatalyst for photoelectrochemical hydrogen generation: An overview," *International Journal of Hydrogen Energy*, vol. 43, pp. 18925-18945, 2018.
- [12] H. Prats and K. Chan, "The determination of the HOR/HER reaction mechanism from experimental kinetic data," *Phys. Chem. Chem. Phys*, vol. 23, pp. 27150-27158, 2021.
- [13] M. Chhowalla, H. Shin, G. Eda, L.-J. Li, K. Loh and H. Zhang, "The chemistry of two-dimensional layered transition metal dichalcogenide nanosheets," *Nature Chemistry*, vol. 5, pp. 263-275, 2013.
- [14] Y. Zhao, G. Mao, Y. Du, G. Cheng and W. Luo, "Colloidal Synthesis of NiWSe Nanosheets for Efficient Electrocatalytic Hydrogen Evolution Reaction in Alkaline Media," *Chemistry An Asian Journal*, vol. 13, pp. 2040-2045, 2018.
- [15] Y. Hwang and N. Shin, "Colloidal Synthesis of MoSe₂/WSe₂ Heterostructure Nanoflowers via Two-Step Growth," *Materials*, vol. 14, p. 7294, 2021.
- [16] M. Sokolikova, P. Sherrell, P. Palczynski, V. Bemmer and Mattevi, "Direct solution-phase synthesis of 1T' WSe₂ nanosheets," *Nature Communications*, vol. 10, p. 712, 2019.
- [17] L.-M. Cao, D. Lu, D.-C. Zhong and T.-B. Lu, "Prussian blue analogues and their derived nanomaterials for electrocatalytic water splitting," *Coordination Chemistry Reviews*, vol. 407, p. 213156, 2020.
- [18] J. Zhang, W. Yao, M. Liu, Q. Xu, Q. Wu and T. Zeng, "Shape Controlled Synthesis of Platinum Nanocrystals with High Catalytic Activities for Methanol Electrooxidation," *Catalyst Letter*, vol. 143, pp. 1030-1034, 2013.
- [19] Z. Ndala, N. Shumbula, S. Nkabinde, T. Kolokoto, O. Nchoe, P. Shumbula, Z. Tetana, E. Linganiso, S. Gqoba and N. Moloto, "Evaluating the Effect of Varying the Metal Precursor in the Colloidal Synthesis of MoSe₂ Nanomaterials

and Their Application as Electrodes in the Hydrogen Evolution Reaction,"
Nanomaterials, vol. 10, p. 1786, 2020.

Chapter 7

General conclusions and recommendations

7.1. Conclusions

This study shows that colloidal synthesis method is an effective technique of synthesizing WSe₂ nanostructures. Generally, the synthesis favours the formation of three-dimensional nanoflower-like structures rather than two-dimensional nanosheets. The reaction parameters (precursor concentration, reaction time, temperature, capping agents and W precursor) were investigated to analyse how they affect the final product. WSe₂ nanoflowers were successfully synthesized at 320 °C for 120 min in OA with a mole ratio of 1:4 (W:Se) using WCl₆ as the metal precursor. When the mole ratio decreased, to 1:2, nanorods were favoured. Shorter reaction times plus lower reaction temperatures (60 min, 150 °C) also resulted in the formation of WSe₂ nanorods. Whereas longer reaction time plus higher reaction temperatures favour WSe₂ nanoflowers being formed. The metal precursor used largely affected the purity of WSe₂ nanostructures. When WCl₆ and W(CO)₆ were used, less impurities were observed. Whereas H₂WO₄ metal precursor tends to form WSe₂ with tungsten oxide which was likely caused by the oxidation of the metal precursor during synthesis. The recommendation would be to conduct synthesis in a closed environment such as a glove box. This would minimize the precursor reacting in air. It was also shown that the precursor used could also cause impurities. WSe₂ nanostructures favoured oleyl alcohol versus oleylamine as it was a better capping agent that could passivate the nanostructures and prevent agglomeration.

Platinum nanocrystals were decorated on the WSe₂ nanostructures via ex-situ method. It was observed that a capping agent is required for the PtNPs as they tend to agglomerate therefore it affects the distribution. To understand the distribution of the nanoparticles recommendations such as Brunaur-Emmett-Teller (BET) would provide information on the specific surface area of the materials.

The electrochemical properties of the Pt/WSe₂ nanohybrid materials were investigated as electrocatalysts for HER. The electrocatalytic activity of the Pt/WSe₂ was fairly good due to the incorporation of Pt on WSe₂. The nanoflower-like structure of WSe₂ provides a high surface area that improves the catalytic activity of the materials. Such results indicate that the Pt/WSe₂ nanohybrids have potential to be cost-effective

electrocatalysts for HER. Whereby the overall cost has been reduced due to small amount of Pt used. The recommendation would be to reduce the loading of Pt on WSe₂ to make it more economically efficient. It would be beneficial to include other electrocatalytic measurements such as cyclic stability studies that would give an indication of the stability of the materials overtime. These results would provide information on the lifetime of the materials.